

Response to Referee #2 (acp-2018-1158)

We Thank Reviewer for his/her constructive comments

Responses to the Specific comments

General comments: This paper conducts ensemble air quality modeling of NO₂, CO, and NH₃ over Asia, and evaluates model performance using measurements data in the North China Plain and Pearl River Delta regions. 14 models including 13 regional models and one global model with common emission inventory, meteorological fields, modeling domain, and horizontal resolutions were used for the ensemble modeling. The results show that NO₂ and CO simulations are mostly underestimated and NH₃ modeling mismatches the observed temporal variations. Possible reasons for the model structural uncertainties and recommendations for the future studies are given by the authors. This paper is good in general and within the scope of Atmospheric Chemistry and Physics. I recommend for publication once the concerns expressed below are addressed.

Reply: The authors appreciate the reviewer for his/her constructive and up-to-point comments. We have carefully considered the comments and revised the manuscript accordingly. Please refer to our responses for more details given below.

Comment 1: Although 14 models are required to use standard meteorological field, the configurations of meteorological models may not be identical. The author also needs to list the configurations of each meteorological model as in Table 1. Meanwhile, since the meteorological parameters have large impact on the modeled concentrations, the modeled meteorological fields also need to be validated against observed data.

Reply: Thanks for this important comment. In MICS-Asia III, most of the CTMs used the standard meteorological fields simulated by WRFv3.4.1, except the WRF-Chem models (M7-M10), GEOS-Chem (M13) and RAMS-CMAQ (M14) which used their own meteorological fields. Following the reviewer's suggestion, a new table listing the configurations of the meteorological simulations were added to the supplementary material (*please see table S1 in the supplementary*). Table R1 presents the configurations of the standard meteorological simulation as well as those used in WRF-Chem models (M7–M10). The GEOS-Chem (M13) was driven by the GEOS-5 assimilated meteorological fields from the Goddard Earth Observing System of NASA Global Modeling Assimilation Office, and the RAMS-CMAQ (M14) was driven by the Regional Atmospheric Modeling System (RAMS). For WRF-Chem models, the

configurations of their meteorological models were only slightly different from the standard model (Table R1). For example, M7 used the same parametrization schemes as the standard model in terms of the microphysics, radiation, boundary layer, cumulus physics and surface physics. The other WRF-Chem models differed from the standard model only in one or two parametrization schemes.

Table R1: Meteorological configurations for the standard meteorological field and different WRF-Chem models

No	Microphysics	Longwave radiation	shortwave radiation	Boundary layer	Cumulus physics	surface physics
Standard	Lin et al. scheme	RRTMG scheme	Goddard shortwave scheme	YSU scheme	Grell 3D ensemble scheme	Unified Noah land-surface model
M7	Lin et al. scheme	RRTM scheme	Goddard shortwave	YSU scheme	Grell 3D ensemble scheme	Unified Noah land-surface model
M8	Lin et al. scheme	RRTMG scheme	RRTMG scheme	Mellor-Yamada-Janjic TKE scheme	Grell 3D ensemble scheme	Unified Noah land-surface model
M9	Lin et al. scheme	RRTMG scheme	RRTMG scheme	YSU scheme	Grell 3D ensemble scheme	Unified Noah land-surface model
M10	Goddard Cumulus Ensemble	Goddard longwave scheme	Goddard shortwave scheme	YSU scheme	Grell 3D ensemble scheme	Unified Noah land-surface model

We agree with the reviewer that the meteorological parameters have large impacts on the simulations of atmospheric chemistry. As suggested, we have added the evaluations of the wind speed (u-wind and v-wind), relative humidity (RH) and air temperature (T) simulated by the standard meteorological model in the revised manuscript (*please see lines 139–143 in the revised manuscript and Sect.S1 in the supplementary*). These parameters are all important meteorological factors that influences the simulations of NO₂, CO and NH₃ concentrations. For example, the wind speed determines the transport of species and the air temperature influences the reaction rates of thermal chemical reactions. The relative humidity and temperature also have impacts on the thermodynamic equilibrium of gases and aerosols.

Three-hourly meteorological observations from the Integrated Surface Database (ISD) compiled by the National Oceanic and Atmospheric Administration (NOAA), U.S. (Smith et al., 2011) were used in this study. We focused on the evaluations of meteorological simulations over the North China Plain (NCP) and the Pearl River Delta region with the observation sites used in evaluation shown in Fig.R1. Figure R2 shows the averaged time series of simulated meteorological parameters and observations over the NCP region from January, 2010 to December, 2010 with an interval of three hours. The evaluation statistics, including correlation coefficient (R), mean bias error (MBE) and root of mean square error (RMSE), were summarized in Table R2. It clearly shows that the standard meteorology simulations well captured the

main features of the observed meteorological conditions in the NCP region throughout the year with high correlation coefficient, small biases and low RMSE for all meteorological parameters. Similar results could be obtained from the evaluations of meteorological conditions over the PRD region (fig R3). These results suggested that the standard meteorological simulations can well reproduce the meteorological conditions of the NCP and PRD region.

Table R2: Evaluation metrics of the standard meteorological simulation

	NCP			PRD		
	R	MBE	RMSE	R	MBE	RMSE
temp (°C)	1.00	0.21	1.08	1.00	-0.22	0.71
RH (%)	0.97	-0.16	5.15	0.97	3.42	4.82
u-wind (m/s)	0.91	-0.08	0.63	0.82	-0.20	0.53
v-wind (m/s)	0.93	0.33	0.76	0.93	0.05	0.81

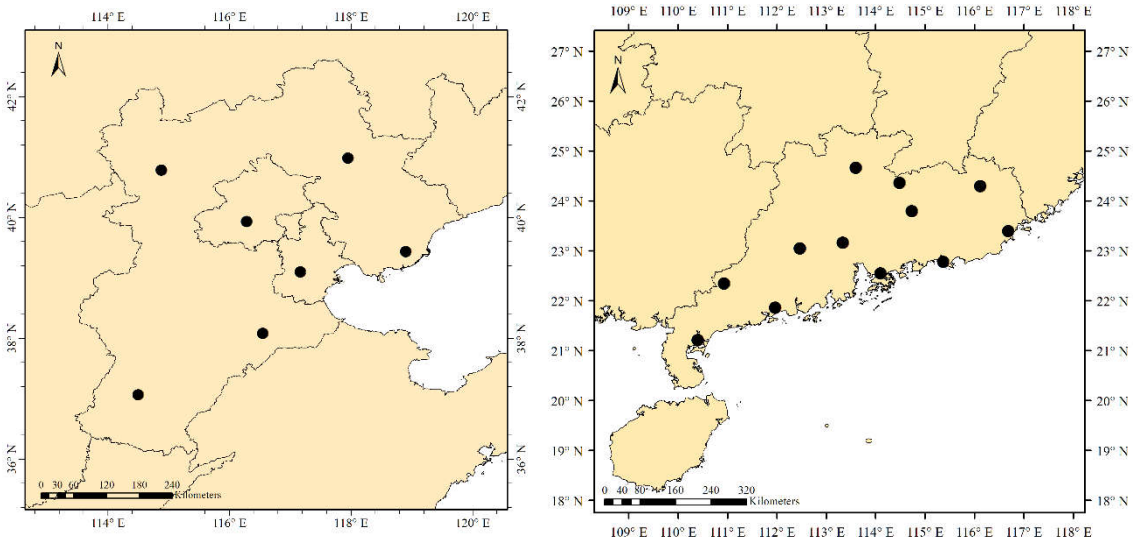


Figure R1: Spatial distributions of the meteorological observation sites from the ISD over the NCP region (left panel) and the PRD region (right panel).

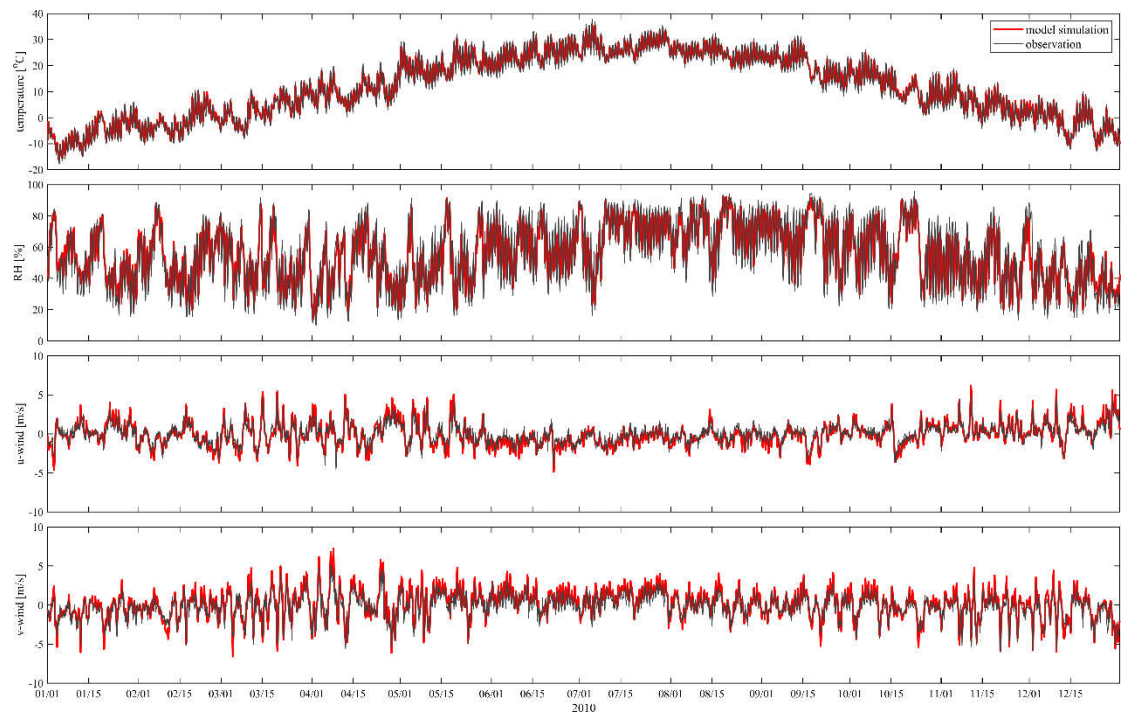


Figure R2: Time series of the simulated and observed meteorological parameters over the NCP region from January 2010 to December 2010 with an interval of three hours.

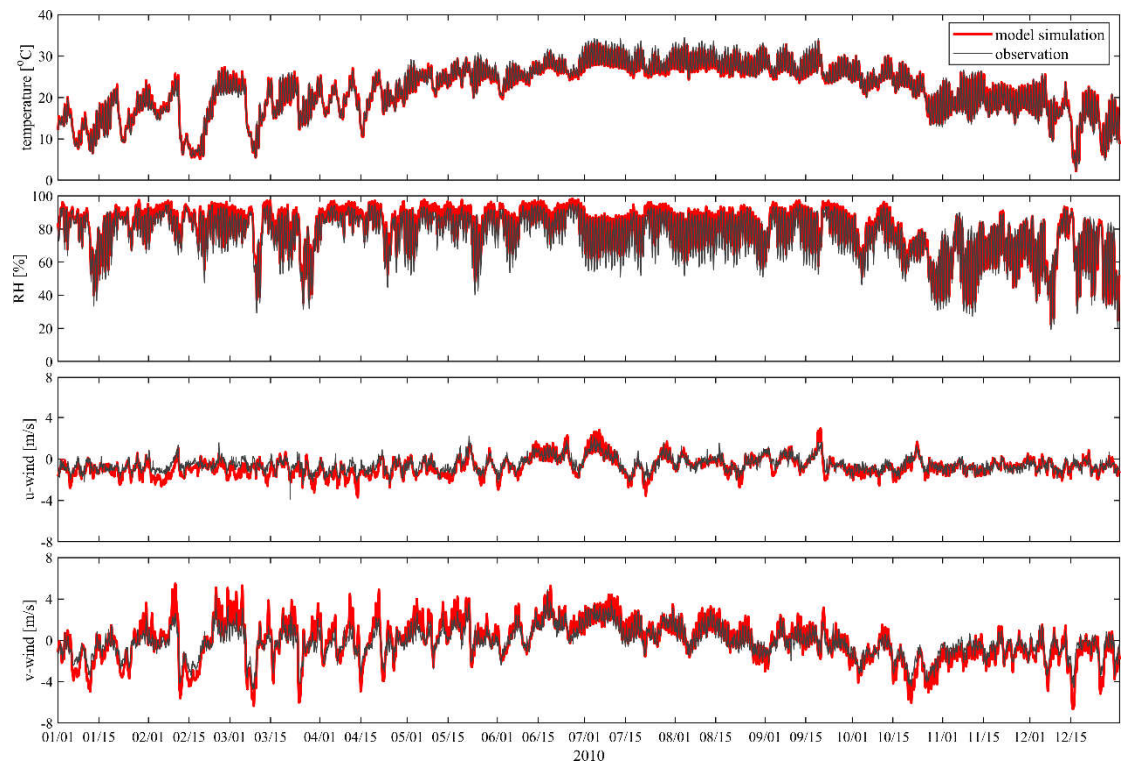


Figure R3: Same as Figure R2 but for the PRD region.

Changes in the manuscript: lines 139–143.

Changes in the supplementary: Sect.S1, Table S1-2 and Figure S1-3.

Comment 2: The model performance in PRD is much worse than that in NCP. The author concludes that it is because of coarse horizontal resolution. I think uncertainties may primarily come from the emission inventory, especially spatial allocations from different emission sectors are not well resolved in the PRD region. I suggest the author use one or two models with finer resolution to test the model performance again in PRD, to see if the horizontal resolution is the main problem as the author demonstrated.

Reply: Thanks for this valuable suggestion. As suggested, a full-year run of NAQPMS model with finer horizontal resolutions has been conducted to investigate the impacts of horizontal resolutions on the simulations of NO₂ and CO over the PRD region. The NAQPMS model is one of the participating CTMs in MICS-Asia III. Two nested domains with finer horizontal resolutions were added to the original modeling domain of MICS-Asia III, which are shown in Fig. R4. The first domain (D1) is identical to the modeling domain of MICS-Asia III with horizontal resolution of 45km. The second domain (D2) covers most part of southeast China with horizontal resolution of 15km; the third domain has the finest horizontal resolution (5km) covering the PRD region and its surrounding areas. The chemical configurations of NAQPMS in each modeling domain were completely identical to those used in MICS-Asia III. Meteorological fields for each modeling domain were simulated by the WRF model version 3.4.1, same as the standard meteorological model in MICS-Asia III. The WRF configurations were also the same as those used in the standard meteorological simulations except two additional nested domains were added (Fig. R4). The emission inventories and boundary conditions in D1 were provided by the standard input datasets of MICS-Asia III. Since MICS-Asia III only provided the emission inventories and boundary conditions at 45km horizontal resolution, in D2 and D3, the emission rates ($\mu\text{g}/\text{m}^2/\text{s}$) and boundary conditions over one model grid were simply obtained from the corresponding model grid in its parent domain. This means that although we used the finer horizontal resolutions in D2 and D3, the resolutions of emission inventories and boundary conditions in D2 and D3 were the same as those used in D1. Therefore, the horizontal resolutions were only dynamically increased in D2 and D3. The simulation results from different modeling domains were then compared with each other to investigate the dynamical impacts of horizontal resolution on the model performance.

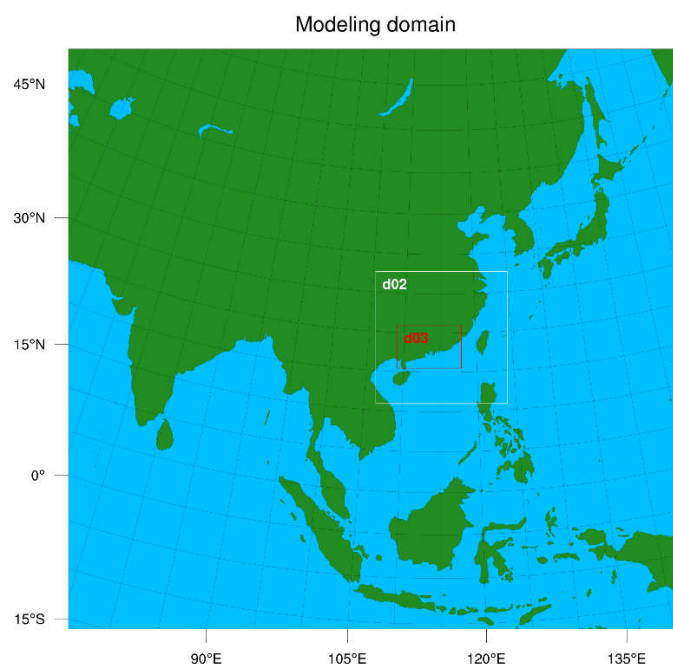


Figure R4: Modeling domain of the sensitivity experiment with different horizontal resolutions.

Figure R5 shows the spatial distributions of the observed annual mean NO_2 concentrations in the PRD region overlay the simulation results using different horizontal resolutions. We can clearly see that the coarse modeling results (D1) cannot resolve the high spatial variability of NO_2 concentrations in the PRD region, which is consistent with what we found from the MICS-Asia III. For simulations using finer horizontal resolutions (D2 and D3), although the spatial scales of NO_2 observations can be resolved by the 15km and 5km resolutions, the modeling results still show poor performance in capturing the observed spatial variability of NO_2 concentrations, with calculated correlation coefficient only of 0.03 and 0.02, respectively (table R2), even worse than the coarse resolutions. Similar results could be obtained from the comparisons of CO observations and simulations with different horizontal resolutions (Fig.R6). These results indicated that the poor model performance in the PRD region may not be attributed to the resolution of model but more related to the resolution and/or spatial allocation of the emission inventories in the PRD region. These results also suggested that only increasing the resolution of the model may not help improve the model performance.

Thus, as the reviewer suggested, the poor model performance in PRD may be more related to coarse resolution and/or inappropriate spatial allocation of the emission inventories in PRD region. Based on these results, we have revised the abstract (*please see lines 43–45 in the revised manuscript*), Section 3.3.1 (*please see lines 244–254 in the revised manuscript*) and Summary (*please see lines 420–424 in the revised manuscript*) part of the manuscript. Analysis of this sensitivity experiments were also added to

the supplementary material (please see Sect.S3 in the supplementary material).

Table R2: Table S3: Evaluation metrics of the simulated annual mean NO₂ and CO concentrations over the PRD region with different horizontal resolutions.

	NO ₂ (ppbv)				CO (ppmv)			
	Spatial R	MBE	NMB (%)	RMSE	Spatial R	MBE	MBE (%)	RMSE
45km	0.09	2.99	13.37	10.53	0.00	-0.51	-52.85	0.57
15km	0.03	2.19	9.81	10.15	0.00	-0.54	-56.25	0.60
5km	0.02	0.58	2.59	10.23	-0.10	-0.58	-59.23	0.62

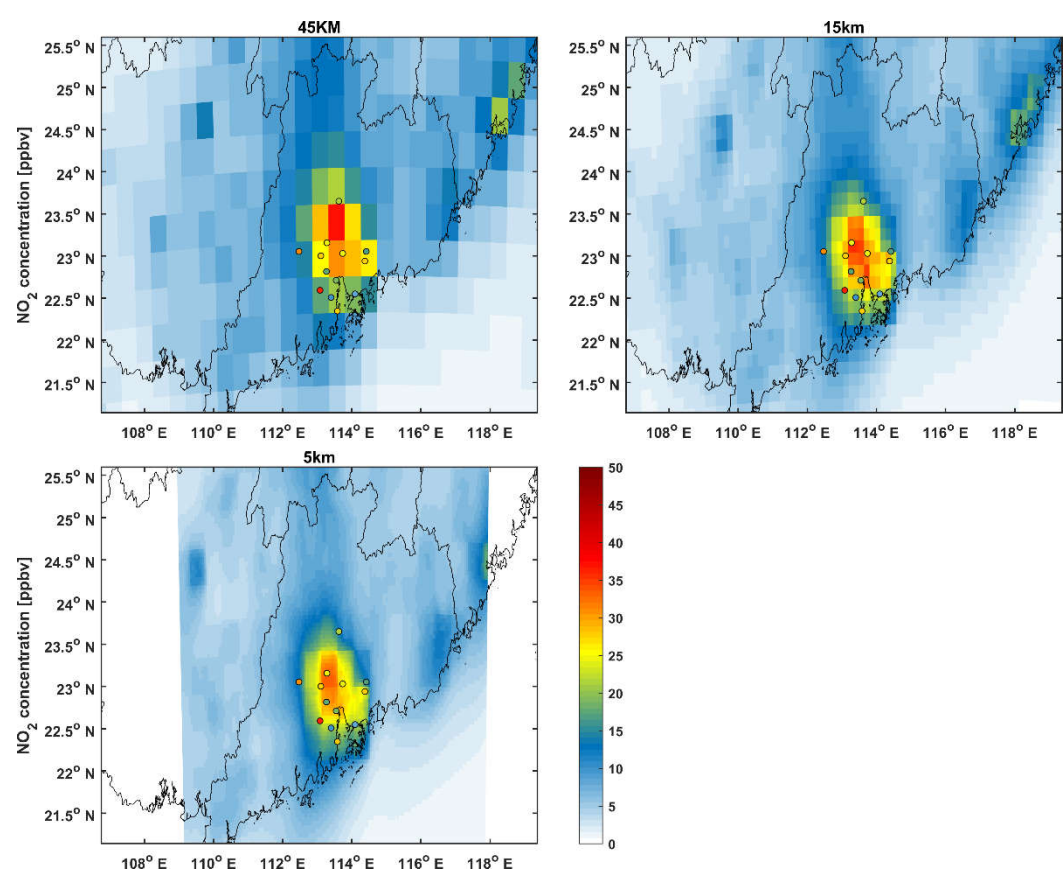


Figure R5: Spatial distributions of the observed and multi-resolution simulated annual mean NO₂ concentrations over the PRD region.

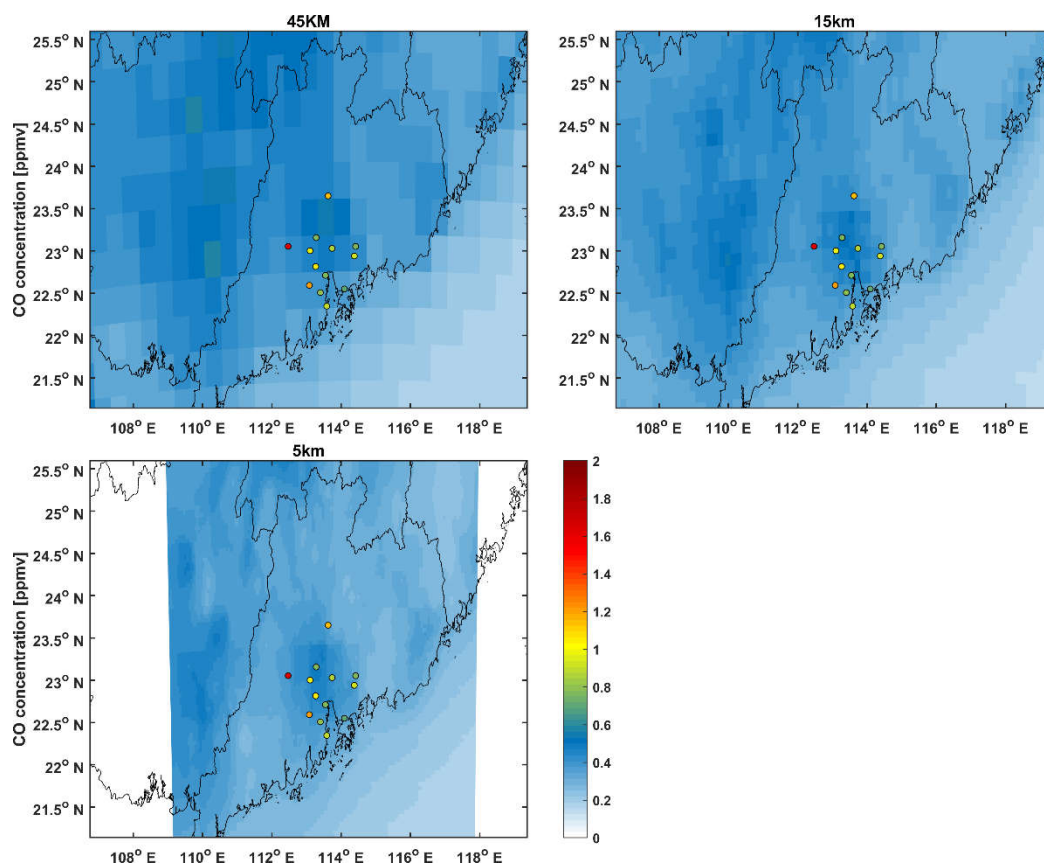


Figure R6: Same as figure R5 but for CO concentrations.

Changes in the manuscript: lines 43–45, lines 244-254 and lines 420-424.

Changes in the supplementary: Sect.S3 and Figure S4-6.

Comment 3: I agreed with the author using the available NH_3 observations from the other years as an alternative to evaluate the performance of different models. However, to evaluate the modeled temporal variations using observed data from different years may not be appropriate, because the NH_3 emissions vary year by year, and control measures may be applied in year of measurement conducted.

Reply: Thanks for this comment. We agree with the reviewer that the use of NH_3 observations from different years may be inappropriate for evaluating the modeled temporal variations due to the emission changes of NH_3 . In the revised manuscript, this problem has been discussed using the satellite retrievals of NH_3 total columns from IASI (Infrared Atmospheric Sounding Interferometer) since we did not obtain the direct surface observations of NH_3 concentration over China in 2010 (*please see lines 202–207 in the revised manuscript*). We used the ANNI-NH3-v2.1R-I retrieval product (Van Damme et al., 2017; Van Damme et al., 2018) in this study which is the reanalysis version of NH_3 retrievals from IASI instruments and provides the daily morning (~9:30 am local time) NH_3 total columns from year 2008 to 2016. The morning orbit was used since IASI is generally more sensitive to the atmospheric boundary layer at this

time due to more favorable thermal conditions, which could provide more information on the NH_3 concentrations in the boundary layer where NH_3 is emitted. This dataset was produced by Van Damme et al., 2018 based on the conversion of hyperspectral range indices (HRIs) using an Artificial Neural Network (Whitburn et al., 2016). It uses the ERA-interim ECWMF meteorological input data rather than the operationally provided EUMETSAT IASI Level 2 (L2) data used for the standard near-real-time version, which is more coherent in time and suitable for the study of temporal variations.

To facilitate comparisons, the NH_3 total columns were averaged to the monthly data at $45\text{km} \times 45\text{km}$ MICS-Asia grids. A comparison of surface NH_3 observation from AMoN-China and NH_3 total columns from IASI was first conducted to see if IASI measurement could reasonably represent the monthly variations of surface NH_3 concentrations, which is shown in Fig. R7. We can see that the IASI measurement can generally well represent the monthly variations of surface NH_3 concentrations over the NCP region. Both two datasets show a very strong summer peak in July and a subpeak in Spring. However, the IASI NH_3 columns show a steeper monthly variations than the surface NH_3 observations suggested. The month of the subpeak in spring is also different between these two datasets. Nevertheless, the IASI measurement well captured the major monthly patterns of the surface NH_3 concentrations, which can be used to qualitatively evaluate the modeled monthly variations.

Figure R8 shows the spatial distributions of the monthly mean IASI NH_3 total columns over the modeling domain of MICS-Asia III in year 2010. The IASI measurement has a good agreement with the modeled results regarding the spatial distributions of the NH_3 concentrations over East Asia with high columns over Indo-Gangetic Plain and the North China Plain (NCP). However, large discrepancy exists in the monthly variations of NH_3 concentrations over the NCP region between model results and IASI measurements. Consistent with Fig. R7, The IASI NH_3 total columns exhibit significant monthly variations over the NCP region with a strong summer peak in July while the model results shows peak values in November (*Fig. 3e in the revised manuscript*). This is consistent with the comparisons of surface NH_3 concentrations, which further confirms the potential deficiency of current CTMs in reproducing the monthly variations of NH_3 concentrations over NCP.

We also plotted the time series of monthly IASI NH_3 total columns averaged over NCP from January, 2008 to December, 2016 to investigate the interannual change of the monthly variations of NH_3 concentrations over NCP, which is shown in Fig. R8. We can see that although there are some interannual changes of magnitude of NH_3 total columns, the monthly pattern of NH_3 total columns is quite similar among different years, which suggests that the interannual change of monthly variation of NH_3

concentrations were very small in these years. Thus, the NH₃ observations from different years could still provide us valuable information on the monthly variation of NH₃ concentrations, which can be used as an alternative to qualitatively evaluate the modeled monthly variation.

These results have been summarized in the revised manuscript (*please see lines 312–323 in the revised manuscript*) and the supplementary (*please see Figure S7-8 in supplementary*)

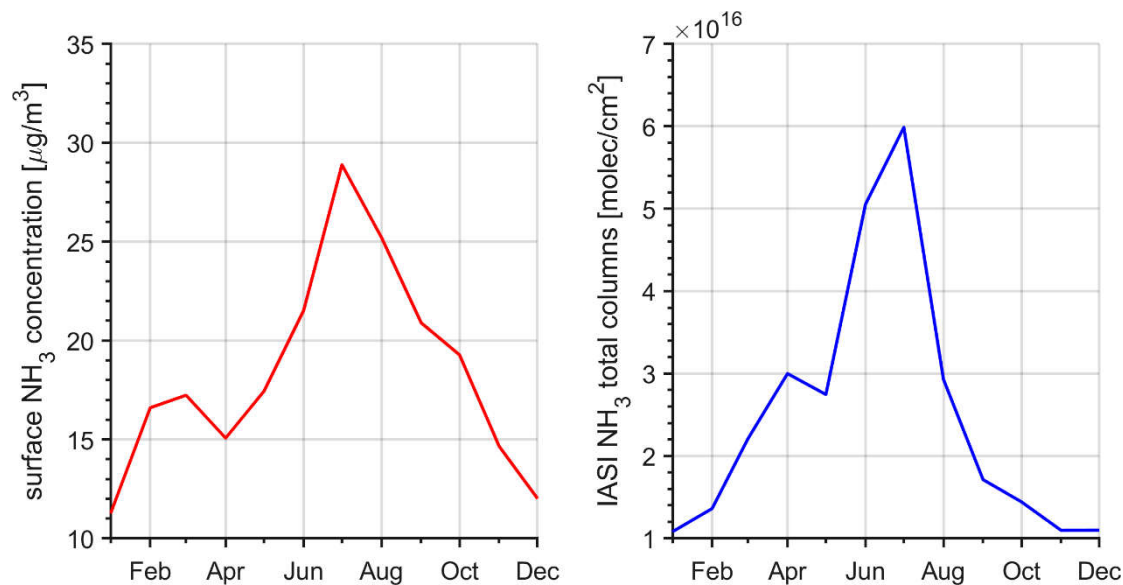


Figure R7: Time series of the surface NH₃ concentrations from AMoN-China (left panel) and NH₃ total columns from IASI (right panel) over the NCP region during September 2015 – August 2016. Note that we reordered the months to better characterize the monthly variations

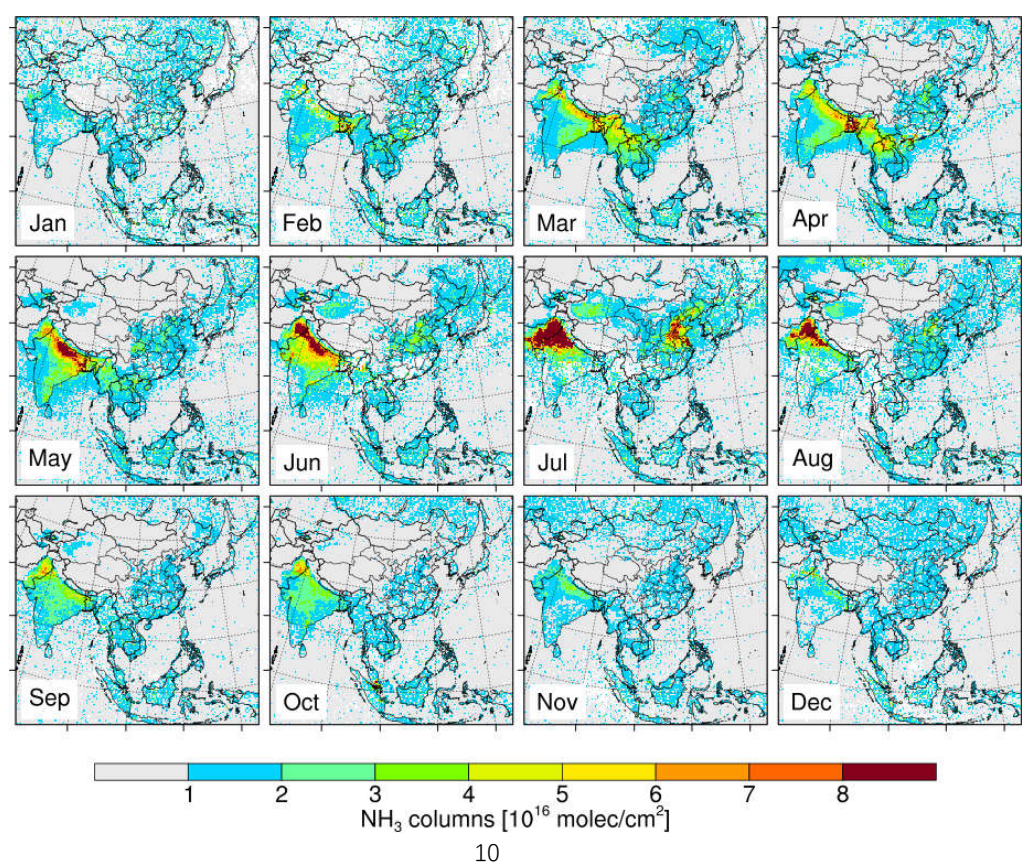


Figure R8: Spatial distributions of the monthly mean IASI NH₃ total columns over the modeling domain of MICS-Asia III

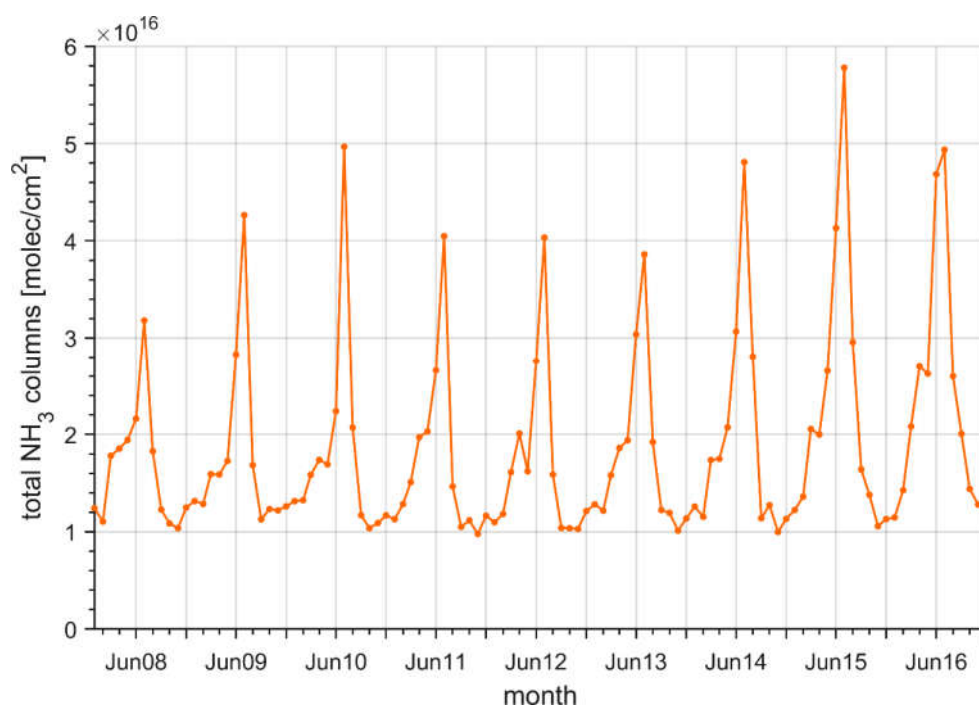


Figure R9: Monthly series of IASI measured NH₃ total columns over the NCP region from year 2008 to 2016.

Changes in the manuscript: lines 202–207 and lines 312–323.

Changes in the supplementary: Sect.S2 and Figure S7-8.

Comment 4: Figure 5 is an interesting finding in this paper. I am surprised that the NH₃ gas-aerosol partitioning simulations from different models have such large discrepancies. Is it because the chemical mechanisms in different models treating NH₃ different? Otherwise, please explain why does such large discrepancy of NH₃ gas-aerosol partitioning occur in different models.

Reply: Thanks for this comment. As the review mentioned, the gas-chemistry mechanism may contribute to the differences in the modeled gas-aerosol partitioning of NH₃. M9 used the RADM2 mechanism which give lower reaction rates of oxidation of SO₂ and NO₂ by OH radical as compiled by Tan et al., 2019, leading to lower productions of acid and thus lower conversion rate of NH₃ to NH₄⁺. Besides, the hydrolysis of N₂O₅ was not considered in M7, which leads to a lower tendency in the prediction of NO₃⁻ (Chen et al., 2019), and partly explains the higher NH₃ predictions of M7. On the contrary, M14 showed a much lower NH₃/NH_x ratio than most models, which would be related to its higher production rates of sulfate than other models (Chen et al., 2019). For M10, the higher NH₃ predictions of M10 would be related to the inorganic aerosol module used in the model (GOCART). The GOCART aerosol module did

not consider the NH_4^+ aerosol, thus the emitted NH_3 would be only presented as the gas phase in the atmosphere, leading to higher NH_3 predictions in M10. This may also help explain the different monthly variations of NH_3 concentrations seen in M10. Without the considerations of NH_4^+ , the monthly variations of NH_3 concentrations in M10 were more consistent with the monthly variations of NH_3 emissions. This again highlighted the importance of gas-aerosol partitioning of NH_3 on the predictions of monthly variations of NH_3 concentrations.

Based on these results, we have added more discussions on the potential reasons for the differences in the modeled gas-aerosol partitioning of NH_3 in the revised manuscript (*please see lines 335–339 and lines 343–349 in the revised manuscript*).

Changes in the manuscript: lines 335–339 and lines 343–349;

Comment 5: In summary, the author makes a few recommendations for future studies. I think inversions of NO_x and CO emissions will help to reduce uncertainties in emission inventory and improve model performance, since many inverse modeling works of NO_x and CO emissions have been done using satellite as well as ground observations. However, I have doubts on inversion of NH_3 because of the reactivity and uncertainties in the chemical pathways of NH_3 gas.

Reply: Thanks for this comment. We agree with the reviewer that the inversion of NH_3 emissions (top-down method) would be more complicated than that for the NO_x and CO emissions due to the larger uncertainties in modeling the atmospheric processes of NH_3 . However, the inversion of NH_3 emissions could still provide valuable clues for verifying bottom-up emission inventories (Zhang et al., 2009) if the models were well validated. In addition, Most of NH_3 is emitted from the non-point sources like livestock or fertilizer uses, which is difficult to be measured over a large domain. As a result, detailed activity data and emission factors for NH_3 emissions are rarely available nationally, leading to high uncertainties in the spatial and temporal patterns of NH_3 emissions. Using the ground or satellite measurements, the top-down methods could give valuable information on the spatial and temporal characteristics of NH_3 emission inventories (Li et al., 2017). Therefore, although there are uncertainties in modeling the processes of NH_3 , several inversion studies has been conducted for NH_3 emissions in U.S., Europe and also China (Gilliland et al., 2003;Paulot et al., 2014;Zhu et al., 2013;Zhang et al., 2018), which has provided valuable suggestions to the improvement of NH_3 emission inventories. Thus, we still believe the top-down methods could help improve the development of NH_3 emissions, however, we have clarified the needs of model validation before the inversion of NH_3 emissions in the revised manuscript (*please see lines 454–461 in*

the revised manuscript), which as follows:

“The inversion of NH₃ emissions would be more complicated than the inversion of CO emissions due to the larger uncertainties in modeling the atmospheric processes of NH₃. Nevertheless, it could still provide valuable clues for verifying the bottom-up emission inventories (Zhang et al., 2009) if the models were well validated. In addition, by using the ground or satellite measurements, the top-down methods could also give valuable information on the spatial and temporal patterns of NH₃ emissions, for example the inversions studies by (Paulot et al., 2014; Zhang et al., 2018). However, more attention should be paid to the validations of model before the inversion estimation of NH₃ emissions. How to represent the model uncertainties in the current framework of emission inversion is also an important aspect in future studies. Things could be better for CO considering its small and weakly spatial-dependent model uncertainties.”

Changes in the revised manuscript: lines 454–461.

Other specific comments:

Comment 6: In page 1, line 40, change “peral” to “pearl”.

Reply: We have revised it.

Changes in the manuscript: lines 41

Comment 7: In page 4, line 4, missing “plain”

Reply: We have revised it.

Changes in the manuscript: lines 111-112.

Comment 8: In Figure 1, I think the color of CO measurement sites in NCP should be “green” instead of “blue”.

Reply: We have revised it.

Changes in the manuscript: lines 776.

References

- Chen, L., Gao, Y., Zhang, M., Fu, J. S., Zhu, J., Liao, H., Li, J., Huang, K., Ge, B., Wang, X., Lam, Y. F., Lin, C. Y., Itahashi, S., Nagashima, T., Kajino, M., Yamaji, K., Wang, Z., and Kurokawa, J. I.: MICS-Asia III: Multi-model comparison and evaluation of aerosol over East Asia, Atmos. Chem. Phys. Discuss., 2019, 1-54, 10.5194/acp-2018-1346, 2019.
- Gilliland, A. B., Dennis, R. L., Roselle, S. J., and Pierce, T. E.: Seasonal NH₃ emission estimates for the eastern United States

- based on ammonium wet concentrations and an inverse modeling method, *J. Geophys. Res.-Atmos.*, 108, 12, 10.1029/2002jd003063, 2003.
- Li, M., Liu, H., Geng, G. N., Hong, C. P., Liu, F., Song, Y., Tong, D., Zheng, B., Cui, H. Y., Man, H. Y., Zhang, Q., and He, K. B.: Anthropogenic emission inventories in China: a review, *Natl. Sci. Rev.*, 4, 834-866, 10.1093/nsr/nwx150, 2017.
- Paulot, F., Jacob, D. J., Pinder, R. W., Bash, J. O., Travis, K., and Henze, D. K.: Ammonia emissions in the United States, European Union, and China derived by high-resolution inversion of ammonium wet deposition data: Interpretation with a new agricultural emissions inventory (MASAGE_NH3), *J. Geophys. Res.-Atmos.*, 119, 4343-4364, 10.1002/2013jd021130, 2014.
- Smith, A., Lott, N., and Vose, R.: The Integrated Surface Database Recent Developments and Partnerships, *Bull. Amer. Meteorol. Soc.*, 92, 704-708, 10.1175/2011bams3015.1, 2011.
- Tan, J., Fu, J. S., Carmichael, G. R., Itahashi, S., Tao, Z., Huang, K., Dong, X., Yamaji, K., Nagashima, T., Wang, X., Liu, Y., Lee, H. J., Lin, C. Y., Ge, B., Kajino, M., Zhu, J., Zhang, M., Hong, L., and Wang, Z.: Why models perform differently on particulate matter over East Asia? – A multi-model intercomparison study for MICS-Asia III, *Atmos. Chem. Phys. Discuss.*, 2019, 1-36, 10.5194/acp-2019-392, 2019.
- Van Damme, M., Whitburn, S., Clarisse, L., Clerbaux, C., Hurtmans, D., and Coheur, P. F.: Version 2 of the IASI NH3 neural network retrieval algorithm: near-real-time and reanalysed datasets, *Atmos. Meas. Tech.*, 10, 4905-4914, 10.5194/amt-10-4905-2017, 2017.
- Van Damme, M., Clarisse, L., Whitburn, S., Hadji-Lazaro, J., Hurtmans, D., Clerbaux, C., and Coheur, P.-F.: Level 2 dataset and Level 3 oversampled average map of the IASI/Metop-A ammonia (NH3) morning column measurements (ANNI-NH3-v2.1R-I) from 2008 to 2016, in, PANGAEA, 2018.
- Whitburn, S., Van Damme, M., Clarisse, L., Bauduin, S., Heald, C. L., Hadji-Lazaro, J., Hurtmans, D., Zondlo, M. A., Clerbaux, C., and Coheur, P. F.: A flexible and robust neural network IASI-NH3 retrieval algorithm, *J. Geophys. Res.-Atmos.*, 121, 6581-6599, 10.1002/2016jd024828, 2016.
- Zhang, L., Chen, Y. F., Zhao, Y. H., Henze, D. K., Zhu, L. Y., Song, Y., Paulot, F., Liu, X. J., Pan, Y. P., Lin, Y., and Huang, B. X.: Agricultural ammonia emissions in China: reconciling bottom-up and top-down estimates, *Atmos. Chem. Phys.*, 18, 339-355, 10.5194/acp-18-339-2018, 2018.
- Zhang, Q., Streets, D. G., Carmichael, G. R., He, K. B., Huo, H., Kannari, A., Klimont, Z., Park, I. S., Reddy, S., Fu, J. S., Chen, D., Duan, L., Lei, Y., Wang, L. T., and Yao, Z. L.: Asian emissions in 2006 for the NASA INTEX-B mission, *Atmos. Chem. Phys.*, 9, 5131-5153, 10.5194/acp-9-5131-2009, 2009.
- Zhu, L., Henze, D. K., Cady-Pereira, K. E., Shephard, M. W., Luo, M., Pinder, R. W., Bash, J. O., and Jeong, G. R.: Constraining U.S. ammonia emissions using TES remote sensing observations and the GEOS-Chem adjoint model, *J.*

Response to Referee #3 (acp-2018-1158)

We Thank Reviewer for his/her constructive comments

Responses to the Specific comments

General comments: This work evaluated 14 model simulations of NO₂, CO and NH₃ over China under the framework of MICS-Asia III with the aim to assess the capability and uncertainty of current CTMs in East Asia. Model results were provided by a larger number of independent groups and covered a full year (2010). The results show that most models well captured the monthly and spatial patterns of NO₂ in NCP though NO₂ levels are slightly underestimated, but relatively poor model performance was observed in the PRD region. All models significantly underpredict CO concentrations both in the NCP and PRD regions and failed to reproduce the observed monthly variation of NH₃ in NCP. This work quantifies the impacts of model uncertainties on simulations of the three primary gases, which shows the large uncertainty (spread) in simulating more reactive and/or short-lived primary pollutants (e.g. NH₃). This work is important and valuable to the scientific and regulatory community as it provides information on the capability and limitations of some widely used models. The manuscript is well organized and well written, and model results (tables and figures) are clearly presented. I recommend its publication after the authors have addressed my comments listed below.

Reply: The authors appreciate the reviewer for his/her valuable suggestions. In the revised manuscript we have considered each comment for improvement, revision, and correction. Please refer to our responses for more details given below.

Comment 1: For comparison with the NO₂ measured from the regular monitoring networks, please note that these networks employ a thermal conversion method which converts NO₂ to NO, followed by detection of NO. This method is known to overestimate NO₂ as it also converts other NO_y species such as HONO and PAN etc (e.g., Xu et al., 2013). It is important to correct this measurement problem before making the comparison, using, for example, the approach by Zhang et al. (2017). After corrections of the measurement data, a closer agreement would be seen between the modelled results and the observations in the present work. If the author cannot make such corrections in view of a large number of groups involved, at least some discussions should be provided on this point.

Reply: Thanks for this important point. According to Xu et al., 2013, the thermal conversion method has

a problem of overestimating the NO₂ concentrations due to the positive interference of other oxidized nitrogen compounds. Zhang et al., 2017 has proposed a method to correct this measurement error based on the model simulations using the equation of:

$$NO_{2\text{ }obs} = NO_{2\text{ }obs}^* \times \frac{NO_{2\text{ }mod}}{NO_{2\text{ }mod} + NO_{z\text{ }mod} - Nitrate_{mod}}$$

where $NO_{2\text{ }obs}$ is the corrected NO₂ observations; $NO_{2\text{ }obs}^*$ is original measurement of NO₂; $NO_{2\text{ }mod}$ is the simulated NO₂ concentration; $NO_{z\text{ }mod}$ is the sum of simulations of HONO, 2×N₂O₅, ClONO₂, ClONO₂, NO₃ HNO₃, HNO₄, PAN, and Nitrate; and $Nitrate_{mod}$ is the simulated nitrate.

However, as the reviewer mentioned, it is hard to make such corrections using a large number of models due to the model uncertainties in predicting the concentrations of NO₂, NO_z and Nitrate. Thus, following the suggestions of reviewer, we have added the discussions of the positive biases in the measurement NO₂ concentrations in the revised manuscript (*see lines 190–192 in the revised manuscript*), which as follows:

“It should be noted that these networks measured the NO₂ concentrations using a thermal conversion method, which would overestimate the NO₂ concentrations due to the positive interference of other oxidized nitrogen compounds (Xu et al., 2013).”

According to this, the underestimated NO₂ predictions by the models may also be related to the positive biases in the NO₂ observations, which has been clarified in the revised manuscript (*please see lines 234–236 and lines 416–417 in the revised manuscript*).

Changes in the manuscript: lines 190-192, lines 234-236 and lines 416-417.

Comment 2: Section 2.2. The comparison of NO₂ and CO concentrations are only for NCP and PRD. Any reasons why not to include other regions?

Reply: Thanks for this comment. This manuscript focuses on the evaluation and uncertainty investigation of NO₂, CO and NH₃ modeling over China under the framework of MICS-Asia III. The CTMs were run at the base year of 2010 when the observations were very limited in China, thus observation data for NO₂ and CO concentrations only included that from Chinese Ecosystem Research Network (NCP), Pearl River Delta Regional Air Quality Monitoring Network (PRD RAQMN) and the Acid Deposition Monitoring Network in East Asia (EANET). Since the observation data from EANET was very limited in China, we only evaluated the CO and NO₂ modeling results in the NCP and PRD regions, the two typical industrialized regions in China. In next phase of MICS-Asia (MICS-Asia IV), more observations will be

available in China, which would allow us a more thorough evaluation of the model performance over China.

Comment 3: For simulations of NO₂ (and NH₃), accurate representation of nitrogen chemistry is critical. Recent studies have shown that the HONO sources may be under-represented in some models which would give rise to larger simulated NO₂ values (as it underestimates the oxidation of NO₂ by OH) (e.g., Zhang et al., 2017; Fu et al., 2019); N₂O₅ uptake on aerosol may be treated differently in models which could also affect the NO₂ simulations. Therefore, in discussing the discrepancy in modelled NO₂, information on how models treat these nitrogen processes would be helpful.

Reply: Thanks for this comment. We agree with the reviewer that the HONO chemistry has an important role in the nitrogen chemistry in the atmosphere, which influences the simulations of NO₂ and NH₃ (Fu et al., 2019; Zhang et al., 2016; Zhang et al., 2017). Previous studies also indicated that the HONO sources were commonly underestimated in models (Zhang et al., 2016). The heterogeneous reactions of NO₂ on the surfaces ($2\text{NO}_{2(g)} + \text{H}_2\text{O}_{(l)} \rightarrow \text{HONO}_{(l)} + \text{HNO}_{3(l)}$) was one of the dominant sources of HONO in the atmosphere, which has been considered in most models of MICS-Asia III, including CMAQ since version 4.7, NAQPMS, NHM-Chem and GEOS-Chem. However, some other important sources of HONO may still be underestimated by models in MICS-Asia III. For example, Fu et al., 2019 suggested that the high relative humidity and strong light could enhance the heterogeneous reaction of NO₂, and the photolysis of total nitrate were also important sources of HONO. These sources have not been included in the models of MICS-Asia III, which would lead to the deviations from observations. As the reviewer suggested, different treatment of hydrolysis of N₂O₅ would help explain the differences in the modeled NH₃ concentrations. The hydrolysis of N₂O₅ has not been considered in M7, which would lead to a lower tendency in the prediction of NO₃⁻ (Chen et al., 2019) and may partly explain the higher NH₃ predictions in M7.

Based on these results, we have added the discussions of HONO chemistry in the revised manuscript (*please see lines 441–449 in the revised manuscript*).

Changes in the manuscript: lines 441-449.

Comment 4: The photo-chemical mechanisms used in this study are CBMZ, CB05, and SAPRC 99, and

some of them have an updated version such as CB06 and SPARC 07. These updated mechanisms could give different results on model performance. The author is advised to discuss this point to alert the reader that their conclusion may not be applicable to the newer version of the respective mechanism.

Reply: Thanks for this important point. We have clarified this point in the revised manuscript (*please see lines 472–474 in the revised manuscript*), which as follows:

“The gas chemistry mechanisms used in this study are SAPRC 99, CB05, CBMZ, RACM and RADM2, and some of them have an updated version such as CB06 and SPARC 07. Our conclusions may not be applicable to these newer versions of mechanisms and thus more comparisons studies can be performed to understand the differences in these new mechanisms.”

Changes in the manuscript: lines 472-474.

Comment 5: The present comparisons focused on yearly and monthly model performance. It would be interesting to show how different models compare during severe pollution episodes. An important application of CTMs in China is to forecast severe episodes based on which emergency source control measures are activated.

Reply: We agree. Comparisons of different model performance in severe pollution episodes would be very important for the understanding of the capability of current CTMs and their applications in air quality forecast and emission controls. However, in current phase of MICS-Asia, only monthly modeling results has been provided by different CTMs, which limited the comparisons at the yearly and monthly scale. The model performances in pollution episodes will be investigated in MICS-Asia IV with more observation data and hourly simulation results at severe pollution episodes.

Comment 6: The model comparisons were conducted for NO₂, CO, and NH₃. How about SO₂, which is another important primary pollutant? I think the reader would be interested in seeing the model performance for SO₂ as well.

Reply: Thanks for this suggestion. Our study mainly focused on the model performance of NO₂, CO and NH₃. The model comparisons of SO₂ has been covered in a companion paper (Tan et al., 2019), where both the performance of SO₂ and sulfate has been investigated.

Comment 7: Conclusion (1) recommends to improve the CO emission inventory which is for year 2010. Does the recent CO emission have similar problem?

Reply: Thanks for this important point. Since we only evaluated the CO simulations for year 2010, the direct evaluations of CO emissions for recent years were not available in this study. However, we have added some discussions on the recent CO emissions in the revised manuscript (*please see lines 427–433 in the revised manuscript*), which as follows:

The underestimations of CO emissions may be alleviated in recent years due to the decreasing trends of the Chinese CO emissions in recent years (Jiang et al., 2017; Zhong et al., 2017; Sun et al., 2018; Muller et al., 2018; Zheng et al., 2018; Zheng et al., 2019). The inversion results of Zheng et al., 2018 also agree well with the regional MEIC (Multi-resolution Emission Inventory for China) inventory for CO emissions in China from 2013 to 2015. However uncertainties still exist in the CO emissions in recent years, according to previous studies, the estimated CO emissions for the whole China for year 2013 ranges from 134–202 Tg/yr (Jiang et al., 2017; Zhong et al., 2017; Sun et al., 2018; Muller et al., 2018; Zheng et al., 2018; Zheng et al., 2019). Zhao et al., 2017 also suggested a -29%–40% uncertainty of CO emissions from industrial sector in year 2012.

Changes in the manuscript: lines 427–433.

Comment 8: This study reveals a large spread of model simulations for reactive gases. As the exact causes for the difference have not been identified for the individual model, I think it is important to emphasize the need to validate the individual model before using its results to make important policy recommendation.

Reply: Thanks for this important point. We have clarified this point in the revised manuscript (*please see lines 462–466 in the revised manuscript*), which as follows:

“For some highly active and/or short-lived primary pollutants, like NH₃, model uncertainty can also take a great part in the forecast uncertainty. Emission uncertainty alone may not be sufficient to explain the forecast uncertainty and may cause underdispersive, and overconfident forecasts. Future studies are needed in how to better represent the model uncertainties in the model predictions to obtain a better forecast skill. Such model uncertainties also emphasize the need to validate the individual model before

using its results to make important policy recommendation.”

Changes in the manuscript: lines 462-466.

Minor Comments:

Line 40 page1, line 4 page 4, the “Peral” should be “Pearl”.

Reply: We have revised it.

Changes in the manuscript: lines 41.

References

- Chen, L., Gao, Y., Zhang, M., Fu, J. S., Zhu, J., Liao, H., Li, J., Huang, K., Ge, B., Wang, X., Lam, Y. F., Lin, C. Y., Itahashi, S., Nagashima, T., Kajino, M., Yamaji, K., Wang, Z., and Kurokawa, J. I.: MICS-Asia III: Multi-model comparison and evaluation of aerosol over East Asia, *Atmos. Chem. Phys. Discuss.*, 2019, 1-54, 10.5194/acp-2018-1346, 2019.
- Fu, X., Wang, T., Zhang, L., Li, Q. Y., Wang, Z., Xia, M., Yun, H., Wang, W. H., Yu, C., Yue, D. L., Zhou, Y., Zheng, J. Y., and Han, R.: The significant contribution of HONO to secondary pollutants during a severe winter pollution event in southern China, *Atmos. Chem. Phys.*, 19, 1-14, 10.5194/acp-19-1-2019, 2019.
- Jiang, Z., Worden, J. R., Worden, H., Deeter, M., Jones, D. B. A., Arellano, A. F., and Henze, D. K.: A 15-year record of CO emissions constrained by MOPITT CO observations, *Atmos. Chem. Phys.*, 17, 4565-4583, 10.5194/acp-17-4565-2017, 2017.
- Muller, J. F., Stavrakou, T., Bauwens, M., George, M., Hurtmans, D., Coheur, P. F., Clerbaux, C., and Sweeney, C.: Top-Down CO Emissions Based On IASI Observations and Hemispheric Constraints on OH Levels, *Geophys. Res. Lett.*, 45, 1621-1629, 10.1002/2017gl076697, 2018.
- Sun, W., Shao, M., Granier, C., Liu, Y., Ye, C. S., and Zheng, J. Y.: Long-Term Trends of Anthropogenic SO₂, NO_x, CO, and NMVOCs Emissions in China, *Earth Future*, 6, 1112-1133, 10.1029/2018ef000822, 2018.
- Tan, J., Fu, J. S., Carmichael, G. R., Itahashi, S., Tao, Z., Huang, K., Dong, X., Yamaji, K., Nagashima, T., Wang, X., Liu, Y., Lee, H. J., Lin, C. Y., Ge, B., Kajino, M., Zhu, J., Zhang, M., Hong, L., and Wang, Z.: Why models perform differently on particulate matter over East Asia? – A multi-model intercomparison study for MICS-Asia III, *Atmos. Chem. Phys. Discuss.*, 2019, 1-36, 10.5194/acp-2019-392, 2019.
- Xu, Z., Wang, T., Xue, L. K., Louie, P. K. K., Luk, C. W. Y., Gao, J., Wang, S. L., Chai, F. H., and Wang, W. X.: Evaluating the uncertainties of thermal catalytic conversion in measuring atmospheric nitrogen dioxide at four differently polluted sites in China, *Atmos. Environ.*, 76, 221-226, 10.1016/j.atmosenv.2012.09.043, 2013.

- Zhang, L., Wang, T., Zhang, Q., Zheng, J. Y., Xu, Z., and Lv, M. Y.: Potential sources of nitrous acid (HONO) and their impacts on ozone: A WRF-Chem study in a polluted subtropical region, *J. Geophys. Res.-Atmos.*, 121, 3645-3662, 10.1002/2015jd024468, 2016.
- Zhang, L., Li, Q. Y., Wang, T., Ahmadov, R., Zhang, Q., Li, M., and Lv, M. Y.: Combined impacts of nitrous acid and nitryl chloride on lower-tropospheric ozone: new module development in WRF-Chem and application to China, *Atmos. Chem. Phys.*, 17, 9733-9750, 10.5194/acp-17-9733-2017, 2017.
- Zhao, Y., Zhou, Y. D., Qiu, L. P., and Zhang, J.: Quantifying the uncertainties of China's emission inventory for industrial sources: From national to provincial and city scales, *Atmos. Environ.*, 165, 207-221, 10.1016/j.atmosenv.2017.06.045, 2017.
- Zheng, B., Chevallier, F., Ciais, P., Yin, Y., Deeter, M. N., Worden, H. M., Wang, Y. L., Zhang, Q., and He, K. B.: Rapid decline in carbon monoxide emissions and export from East Asia between years 2005 and 2016, *Environ. Res. Lett.*, 13, 9, 10.1088/1748-9326/aab2b3, 2018.
- Zheng, B., Chevallier, F., Yin, Y., Ciais, P., Fortems-Cheiney, A., Deeter, M. N., Parker, R. J., Wang, Y. L., Worden, H. M., and Zhao, Y. H.: Global atmospheric carbon monoxide budget 2000-2017 inferred from multi-species atmospheric inversions, *Earth Syst. Sci. Data*, 11, 1411-1436, 10.5194/essd-11-1411-2019, 2019.
- Zhong, Q. R., Huang, Y., Shen, H. Z., Chen, Y. L., Chen, H., Huang, T. B., Zeng, E. Y., and Tao, S.: Global estimates of carbon monoxide emissions from 1960 to 2013, *Environ. Sci. Pollut. Res.*, 24, 864-873, 10.1007/s11356-016-7896-2, 2017.

Evaluation and uncertainty investigation of the NO₂, CO and NH₃ modeling over China under the framework of MICS-Asia III

Lei Kong^{1,3}, Xiao Tang^{2,3}, Jiang Zhu^{1,3}, Zifa Wang^{2,3}, Joshua S. Fu⁴, Xuemei Wang⁵, Syuichi Itahashi^{6,7}, Kazuyo Yamaji⁸, Tatsuya Nagashima⁹, Hyo-Jung Lee¹⁰, Cheol-Hee Kim¹⁰, Chuan-Yao Lin¹¹, Lei Chen^{2,3}, Meigen Zhang^{2,3}, Zhining Tao^{12,13}, Jie Li^{2,3}, Mizuo Kajino^{14,15}, Hong Liao¹⁶, Zhe Wang^{17,2}, Kengo Sudo¹⁸, Yuesi Wang^{2,3}, Yuepeng Pan^{2,3}, Guiqian Tang^{2,3}, Meng Li^{19,20}, Qizhong Wu^{21,22}, Baozhu Ge^{2,3}, Gregory R. Carmichael²³

¹ICCES, Institute of Atmospheric Physics, Chinese Academy of Sciences, Beijing, 100029, China

²LAPC, Institute of Atmospheric Physics, Chinese Academy of Sciences, Beijing, 100029, China

³University of Chinese Academy of Sciences, Beijing, 100049, China

⁴Department of Civil and Environmental Engineering, University of Tennessee, Knoxville, TN, 37996, USA

⁵Institute for Environment and Climate Research, Jinan University, Guangzhou, 510632, China

⁶Central Research Institute of Electric Power Industry, Abiko, Chiba, 270-1194, Japan

⁷Department of Marine, Earth, and Atmospheric Sciences, North Carolina State University, Raleigh, NC 27607, USA

⁸Graduate School of Maritime Sciences, Kobe University, Kobe, Hyogo 658-0022, Japan

⁹National Institute for Environmental Studies, Onogawa, Tsukuba 305-8506, Japan

¹⁰Department of Atmospheric Sciences, Pusan National University, Busan, 46241, South Korea

¹¹Research Center for Environmental Changes, Academia Sinica, Taipei, 115, Taiwan

¹²Universities Space Research Association, Columbia, MD, USA

¹³NASA Goddard Space Flight Center, Greenbelt, MD, 130, USA

¹⁴Meteorological Research Institute, Japan Meteorological Agency, Tsukuba, Ibaraki, 305-0052, Japan

¹⁵Faculty of Life and Environmental Sciences, University of Tsukuba, Tsukuba, Ibaraki, 305-8577, Japan

¹⁶School of Environmental Science and Engineering, Nanjing University of Information Science & Technology, Nanjing 210044, China

¹⁷Research Institute for Applied Mechanics (RIAM), Kyushu University, Fukuoka, Japan

¹⁸Graduate School of Environmental Studies, Nagoya University, Nagoya, Japan

¹⁹Ministry of Education Key laboratory for Earth System Modeling, Department of Earth System Science, Tsinghua University, Beijing, 100084, China

²⁰Multiphase Chemistry Department, Max Planck Institute for Chemistry, Mainz, 55128, Germany

²¹College of Global Change and Earth System Science, Beijing Normal University, Beijing 100875, China

²²Joint Centre for Global Changes Studies, Beijing Normal University, Beijing 100875, China

²³Center for Global and Regional Environmental Research, University of Iowa, Iowa City, IA, 52242, USA

Correspondence to: Xiao Tang(tangxiao@mail.iap.ac.cn)

Abstract. Despite the significant progress in improving the chemical transport models (CTMs), applications of these modeling endeavours are still subject to the large and complex model uncertainty. Model Inter-Comparison Study for Asia III (MICS-Asia III) has provided the opportunity to assess the capability and uncertainty of current CTMs in East Asia applications. In this study, we have evaluated the multi-model simulations of nitrogen dioxide (NO₂), carbon monoxide (CO) and ammonia (NH₃) over China under the framework of MICS-Asia III. Thirteen modeling results, provided by several independent groups from different countries/regions, were used in this study. Most of these models used some modeling domain with a horizontal resolution of 45km, and were driven by common emission inventories and meteorological inputs. New observations over North China Plain (NCP) and Pearl River Delta (PRD) regions were also available in MICS-Asia III, allowing the model evaluations

over highly industrialized regions. The evaluation results show that most models well captured the monthly and spatial patterns of NO₂ concentrations in the NCP region though NO₂ levels were slightly underestimated. Relatively poor performance in NO₂ simulations was found in the PRD region with larger root mean square error and lower spatial correlation coefficients, which may be related to the coarse resolution or inappropriate spatial allocations of the emission inventories in the PRD region. All models significantly underpredicted CO concentrations in both the NCP and PRD regions, with annual mean concentrations 65.4% and 61.4% underestimated by the ensemble mean. Such large underestimations suggest that CO emissions might be underestimated in current emission inventory. In contrast to the good skills in simulating the monthly variations of NO₂ and CO concentrations, all models failed to reproduce the observed monthly variations of NH₃ concentrations in the NCP region. Most models mismatched the observed peak in July and showed negative correlation coefficients with observations, which may be closely related to the uncertainty in the monthly variations of NH₃ emissions and the NH₃ gas-aerosol partitioning. Finally, model inter-comparisons have been conducted to quantify the impacts of model uncertainty on the simulations of these gases which are shown increase with the reactivity of species. Models contained more uncertainty in the NH₃ simulations. This suggests that for some highly active and/or short-lived primary pollutants, like NH₃, model uncertainty can also take a great part in the forecast uncertainty besides the emission uncertainty. Based on these results, some recommendations are made for future studies.

1 Introduction

As the rapid growth in East Asia's economy with surging energy consumption and emissions, air pollution has become an increasingly important scientific topic and political concern in East Asia due to its significant environmental and health effects (Anenberg et al., 2010; Lelieveld et al., 2015). Chemical transport models (CTMs), serving as a critical tool in both the scientific research and policy makings, have been applied into various air quality issues, such as air quality prediction, long-range transport of atmospheric pollutants, development of emission control strategies and understanding of observed chemical phenomena (e.g. Cheng et al., 2016; Li et al., 2017a; Lu et al., 2017; Ma et al., 2019; Tang et al., 2011; Xu et al., 2019; Zhang et al., 2019). Nevertheless, air quality modeling remains a challenge due to the multi-scale and non-linear nature of the complex atmospheric processes (Carmichael et al., 2008). It still suffers from large uncertainties related to the missing or poorly parameterized physical and chemical processes, inaccurate and/or incomplete emission inventories as well as the poorly represented initial and boundary conditions (Carmichael et al., 2008; Dabberdt and Miller, 2000; Fine et al., 2003; Gao et al., 1996; Mallet and Sportisse, 2006). Understanding such uncertainties and their impacts on the air quality modeling is of great importance in assessing the robustness of models for their applications in scientific research and operational use.

There are specific techniques to assess these uncertainties. Monte Carlo simulations, based on different values of model parameters or input fields sampled from a predefined probability density function (PDF), can provide an approximation to the PDF of possible model output and serves as an excellent characterization of the uncertainties in simulations (Hanna et al., 2001). However, this method is more suited to deal with the uncertainty related to the continuous variables, such as input data

74 or parameters in parameterization. The ensemble method, based on a set of different models, is an alternative approach to
75 accounting for the range of uncertainties (Galmarini et al., 2004; Mallet and Sportisse, 2006). For example, the Air Quality
76 Model Evaluation International Initiative (AQMEII) has been implemented in Europe and North America to investigate the
77 model uncertainties of their regional-scale model predictions (Rao et al., 2011). To assess the model performances and
78 uncertainties in East Asia applications, the Model Inter-Comparison Study for Asia (MICS-Asia) has been initiated in year
79 1998. The first Phase of MICS-Asia (MICS-Asia I) was carried out during period 1998–2002, mainly focusing on the long-
80 range transport and depositions of sulfur in Asia (Carmichael et al., 2002). In 2003, the second phase (MICS-Asia II) was
81 initiated and took more species related to the regional health and ecosystem protection into account, including nitrogen
82 compounds, O₃ and aerosols. Launched in 2010, MICS-Asia III has greatly expanded its study scope by covering three
83 individual and interrelated topics: (1) evaluate strength and weaknesses of current multi-scale air quality models and provide
84 techniques to reduce uncertainty in Asia; (2) develop a reliable anthropogenic emission inventories in Asia and understanding
85 uncertainty of bottom-up emission inventories in Asia; (3) provide multi-model estimates of radiative forcing and sensitivity
86 analysis of short-lived climate pollutants.

87 This study addresses one component of topic 1, focusing on the three gas pollutants of NO₂, CO and NH₃. Compared with
88 MICS-Asia II, more modeling results (fourteen different models with thirteen regional models and one global model) were
89 brought together within the topic 1 of MICS-Asia III, run by independent modeling groups from China, Japan, Korea, United
90 States of America and other countries/regions. The different models contain differences in their numerical approximations
91 (time step, chemical solver, etc.) and parameterizations, which represent a sampling of uncertainties residing in the air quality
92 modeling. However, it would be difficult to interpret the results from inter-comparison studies when the models were driven
93 by different meteorological fields and emission inventories. Thus, in MICS-Asia III the models were constrained to be operated
94 under the same conditions by using the common emission inventories, meteorological fields, modeling domain and horizontal
95 resolutions. The simulations were also extended from the four months in MICS-Asia II to one-full year of 2010.

96 NO₂, CO and NH₃ are three important primary gas pollutants that has wide impacts on the atmospheric chemistry. As a
97 major precursor of O₃, NO₂ plays an important role in the tropospheric O₃ chemistry, and also contributes to the rainwater
98 acidification and the formation of secondary aerosols (Dentener and Crutzen, 1993; Evans and Jacob, 2005). CO is a colorless
99 and toxic gas ubiquitous throughout the atmosphere which is of interest as an indirect greenhouse gas (Gillenwater, 2008) and
100 a precursor for tropospheric O₃ (Steinfeld, 1998). Being the major sink of OH, CO also controls the atmosphere's oxidizing
101 capacity (Levy, 1971; Novelli et al., 1998). As the only primary alkaline gas in the atmosphere, NH₃ is closely associated with
102 the acidity of precipitations for one thing, for another it can react with sulfuric acid and nitric acid forming ammonium sulfate
103 and ammonium nitrate which account for a large proportion of fine particulate matter (Sun et al., 2012; Sun et al., 2013).
104 Assessing their model performances is thus important to help us better understand their environmental consequences and also
105 help explain the model performances for their related secondary air pollutants, such as O₃ and fine particulate matter.

106 In previous phase of MICS-Asia, no specific evaluation and inter-comparison work has been conducted for these gases,
107 especially for CO and NH₃. In MICS-Asia II, model performance of NO₂ was evaluated as a relevant species to O₃ (Han et al.,

2008b), however such evaluations were limited to the observation sites from EANET (Acid Deposition Monitoring Network in East Asia). Model evaluations and inter-comparisons in industrialized regions of China has not been performed due to the limited number of monitoring sites in China from EANET, which hindered our understanding of the model performance in industrialized regions. More densely observations over highly industrialized regions of China, namely the North China (NCP) Plain and Pearl River Delta (PRD) regions, were first included in MICS-Asia III, allowing the model evaluations over highly industrialized regions. Meanwhile, the emission inventories of these three gases still subject to the large uncertainties (Kurokawa et al., 2013; Li et al., 2017b), which is a major source of uncertainties in air quality modeling and forecast. Evaluating these gases' emission inventories from a model perspective is also a useful way to identify the uncertainties in emission inventories (Han et al., 2008a; Noije et al., 2006; Pinder et al., 2006; Stein et al., 2014; Uno et al., 2007).

In all, this paper is aimed at evaluating the NO₂, CO and NH₃ simulations using the multi-model data from MICS-Asia III, three questions are trying to be addressed: (1) what is the performance of current CTMs in simulating the NO₂, CO and NH₃ concentrations over highly industrialized regions of China, (2) what are the potential factors responsible for the model deviations from observations and differences among models, and (3) how large are the impacts of model uncertainties on the simulations of these gases.

2 Inter-comparison frameworks

2.1 Description on the participating models and input datasets

Six different chemical transport models have participated in MICS-Asia III with their major configurations summarized in Table 1. These models included NAQPMS (Wang et al., 2001), three versions of CMAQ (Byun and Schere, 2006), WRF-Chem (Grell et al., 2005), NU-WRF (Peters-Lidard et al., 2015), NHM-Chem (Kajino et al., 2012) and GEOS-Chem (<http://acmg.seas.harvard.edu/geos/>). All models employed a same modeling domain (Fig. 1) with a horizontal resolution of 45km except M13 (0.5° of latitude×0.667° of longitude) and M14 (64km×64km). Detailed information on each component of these CTMs can be obtained from the companion paper Chen et al., 2019 and Tan et al., 2019.

Standard model input datasets of raw meteorological fields, emission inventory and boundary conditions were provided by MICS-Asia III for all participants. Raw meteorological fields were generated from a whole year simulations of 2010 using Weather Research and Forecasting Model (WRF) version 3.4.1 (Skamarock, 2008) with horizontal resolution of 45km and vertically 40 layers from surface to the model top (10hPa). Initial and lateral boundary conditions for meteorological simulation were generated every six hours by using the 1°×1° NCEP FNL (Final) Operational Global Analysis data (ds083.2). Real-time, global, sea surface temperature (RTG_SST_HR) analysis were used to generate and update lower boundary conditions for sea areas. Four-dimensional data assimilation nudging (Gridded FDDA & SFDDA) was performed during the simulation to increase the accuracy of WRF after the objective analysis with NCEP FNL (Final) Operational Global Analysis data (ds083.2), NCEP ADP Global Surface Observation Weather Data (ds461.0) and NCEP ADP Global Upper Air and Surface Weather Data (ds337.0). Detailed configurations of the standard meteorological model are available in supplementary Table S1. The

140 simulated wind speed, relative humidity and air temperature were evaluated against the observations over the NCP and PRD
141 regions with detailed results shown in supplementary Sect. S1. In general, the standard meteorological simulations well
142 captured the main features of meteorological conditions in the NCP and PRD regions with high correlation coefficient, small
143 biases and low errors for all meteorological parameters (supplementary Fig.S1-S3 and Table S2).

144 Standard emission inventories provided by the MICS-Asia III were used by all participants. The anthropogenic emissions
145 were provided by a newly developed anthropogenic emission inventory for Asia (MIX) which integrated five national or
146 regional inventories, including Regional Emission inventory in Asia (REAS) inventory for Asia developed at the Japan
147 National Institute for Environment Studies, the Multi-resolution Emission Inventory for China (MEIC) developed at Tsinghua
148 University, the high-resolution ammonia emission inventory in China developed at Peking University, the Indian emission
149 inventory developed at Argonne National Laboratory in the United States, and the Clean Air Policy Support System (CAPSS)
150 Korean emission inventory developed at Konkuk University (Li et al., 2017b). Hourly biogenic emissions for the entire year
151 of 2010 in MICS-Asia III were provided by the Model of Emissions of Gases and Aerosols from Nature version 2.04 (Guenther
152 et al., 2006). The Global Fire Emissions Database 3 (Randerson et al., 2013) was used for biomass burning emissions. Volcanic
153 SO₂ emissions were provided by the Asia Center for Air Pollution Research (ACAP) with a daily temporal resolution. Air and
154 ship emissions with an annual resolution were provided by the HTAPv2 emission inventory for 2010 (Janssens-Maenhout et
155 al., 2015). NMVOC emissions were spectated into the model-ready inputs for three chemical mechanisms: CBMZ, CB05 and
156 SAPRC-99 and the weekly and diurnal profiles for emissions were also provided.

157 MICS-Asia III has provided two sets of top and lateral boundary conditions for year 2010, which were derived from the
158 3-hourly global CTM outputs of CHASER (Sudo et al., 2002a; Sudo et al., 2002b) and GEOS-Chem
159 (<http://acmg.seas.harvard.edu/geos/>), run by Nagoya University (Japan) and the University of Tennessee (USA) respectively.
160 GEOS-Chem was run with 2.5°×2° resolution and 47 vertical layers while CHASER model was run with 2.8°×2.8° and 32
161 vertical layers.

162 All participants were required to use the standard model input data to drive their model run so that impacts of model input
163 data on simulations could be minimized. However, models are quite different from each other, and it is difficult to keep all the
164 inputs the same. The majority of models have applied the standard meteorology fields, while the GEOS-Chem and RAMS-
165 CMAQ utilized their own meteorology models. The GEOS-Chem was driven by the GEOS-5 assimilated meteorological fields
166 from the Goddard Earth Observing System of the NASA Global Modeling Assimilation Office, and the RAMS-CMAQ was
167 driven by meteorological fields provided by Regional Atmospheric Modeling System (RAMS) (Pielke et al., 1992). WRF-
168 Chem utilized the same meteorology model (WRF) as the standard meteorological simulation, but two of them considered the
169 two-way coupling effects of pollutants and meteorological fields. The meteorological configurations of these WRF-Chem
170 models were compared to the configurations of the standard meteorological model (supplementary table S1), which shows
171 slight differences from the standard meteorological model. The CTM part of NHM-Chem is coupled with the JMA's non-
172 hydrostatic meteorological model (NHM) (Saito et al., 2006), but an interface to convert a meteorological model output of

173 WRF to a CTM input was implemented (Kajino et al., 2018). Thus, the standard meteorology field was used in the NHM-
174 Chem simulation, too.

175 2.2 Data and statistical methods

176 All modeling groups have performed a base year simulations of 2010 and were required to submit their modeling results
177 according to the data protocol designed in MICS-Asia III. Gridded monthly concentrations of NO₂, CO, NH₃ and ammonium
178 (NH₄⁺) in the surface layer were used in this study. Note that modeling results from M3 and NH₃ simulations from M8 were
179 excluded due to their incredible results, thus only thirteen modeling results were used in this study.

180 Hourly observed concentrations of NO₂ and CO were collected over the NCP (19 stations) and PRD (13 stations) regions,
181 obtained from the air quality network over North China (Tang et al., 2012) and the Pearl River Delta regional air quality
182 monitoring network (PRD RAQMN), respectively. The air quality monitoring network over North China was set up by the
183 Chinese Ecosystem Research Network (CERN), the Institute of Atmospheric Physics (IAP) and the Chinese Academy of
184 Sciences (CAS) since 2009 within an area of 500×500 km² in northern China. All monitoring stations were selected and set
185 up according to the US EPA method designations (Ji et al., 2012). The PRD RAQMN network was jointly established by the
186 government of the Guangdong Province and the Hong Kong Special Administrative Region, consisting of 16 automatic air
187 quality monitoring stations across the PRD region (Zhong et al., 2013). Thirteen of these stations are operated by the
188 Environmental Monitoring Centers in the Guangdong Province which were used in this study, while the other three are located
189 in Hong Kong (not included in this study) and are managed by the Hong Kong Environmental Protection Department. Monthly
190 averaged observations were calculated for the comparisons with the simulated monthly surface NO₂ and CO concentrations. It
191 should be noted that these networks measured the NO₂ concentrations using a thermal conversion method, which would
192 overestimate the NO₂ concentrations due to the positive interference of other oxidized nitrogen compounds (Xu et al., 2013).

193 NH₃ observations for long-term period are indeed challenging and limited due to its strong spatial and temporal variability,
194 quick conversion from one phase to another and also its stickiness to the observational instruments (von Bobruzki et al., 2010).
195 Measurements of surface NH₃ concentrations in year 2010 were not available in this study, however, one-year surface
196 measurement of monthly NH₃ concentrations over China from September of 2015 to August of 2016 were used as a reference
197 dataset in this study, which were obtained from the Ammonia Monitoring Network in China (AMoN-China) (Pan et al., 2018)
198 The AMoN-China was established based on the CERN and the Regional Atmospheric Deposition Observation Network in
199 North China Plain (Pan et al., 2012), which consists of 53 sites over the whole China and measured the monthly ambient NH₃
200 concentrations using the passive diffusive technique. Eleven stations located in the NCP region were used in this study.
201 Distributions of the observation sites of NO₂, CO and NH₃ over the NCP and PRD regions as well as their total emissions in
202 year 2010 provided by MICS-Asia III are shown in Fig. 1. Besides the surface observations, the satellite retrievals of NH₃ total
203 columns from IASI (Infrared Atmospheric Sounding Interferometer) were also used in this study to quantitatively evaluate the
204 modeled monthly variations of NH₃ concentrations. The ANNI-NH3-v2.1R-I retrieval product (Van Damme et al., 2017; Van
205 Damme et al., 2018) was used in this study which is the reanalysis version of NH₃ retrievals from IASI instruments and

206 provides the daily morning (~9:30 am local time) NH_3 total columns from year 2008 to 2016. More detailed information and
207 the process of satellite data are available in supplementary sect. S2.

208 Mean bias error (MBE), normalized mean bias (NMB), root mean square error (RMSE) and correlation coefficient (R)
209 were calculated for the assessment of model performances. Standard deviation of the ensemble models was used to measure
210 the ensemble spread and the impacts of model uncertainty. Coefficient of variation (hereinafter, CV), defined as the standard
211 deviation divided by the average with larger value denoting lower consistency among models, was also used to measure the
212 impacts of model uncertainty in a relative sense. However, by this definition, there is a tendency that lower concentrations are
213 more likely associated with higher value of CV, thus we did not calculate the values of CV over model grids whose simulated
214 concentrations were lower than 0.1 ppbv for NO_2 and NH_3 , and 0.1 ppmv for CO, respectively. March–May, Jun–August,
215 September–November and December–February were used to define the four seasons that are spring, summer, autumn and
216 winter, respectively.

217 **3 Results**

218 **3.1 Evaluating the ensemble models with observations**

219 To facilitate comparisons, the modeling results were interpolated to the observation sites by taking the values from the
220 grid cell where the monitoring stations located. Model evaluation metrics defined in Sect. 2.2 were then calculated to evaluate
221 the modeling results against the observations.

222 **3.1.1 NO_2**

223 Figure 2 displays the comparisons between the observed and simulated annual mean NO_2 concentrations over the NCP
224 (2a) and PRD(2b) regions with calculated model evaluation metrics summarized in Table 2. M13 is not included in the
225 evaluation of NO_2 since it did not submitted the NO_2 concentrations. In general, the majority of models underpredicted NO_2
226 levels in both the NCP and PRD regions. Calculated MBE (NMB) ranges from -6.54 ppbv (-28.4%) to -2.45 (-10.6%) ppbv
227 over the NCP region and from -9.84 ppbv (-44.0%) to -1.84 ppbv (-8.2%) over the PRD regions among these negatively-biased
228 models. These underpredicted NO_2 concentrations are consistent with the overpredicted O_3 concentrations by these models
229 found in the companion paper by Li et al., 2019. O_3 productions can either increase with NO_x under NO_x limited conditions or
230 decrease under the NO_x saturated (also called volatile organic compounds (VOCs) limited) conditions (Sillman, 1999). Both
231 the NCP and PRD regions are industrialized regions in China with high NO_x emissions (Fig. 1). Observations also showed that
232 the NCP and PRD regions are falling into or changing into the NO_x saturated regimes (Shao et al., 2009; Jin and Holloway,
233 2015). Therefore, the underestimated NO_2 concentrations may contribute to the overpredicted O_3 concentrations in these two
234 regions. More details about the O_3 predictions can be found in the companion paper by Li et al., 2019. In addition, as we
235 mentioned in Sect.2.2, the negative biases in the simulated NO_2 concentrations can be also partly attributed to the positive
236 biases in the NO_2 observations. M5, M8, M9 and M11 in the NCP region and M5, M8 and M11 in the PRD region were

237 exceptions that overpredicted NO₂ concentrations. M11 showed good performances in predicting NO₂ levels in the NCP region
238 with smallest RMSE, while M9 significantly overestimated NO₂ with largest MBE and RMSE values. NO₂ predictions by M8
239 were close to the observations over the PRD region with smallest RMSE value. Meanwhile, we also found that models
240 exhibited better NO₂ modeling skills in the NCP region than that in the PRD region with smaller bias and RMSE values.

241 According to the spatial correlation coefficients (Table 2), all models well reproduced the main features of the spatial
242 variability of NO₂ concentrations in the NCP region with correlation coefficients ranging from 0.57 to 0.70. However, models
243 failed in capturing the spatial variability of NO₂ concentrations in the PRD region with correlation coefficients only ranged
244 from 0.00 to 0.38. Such low correlation might be attributed to the coarser model resolution (45km) that some local impacts on
245 the NO₂ concentrations might not be well resolved in the model, and/or related to the uncertainties in emission inventories
246 which were not well resolved in the PRD region. To investigate it, we have conducted an additional one-year simulation with
247 finer horizontal resolutions (15km and 5km, supplementary Fig.S4) in the PRD region using the NAQPMS model. Detailed
248 experimental settings are presented in supplementary Sect.S3. The experiment results indicate that when using the same
249 emission inventory as the coarse-resolution simulation, the high-resolution simulation still show poor model performances in
250 capturing the spatial variability of NO₂ concentrations in the PRD region, with calculated correlation coefficient only of 0.03
251 and 0.02 for 15km and 5km resolutions, respectively (supplementary Sect. S3, Fig. S5-6 and Table S3). Thus, the poor model
252 performance in the PRD region could be more related to the coarse resolution and/or inappropriate spatial allocation of the
253 emission inventories. These results also suggested that only increasing the resolutions of model may not help improve the
254 model performance.

255 Figure 3 presents the monthly timeseries of the observed and simulated regional mean NO₂ concentrations over the NCP
256 (3a) and PRD (3b) regions from January to December in 2010. The models well captured the monthly variations of NO₂
257 concentrations both in the NCP and PRD regions. According to Table 2, the correlation coefficient ranges from 0.28 to 0.96
258 in the NCP region and from 0.52 to 0.95 in the PRD region. M8 showed the largest overestimation among all models in summer
259 that MBE (NMB) can reach 12.1 ppbv (75.8%) in the NCP region, which may help explain the low correlation of this model.
260 M9 exhibited a significant overestimation in winter in the NCP region with MBE (NMB) up to 22.0 ppbv (79.3%) while much
261 less overestimation or even underestimation (summer) in other seasons. This discrepancy may be explained by that M9 was
262 an online coupled model which considers two-way coupling effects between the meteorology and chemistry. During the period
263 with heavy haze, the radiation can be largely reduced by aerosol dimming effects, leading to weakened photochemistry,
264 lowered boundary layer height and thus the increase of NO₂ concentrations. Severe haze was reported to occur in North China
265 in January 2010, with maximum hourly PM_{2.5} concentration even reached as high as ~500 µg/m³ in urban Beijing (Gao et
266 al., 2018). Such high aerosol loadings in atmosphere could trigger interactions between chemistry and meteorology.
267 Interestingly, M9 did not overestimate NO₂ during winter in the PRD region. This might be related to the lower aerosol
268 concentrations and weaker chemistry-and-meteorology coupling effects in the PRD region.

269 3.1.2 CO

270 Similar analyses were performed for modeling results of CO. All models significantly underestimated the annual mean
271 CO concentrations both in the NCP and PRD regions (Figs. 2c-d and Table 2). Calculated MBE (NMB) ranges from -1.69
272 ppmv (-76.2%) to -1.16 ppmv (-52.0%) in the NCP region and from -0.67 ppmv (-69.6%) to -0.50 ppmv (-52.3%) in the PRD
273 region (Table 2). Such large negative biases in all models were not likely to be explained by the model uncertainties, suggesting
274 the negative biases in the CO emissions over China. This is consistent with the inversion results of Tang et al., 2013 which
275 indicates a significant underestimation of CO emissions over the Beijing and surrounding areas in the summer of 2010. Over
276 the latest decades, global models also reported CO underestimations in north hemisphere (Naik et al., 2013; Stein et al., 2014)
277 and a number of global model inversion studies have been conducted to derive the optimized CO emissions. Most of these
278 studies have reported a significant underestimation of CO emissions in their *a priori* estimates (Bergamaschi et al.,
279 2000; Miyazaki et al., 2012; Petron et al., 2002; Petron et al., 2004). Our findings agree with these studies and indicate that more
280 accurate CO emissions are needed in future studies. Model performances in simulating spatial variability of CO concentrations
281 were still poor in the PRD region according to Table 2 with most models showing negative correlation coefficients.

282 Timeseries of the observed and simulated regional mean CO concentrations in the NCP and PRD regions are presented
283 in Fig. 3c-d. It shows that the models well reproduced the monthly variations of CO concentrations in both the NCP and PRD
284 regions with high temporal correlation coefficient except M5 (Table 2). All models, however, underestimated CO
285 concentrations throughout the year and showed largest underestimations in winter with MBE (NMB) by ensemble mean up to
286 -2.1 ppmv (-64.9%) in the NCP region and -0.75 ppmv (-60.6%) in the PRD region.

287 3.1.3 NH₃

288 Figure 2e shows the comparisons of the observed and simulated annual mean NH₃ concentrations in the NCP region.
289 Since we used the NH₃ observations from September 2015 to August 2016, negative biases are expected according to the
290 increasing trend of atmospheric ammonia during period 2003–2016 detected by recently retrievals from the Atmospheric
291 Infrared Sounder (AIRS) aboard NASA's Aqua satellite (Warner et al., 2016; Warner et al., 2017). Due to the interannual
292 uncertainty, we mainly focused on the disparities among different models rather than the deviation from observations.

293 Large differences can be seen in simulated NH₃ concentrations from different models. M14 simulated very low
294 concentrations and exhibited the largest negative biases with MBE (NMB) of -12.2 ppbv (-66.3%), which may be related to
295 the higher conversion rate of NH₃ to NH₄⁺ in M14 (discussed in later part of this section). On the contrary, M9 provided much
296 higher NH₃ concentrations than other models with MBE (NMB) up to 21.8 ppbv (118.7%). For the CMAQ models, M1 and
297 M2 exhibited higher NH₃ concentrations and larger spatial variability compared to other CMAQ models. Such discrepancy
298 may be explained by that M1 and M2 are two model runs using CMAQ v5.0.2. The bi-directional exchange of NH₃ has been
299 integrated into CMAQ from version 5.0. This module can simulate the emitted and deposited processes of NH₃ between

300 atmosphere and the surfaces, allowing the additional NH_3 emissions to the atmosphere (US EPA Office of Research and
301 Development).

302 As can be seen in Table 2, the observed spatial variations of NH_3 over the NCP region can be well reproduced by all
303 models ($R = 0.57\text{--}0.71$), indicating that the spatial variations of current NH_3 emissions over the NCP region are well represented
304 in emission inventories. However, all models failed to capture the observed monthly variations of NH_3 concentrations with
305 most models mismatching the observed NH_3 peak (July) and showing negative correlation coefficients. M10 and M13 are
306 exceptions showing good temporal correlations of 0.64 and 0.65, respectively (Fig. 3e and Table 2). This is quite different
307 from the model behavior in simulating the monthly variations of NO_2 and CO concentrations. As seen in Fig. 3e, the
308 observation showed the peak concentrations of NH_3 in summer months and lower concentrations in autumn and winter, which
309 is consistent with the previous NH_3 observations in the NCP region (Shen et al., 2011; Xu et al., 2016; Meng et al., 2011).
310 Newly derived satellite-measured NH_3 at 918 hPa averaged between September 2002 and August 2015 also demonstrated
311 higher concentrations in spring and summer and lower concentrations in autumn and winter (Warner et al., 2016). However,
312 all models predicted a peak concentration in November except M10 in August in and M13 in June. We also used the satellite
313 retrievals of NH_3 total columns from IASI to further evaluate the modeled monthly variations of NH_3 concentrations, since
314 evaluating the model results using observations from different years may be inappropriate due to the emission change of NH_3 .
315 Comparisons of the surface NH_3 observations from AMoN-China and NH_3 total columns from IASI (supplementary Fig.S7)
316 suggest that the IASI measurement can well represent the monthly variations of surface NH_3 concentrations, which can be
317 used to qualitatively evaluate the modeled monthly variations of surface NH_3 concentrations. The monthly time series of the
318 regional mean NH_3 total columns over the NCP region from January, 2008 to December, 2016 are shown in supplementary
319 Fig. S8, which shows similar monthly variations to the surface NH_3 observations with highest value in July and confirms the
320 poor model performances in reproducing the monthly variations of NH_3 concentrations. The IASI measurement also indicates
321 that the interannual variability of monthly variations of NH_3 concentrations over the NCP region was small from year 2008 to
322 2016, which suggest that using observations from different years could still provide valuable clues for verifying the modeled
323 monthly variations.

324 The simulated monthly variations of NH_3 concentrations were closely related to the monthly variations of the NH_3
325 emissions. Most models predicted three peak values of NH_3 concentrations in June, August and November but exhibited a
326 significant decrease in July, which was in good agreement with the peaks and drops of the NH_3 emission rates in these months
327 (Fig.4). The strong relationship between the simulated NH_3 concentrations and the emission rates suggests that the poor model
328 performance in reproducing the monthly variations of NH_3 concentrations is probably related to the uncertainties in the monthly
329 variations of NH_3 emissions. This is consistent with the recent bottom-up and top-down estimates of agriculture ammonia
330 emissions in China by (Zhang et al., 2018), which shows more distinct seasonality of Chinese NH_3 emissions.

331 It is worth noting that there are also important uncertainties in the models beyond emission uncertainty. In order to
332 investigate this issue, we have analyzed the impact of gas-aerosol partitioning of NH_3 on the simulations of NH_3 concentrations.
333 Figure 5 shows the timeseries of the simulated total ammonium ($\text{NH}_x = \text{NH}_3 + \text{NH}_4^+$) in the atmosphere along with the ratio

of gaseous NH_3 to the total ammonium. M10 is excluded in Fig.5 since the GOCART model does not predict NH_4^+ concentrations. As a result, the emitted NH_3 would be only presented as the gas phase in M10, leading to higher NH_3 predictions. This may also help explain the different monthly variations of NH_3 concentrations seen in M10. Without the considerations of NH_4^+ , the monthly variations of NH_3 concentrations in M10 were more consistent with the monthly variations of NH_3 emissions, which highlighted the importance of gas-aerosol partitioning of NH_3 on the predictions of monthly variations of NH_3 concentrations. As seen in fig.5, there are large discrepancy in the simulated gas-aerosol partitioning of NH_3 from different models. M7 and M9 showed higher NH_3/NH_x ratio than other models, which means that these two models tended to retain the NH_3 in the gas phase and thus predicted higher NH_3 concentrations than other models. For example, M7 predicted comparable magnitude of total ammonium with most models, while gas NH_3 concentration in M7 accounted for more than 60% of total ammonium in summer and even 90% in winter. The lower conversion rate of NH_3 to NH_4^+ in M9 may be related to the gas phase chemistry used in the model. M9 used the RADM2 mechanism which gives lower reaction rates of oxidation of SO_2 and NO_2 by the OH radical as compiled by Tan et al., 2019, leading to lower productions of acid and thus lower conversion rate of NH_3 to NH_4^+ . In case of M7, the hydrolysis of N_2O_5 was not considered in M7, which leads to a lower tendency in the prediction of NO_3^- (Chen et al., 2019) and partly explains the higher NH_3 predictions in M7. On the contrary, M14 showed a much lower NH_3/NH_x ratio than most models, which would be related to its higher production rates of sulfate than other models as seen in Chen et al., 2019. In terms of monthly variations, most models predicted lower NH_3/NH_x ratio in summer than that in other seasons, suggesting the higher conversion rates of NH_3 from gas phase to aerosol phase in summer. This would be related to the higher yield of ammonium sulfate due to the enhanced photochemical oxidation activity in summer. However, different from the modeling results, the NH_3 and NH_4^+ observations over the NCP region indicated a lower NH_3/NH_x ratio with higher ammonium concentrations in autumn and winter (Shen et al., 2011; Xu et al., 2016). Although observed NH_4^+ was largest in summer at a rural site in Beijing, observed NH_3/NH_x ratio was still highest in summer according to observations from Meng et al., 2011. These results indicate that there would be large uncertainties in the modeling of seasonal variations of the gas-aerosol partitioning of NH_3 over the NCP region. The formation of NH_4^+ mainly depends on the acid gas concentrations, temperature, water availability (Khoder, 2002) and the flux rates of NH_3 (Nemitz et al., 2001). Compared with spring and summer, the lower temperature and higher SO_2 and NO_x emissions should favor the gas-to-particle phase conversion of NH_3 and lead to higher NH_4^+ concentrations. This contrast indicates that some reaction pathways of acid productions (H_2SO_4 or HNO_3) may be missing in current models, such as aqueous-phase and heterogeneous chemistry (Cheng et al., 2016; Wang et al., 2016; Zheng et al., 2015). Such uncertainty may be another important factor contributing to the poor model performances in reproducing the monthly variations of NH_3 concentrations over the NCP region.

3.2 Quantifying the impacts of model uncertainty

In this section, we further investigate the discrepancies among the different models to quantify the impacts of model uncertainty on the simulations of these gases. As we mentioned in Sect. 2, most of these models employed common

366 meteorology fields and emission inventories over China under the same modeling domain and horizontal resolutions, which
367 composed an appropriate set for the investigations of model uncertainties.

368 Figures 6–8 present the simulated annual mean concentrations of NO₂, CO and NH₃ from different models. The spatial
369 distributions of the simulated NO₂, CO and NH₃ concentrations from different models agreed well with each other, similar to
370 the spatial distributions of their emissions (Fig. 1). High NO₂ concentrations were mainly located in the north and central-east
371 China, and several hot-spots of NO₂ were also detected in the northeast China and the PRD region. M5, M8, M9, and M11
372 predicted higher NO₂ concentrations than other models especially for M8 which also predicted very high NO₂ levels over
373 southeast China. Similar to NO₂, high CO concentrations were generally located over the north and central-east China as well
374 as the east of Sichuan basin. M8, M9 and M11 predicted higher CO concentrations than other models as well. In terms of NH₃,
375 although most models shared similar spatial patterns of NH₃ simulations, the simulated NH₃ concentrations varied largely from
376 different models. High NH₃ concentrations were mainly located over the north China and India peninsula, which was in
377 accordance with the distribution of agricultural activity intensity over East Asia. Among these models, M9 and M10 produced
378 much higher NH₃ concentrations over East Asia while M4, M5, M6, M13 and M14 produced much lower concentrations.

379 The impacts of model uncertainty on the simulations of NH₃ (9a), CO (9b) and NO₂ (9c) were then quantified in Fig.9,
380 denoted by the spatial distributions of the standard deviation (ensemble spread) and the corresponding distributions of CV on
381 the annual and seasonal basis. Note that M13 and M14 are excluded in the calculation of ensemble spread and CV to reduce
382 the influences of the meteorological input data and horizontal resolutions. It seems that the impacts of model uncertainty
383 increase with the reactivity of gases. NH₃ simulations were affected most by the model uncertainty, while CO suffered least
384 from the uncertainty in models.

385 The ensemble spread of NH₃ simulations exhibited a strong spatial variability with higher values mainly located in the
386 NCP region. Standard deviation of the annual mean NH₃ concentrations can be over 20 ppbv in Henan province and 15 ppbv
387 in the south of Hebei province, which is about 60–80% and 40–60% of the ensemble mean respectively according to the CV
388 distribution. As we mentioned in Sect. 3.1.3, these large modeling differences can be partly explained by the differences in the
389 bi-directional exchange and gas-aerosol partitioning of NH₃ in different models. A strong seasonal pattern was also found in
390 the differences of NH₃ simulations over the NCP region. The ensemble spread was smallest in spring while largest in autumn,
391 up to 25 ppbv in most areas of the NCP region. However, in the relative sense, the modeling differences were larger in summer
392 and winter while less in spring and autumn. The southeast China shared a similar magnitude of the ensemble spread (2–5 ppbv)
393 and showed weaker seasonal variability. However, the modeling differences in the relative sense were larger than that in the
394 NCP region with CV over 1.0 in all seasons except that in Summer. This can be due to that the simulated concentrations may
395 be more influenced by the model processes over the areas with low emissions, while more constrained by the emissions over
396 high emission rate areas.

397 CO was least affected by the model uncertainty among the three gases which is consistent with its weaker chemical
398 activity and longer lifetime in the atmosphere. The ensemble spread of annual mean CO concentration was about 0.05–0.2
399 ppmv in the east China, only about 20%–30% of the ensemble mean. Meanwhile, CO modeling differences was more

uniformly distributed in east China with CV less than 0.3 over most areas of east China. However, large modeling differences were visible over Myanmar during spring when there were high CO emissions from biomass burning. Model differences turned to be larger during winter in the NCP region with ensemble spread and CV about 0.3–0.5 ppmv and 0.3–0.4, respectively.

NO₂ was mediumly affected by the model uncertainty among the three gases. Ensemble spread of annual mean NO₂ concentration was 5–7.5 ppbv in the NCP region and 2.5–5 ppbv in the southeast China, which accounted for about 20%–30% of the ensemble mean in the former but more than 70% in the latter. The ensemble spread was largest in winter which was over 10 ppbv in the NCP region (30%–40%) and 5–7.5 ppbv in southeast China (over 70%). Similar to NH₃, southeast China exhibited more modeling differences than the NCP region in relative sense with CV higher than 0.7 in most areas of southeast China.

4 Summary

In this study, thirteen modeling results of surface NO₂, CO and NH₃ concentrations from MICS-Asia III were compared with each other and evaluated against the observations over the NCP and PRD regions. Three questions are trying to be addressed which are related to the performance of current CTMs in simulating the NO₂, CO and NH₃ concentrations over the highly industrialized regions of China, potential factors responsible for the model deviations from observations and differences among models, and the impacts of model uncertainty on the simulations of these gases.

Most models showed underestimations of NO₂ concentrations in the NCP and PRD regions, which could be an important potential factor contributing to the overpredicted O₃ concentrations in these regions. According to Xu et al., 2013, such underestimations would also be related to the positive biases in the NO₂ observations. The models showed better NO₂ model performance in the NCP region than that in the PRD region with smaller biases and RMSE. Most models well reproduced the observed temporal and spatial patterns of NO₂ concentrations in the NCP region, while relatively poor model performance was found in the PRD region in terms of the spatial variations of NO₂ concentrations. A sensitivity test with finer horizontal resolutions has been conducted to investigate the potential reasons for the poor model performance in the PRD region. The results shows that only increasing the model resolution cannot improve the model performance in the PRD region, which suggest that the poor model performance in the PRD region would be more related to the coarse resolution and/or inappropriate spatial allocations of the emission inventories in the PRD regions. All models significantly underestimated the CO concentrations in the NCP and PRD regions throughout the year. Such large underestimations of all models are not likely to be fully explained by the model uncertainty, which suggests that CO emissions may be underestimated in current emission inventories. More accurate estimate of CO emissions is thus needed for year 2010. Underestimations of CO emissions may be alleviated in recent years due to the decreasing trends of the Chinese CO emissions in recent years(Jiang et al., 2017;Zhong et al., 2017;Sun et al., 2018;Muller et al., 2018;Zheng et al., 2018;Zheng et al., 2019). The inversion results of Zheng et al., 2018 also agree well with the MEIC inventory for CO emissions in China from 2013 to 2015. However uncertainties still exist in the CO emissions for recent years, according to previous studies, the estimated CO emissions in China ranges from 134–202

432 Tg/yr in year 2013 (Jiang et al., 2017;Zhong et al., 2017;Sun et al., 2018;Muller et al., 2018;Zheng et al., 2018;Zheng et al.,
433 2019). Zhao et al., 2017 also suggested a -29%–40% uncertainty of CO emissions from the industrial sector in year 2012. For
434 NH₃ simulations, in contrast to the good skills in the monthly variations of NO₂ and CO concentrations, all models failed to
435 reproduce the observed monthly variations of NH₃ concentrations in the NCP region, as shown by both the surface and satellite
436 measurements. Most models mismatched the observed peak and showed negative correlation coefficient with observations,
437 which may be closely related to the uncertainty in the monthly variations of NH₃ emissions and also the uncertainty in the gas-
438 aerosol partitioning of NH₃.

439 Several potential factors were found to be responsible for the model deviation and differences, including the emission
440 inventories, chemistry-and-meteorology coupling effects, bi-directional exchange of NH₃ and the NH₃ gas-aerosol partitioning,
441 which would be important aspects with respect to the model improvements in future. Previous studies also suggest that the
442 nitrous acid (HONO) chemistry plays an important role in the atmospheric nitrogen chemistry, which influences the
443 simulations of NO₂ and NH₃ (Fu et al., 2019;Zhang et al., 2017;Zhang et al., 2016). Heterogeneous conversion from NO₂ to
444 HONO ($2\text{NO}_{2(g)} + \text{H}_2\text{O}_{(l)} \rightarrow \text{HONO}_{(l)} + \text{HNO}_{3(l)}$) is one of the dominant sources of HONO in the atmosphere, which has been
445 considered in most models of MICS-Asia III, including CMAQ since version 4.7, NAQPMS, NHM-Chem and GEOS-Chem.
446 However, some other important sources of HONO may still be underestimated by models in MICS-Asia III. For example, Fu
447 et al., 2019 suggested that the high relative humidity and strong light could enhance the heterogeneous reaction of NO₂, and
448 the photolysis of total nitrate were also important sources of HONO. These sources has not been included in the models of
449 MICS-Asia III, which would lead to the deviations from observations. The inter-comparisons of the ensemble models
450 quantified the impacts of model uncertainty on the simulations of these gases, which shows that the impacts of model
451 uncertainty increases with the reactivity of these gases. Models contained more uncertainties in the prediction of NH₃ than the
452 other two gases. Based on these findings, some recommendations are made for future studies:

453 1) More accurate estimation of CO and NH₃ emissions are needed in future studies. Both bottom-up and top-down
454 method (inversion technique) can help address this problem. The inversion of NH₃ emissions would be more complicated than
455 the inversion of CO emissions due to the larger uncertainties in modeling the atmospheric processes of NH₃. Nevertheless, it
456 could still provide valuable clues for verifying the bottom-up emission inventories (Zhang et al., 2009) if the models were well
457 validated. In addition, by using the ground or satellite measurements, the top-down methods could also give valuable
458 information on the spatial and temporal patterns of NH₃ emissions, for example the inversions studies by Paulot et al., 2014
459 and Zhang et al., 2018. However, more attention should be paid to the validations of model before the inversion estimation of
460 NH₃ emissions. How to represent the model uncertainties in the current framework of emission inversion is also an important
461 aspect in future studies. Things could be better for CO considering its small and weakly spatial-dependent model uncertainties.

462 2) For some highly active and/or short-lived primary pollutants, like NH₃, model uncertainty can also take a great part in
463 the forecast uncertainty. Emission uncertainty alone may not be sufficient to explain the forecast uncertainty and may cause
464 underdispersive, and overconfident forecasts. Future studies are needed in how to better represent the model uncertainties in

465 the model predictions to obtain a better forecast skill. Such model uncertainties also emphasize the need to validate the
466 individual model before using its results to make important policy recommendation.

467 3) Gas-aerosol partition of NH_3 is shown to be an important source of uncertainties in NH_3 simulation. The formation of
468 NH_4^+ particles is mainly limited by the availability of H_2SO_4 and HNO_3 under ammonia-rich conditions, which involves
469 complex chemical reactions, including gas-phase, aqueous-phase and heterogeneous chemistry (Cheng et al., 2016; Wang et
470 al., 2016; Zheng et al., 2015). These processes are needed to be verified and incorporated into models to better represent the
471 chemistry in the atmosphere.

472 4) The gas chemistry mechanisms used in this study are SAPRC 99, CB05, CBMZ, RACM and RADM2, and some of
473 them have an updated version such as CB06 and SPARC 07. Our conclusions may not be applicable to these newer versions
474 of mechanisms and thus more comparisons studies can be performed to understand the differences in these new mechanisms.

475 **Competing interests**

476 The authors declare that they have no conflict of interest.

477 **Author contribution**

478 X.T., J.Z., Z.F.W and G.C. conducted the design of this study. J.F., X.W., S.I., K.Y., T.N., H.L., C.K., C.L., L.C., M.Z., Z.T.,
479 J.L., M.K., H.L., B.G. contributed to the modelling data. Z.W. performed the simulations of standard meteorological field.
480 M.L. and Q.W. provided the emission data. K.S. provided the CHASER output for boundary conditions. Y.W., Y.P., G.T.
481 provided the observation data. L.K. and X.T. performed the analysis and prepared the manuscript with contributions from all-
482 authors.

483 **Acknowledgements**

484 This study was supported by the National Natural Science Foundation (Grant Nos. 91644216 & 41620104008), the National
485 Key R&D Program (Grant Nos. 2018YFC0213503) and Guangdong Provincial Science and Technology Development Special
486 Fund (No.2017B020216007). Yuepeng Pan acknowledges the National Key Research and Development Program of China
487 (Grants 2017YFC0210100, 2016YFC0201802) and the National Natural Science Foundation of China (Grant 41405144) for
488 financial support. We are indebted to the staff who collected the samples at the AMoN-China sites during the study period.

489 References

- 490 Anenberg, S. C., Horowitz, L. W., Tong, D. Q., and West, J. J.: An Estimate of the Global Burden of Anthropogenic Ozone
491 and Fine Particulate Matter on Premature Human Mortality Using Atmospheric Modeling, *Environ. Health Perspect.*,
492 118, 1189-1195, 10.1289/ehp.0901220, 2010.
- 493 Bergamaschi, P., Hein, R., Heimann, M., and Crutzen, P. J.: Inverse modeling of the global CO cycle 1. Inversion of CO
494 mixing ratios, *J. Geophys. Res.-Atmos.*, 105, 1909-1927, 10.1029/1999jd900818, 2000.
- 495 Byun, D., and Schere, K. L.: Review of the governing equations, computational algorithms, and other components of the
496 models-3 Community Multiscale Air Quality (CMAQ) modeling system, *Appl. Mech. Rev.*, 59, 51-77,
497 10.1115/1.2128636, 2006.
- 498 Carmichael, G., Sakurai, T., Streets, D., Hozumi, Y., Ueda, H., Park, S., Fung, C., Han, Z., Kajino, M., and Engardt, M.:
499 MICS-Asia II: The model intercomparison study for Asia Phase II methodology and overview of findings, *Atmos.*
500 *Environ.*, 42, 3468-3490, 10.1016/j.atmosenv.2007.04.007, 2008.
- 501 Carmichael, G. R., Calori, G., Hayami, H., Uno, I., Cho, S. Y., Engardt, M., Kim, S. B., Ichikawa, Y., Ikeda, Y., Woo, J. H.,
502 Ueda, H., and Amann, M.: The MICS-Asia study: model intercomparison of long-range transport and sulfur deposition
503 in East Asia, *Atmos. Environ.*, 36, 175-199, 10.1016/s1352-2310(01)00448-4, 2002.
- 504 Chen, L., Gao, Y., Zhang, M., Fu, J. S., Zhu, J., Liao, H., Li, J., Huang, K., Ge, B., Wang, X., Lam, Y. F., Lin, C. Y., Itahashi,
505 S., Nagashima, T., Kajino, M., Yamaji, K., Wang, Z., and Kurokawa, J. I.: MICS-Asia III: Multi-model comparison and
506 evaluation of aerosol over East Asia, *Atmos. Chem. Phys. Discuss.*, 2019, 1-54, 10.5194/acp-2018-1346, 2019.
- 507 Cheng, Y. F., Zheng, G. J., Wei, C., Mu, Q., Zheng, B., Wang, Z. B., Gao, M., Zhang, Q., He, K. B., Carmichael, G., Poschl,
508 U., and Su, H.: Reactive nitrogen chemistry in aerosol water as a source of sulfate during haze events in China, *Sci. Adv.*,
509 2, 11, 10.1126/sciadv.1601530, 2016.
- 510 Dabberdt, W. F., and Miller, E.: Uncertainty, ensembles and air quality dispersion modeling: applications and challenges,
511 *Atmos. Environ.*, 34, 4667-4673, 10.1016/s1352-2310(00)00141-2, 2000.
- 512 Dentener, F. J., and Crutzen, P. J.: REACTION OF N₂O₅ ON TROPOSPHERIC AEROSOLS - IMPACT ON THE GLOBAL
513 DISTRIBUTIONS OF NO_x, O₃, AND OH, *J. Geophys. Res.-Atmos.*, 98, 7149-7163, 10.1029/92jd02979, 1993.
- 514 Evans, M. J., and Jacob, D. J.: Impact of new laboratory studies of N₂O₅ hydrolysis on global model budgets of tropospheric
515 nitrogen oxides, ozone, and OH, *Geophys. Res. Lett.*, 32, 4, 10.1029/2005gl022469, 2005.
- 516 Fine, J., Vuilleumier, L., Reynolds, S., Roth, P., and Brown, N.: Evaluating uncertainties in regional photochemicalair quality
517 modeling, *Annu. Rev. Environ. Resour.*, 28, 59-106, 10.1146/annurev.energy.28.011503.163508, 2003.
- 518 Fu, X., Wang, T., Zhang, L., Li, Q. Y., Wang, Z., Xia, M., Yun, H., Wang, W. H., Yu, C., Yue, D. L., Zhou, Y., Zheng, J. Y.,
519 and Han, R.: The significant contribution of HONO to secondary pollutants during a severe winter pollution event in
520 southern China, *Atmos. Chem. Phys.*, 19, 1-14, 10.5194/acp-19-1-2019, 2019.

Galmarini, S., Bianconi, R., Klug, W., Mikkelsen, T., Addis, R., Andronopoulos, S., Astrup, P., Baklanov, A., Bartniki, J.,
 Bartzis, J. C., Bellasio, R., Bompay, F., Buckley, R., Bouzom, M., Champion, H., D'Amours, R., Davakis, E., Eleveld,
 H., Geertsema, G. T., Glaab, H., Kollax, M., Ilvonen, M., Manning, A., Pechinger, U., Persson, C., Polreich, E., Potemski,
 S., Prodanova, M., Saltbones, J., Slaper, H., Sofiev, M. A., Syrakov, D., Sørensen, J. H., Auwera, L. V. d., Valkama, I.,
 and Zelazny, R.: Ensemble dispersion forecasting—Part I: concept, approach and indicators, *Atmos. Environ.*, 38, 4607-
 4617, <https://doi.org/10.1016/j.atmosenv.2004.05.030>, 2004.

Gao, D. F., Stockwell, W. R., and Milford, J. B.: Global uncertainty analysis of a regional-scale gas-phase chemical mechanism,
J. Geophys. Res.-Atmos., 101, 9107-9119, 10.1029/96jd00060, 1996.

Gao, M., Han, Z. W., Liu, Z. R., Li, M., Xin, J. Y., Tao, Z. N., Li, J. W., Kang, J. E., Huang, K., Dong, X. Y., Zhuang, B. L.,
 Li, S., Ge, B. Z., Wu, Q. Z., Cheng, Y. F., Wang, Y. S., Lee, H. J., Kim, C. H., Fu, J. S. S., Wang, T. J., Chin, M. A.,
 Woo, J. H., Zhang, Q., Wang, Z. F., and Carmichael, G. R.: Air quality and climate change, Topic 3 of the Model Inter-
 Comparison Study for Asia Phase III (MICS-Asia III) - Part 1: Overview and model evaluation, *Atmos. Chem. Phys.*, 18,
 4859-4884, 10.5194/acp-18-4859-2018, 2018.

Gillenwater, M.: Forgotten carbon: indirect CO₂ in greenhouse gas emission inventories, *Environ. Sci. Policy*, 11, 195-203,
 10.1016/j.envsci.2007.09.001, 2008.

Grell, G. A., Peckham, S. E., Schmitz, R., McKeen, S. A., Frost, G., Skamarock, W. C., and Eder, B.: Fully coupled "online"
 chemistry within the WRF model, *Atmos. Environ.*, 39, 6957-6975, 10.1016/j.atmosenv.2005.04.027, 2005.

Guenther, A., Karl, T., Harley, P., Wiedinmyer, C., Palmer, P. I., and Geron, C.: Estimates of global terrestrial isoprene
 emissions using MEGAN (Model of Emissions of Gases and Aerosols from Nature), *Atmos. Chem. Phys.*, 6, 3181-3210,
 2006.

Han, K. M., Song, C. H., Ahn, H. J., Park, R. S., Woo, J. H., Lee, C. K., Richter, A., Burrows, J. P., Kim, J. Y., and Hong, J.
 H.: Investigation of NO_x emissions and NO_x-related chemistry in East Asia using CMAQ-predicted and GOME-derived
 NO₂ columns, *Atmos. Chem. Phys.*, 9, 17297-17341, 2008a.

Han, Z., Sakurai, T., Ueda, H., Carmichael, G., Streets, D., Hayami, H., Wang, Z., Holloway, T., Engardt, M., and Hozumi,
 Y.: MICS-Asia II: Model intercomparison and evaluation of ozone and relevant species, *Atmos. Environ.*, 42, 3491-3509,
 10.1016/j.atmosenv.2007.07.031, 2008b.

Janssens-Maenhout, G., Crippa, M., Guizzardi, D., Dentener, F., Muntean, M., Pouliot, G., Keating, T., Zhang, Q., Kurokawa,
 J., Wankmuller, R., van der Gon, H. D., Kuenen, J. J. P., Klimont, Z., Frost, G., Darras, S., Koffi, B., and Li, M.:
 HTAP_v2.2: a mosaic of regional and global emission grid maps for 2008 and 2010 to study hemispheric transport of air
 pollution, *Atmos. Chem. Phys.*, 15, 11411-11432, 10.5194/acp-15-11411-2015, 2015.

Ji, D. S., Wang, Y. S., Wang, L. L., Chen, L. F., Hu, B., Tang, G. Q., Xin, J. Y., Song, T., Wen, T. X., Sun, Y., Pan, Y. P., and
 Liu, Z. R.: Analysis of heavy pollution episodes in selected cities of northern China, *Atmos. Environ.*, 50, 338-348,
 10.1016/j.atmosenv.2011.11.053, 2012.

554 Jiang, Z., Worden, J. R., Worden, H., Deeter, M., Jones, D. B. A., Arellano, A. F., and Henze, D. K.: A 15-year record of CO
555 emissions constrained by MOPITT CO observations, *Atmos. Chem. Phys.*, 17, 4565-4583, 10.5194/acp-17-4565-2017,
556 2017.

557 Jin, X. M., and Holloway, T.: Spatial and temporal variability of ozone sensitivity over China observed from the Ozone
558 Monitoring Instrument, *J. Geophys. Res.-Atmos.*, 120, 7229-7246, 10.1002/2015jd023250, 2015.

559 Kajino, M., Inomata, Y., Sato, K., Ueda, H., Han, Z., An, J., Katata, G., Deushi, M., Maki, T., Oshima, N., Kurokawa, J.,
560 Ohara, T., Takami, A., and Hatakeyama, S.: Development of the RAQM2 aerosol chemical transport model and
561 predictions of the Northeast Asian aerosol mass, size, chemistry, and mixing type, *Atmos. Chem. Phys.*, 12, 11833-11856,
562 10.5194/acp-12-11833-2012, 2012.

563 Kajino, M., Deushi, M., Sekiyama, T. T., Oshima, N., Yumimoto, K., Tanaka, T. Y., Ching, J., Hashimoto, A., Yamamoto, T.,
564 Ikegami, M., Kamada, A., Miyashita, M., Inomata, Y., Shima, S. I., Adachi, K., Zaizen, Y., Igarashi, Y., Ueda, H., Maki,
565 T., and Mikami, M.: NHM-Chem, the Japan Meteorological Agency's regional meteorology – chemistry model (v1.0):
566 model description and aerosol representations, *Geosci. Model Dev. Discuss.*, 2018, 1-45, 10.5194/gmd-2018-128, 2018.

567 Khoder, M. I.: Atmospheric conversion of sulfur dioxide to particulate sulfate and nitrogen dioxide to particulate nitrate and
568 gaseous nitric acid in an urban area, *Chemosphere*, 49, 675-684, 10.1016/s0045-6535(02)00391-0, 2002.

569 Kurokawa, J., Ohara, T., Morikawa, T., Hanayama, S., Janssens-Maenhout, G., Fukui, T., Kawashima, K., and Akimoto, H.:
570 Emissions of air pollutants and greenhouse gases over Asian regions during 2000-2008: Regional Emission inventory in
571 ASia (REAS) version 2, *Atmos. Chem. Phys.*, 13, 11019-11058, 10.5194/acp-13-11019-2013, 2013.

572 Lelieveld, J., Evans, J. S., Fnais, M., Giannadaki, D., and Pozzer, A.: The contribution of outdoor air pollution sources to
573 premature mortality on a global scale, *Nature*, 525, 367-+, 10.1038/nature15371, 2015.

574 Levy, H.: NORMAL ATMOSPHERE - LARGE RADICAL AND FORMALDEHYDE CONCENTRATIONS PREDICTED,
575 *Science*, 173, 141-&, 10.1126/science.173.3992.141, 1971.

576 Li, J., Du, H. Y., Wang, Z. F., Sun, Y. L., Yang, W. Y., Li, J. J., Tang, X., and Fu, P. Q.: Rapid formation of a severe regional
577 winter haze episode over a mega-city cluster on the North China Plain, *Environ. Pollut.*, 223, 605-615,
578 10.1016/j.envpol.2017.01.063, 2017a.

579 Li, J., Nagashima, T., Kong, L., Ge, B., Yamaji, K., Fu, J. S., Wang, X., Fan, Q., Itahashi, S., Lee, H. J., Kim, C. H., Lin, C.
580 Y., Zhang, M., Tao, Z., Kajino, M., Liao, H., Li, M., Woo, J. H., Kurokawa, J. I., Wu, Q., Akimoto, H., Carmichael, G.
581 R., and Wang, Z.: Model evaluation and inter-comparison of surface-level ozone and relevant species in East Asia in the
582 context of MICS-Asia phase III Part I: overview, *Atmos. Chem. Phys. Discuss.*, 2019, 1-56, 10.5194/acp-2018-1283,
583 2019.

584 Li, M., Zhang, Q., Kurokawa, J. I., Woo, J. H., He, K., Lu, Z., Ohara, T., Song, Y., Streets, D. G., Carmichael, G. R., Cheng,
585 Y., Hong, C., Huo, H., Jiang, X., Kang, S., Liu, F., Su, H., and Zheng, B.: MIX: a mosaic Asian anthropogenic emission
586 inventory under the international collaboration framework of the MICS-Asia and HTAP, *Atmos. Chem. Phys.*, 17, 935-
587 963, 10.5194/acp-17-935-2017, 2017b.

588 Lu, M. M., Tang, X., Wang, Z. F., Gbaguidi, A., Liang, S. W., Hu, K., Wu, L., Wu, H. J., Huang, Z., and Shen, L. J.: Source
 589 tagging modeling study of heavy haze episodes under complex regional transport processes over Wuhan megacity,
 590 Central China, *Environ. Pollut.*, 231, 612-621, 10.1016/j.envpol.2017.08.046, 2017.

591 Ma, C. Q., Wang, T. J., Mizzi, A. P., Anderson, J. L., Zhuang, B. L., Xie, M., and Wu, R. S.: Multiconstituent Data Assimilation
 592 With WRF-Chem/DART: Potential for Adjusting Anthropogenic Emissions and Improving Air Quality Forecasts Over
 593 Eastern China, *J. Geophys. Res.-Atmos.*, 124, 7393-7412, 10.1029/2019jd030421, 2019.

594 Mallet, V., and Sportisse, B.: Uncertainty in a chemistry-transport model due to physical parameterizations and numerical
 595 approximations: An ensemble approach applied to ozone modeling, *J. Geophys. Res.-Atmos.*, 111, 15,
 596 10.1029/2005jd006149, 2006.

597 Meng, Z. Y., Lin, W. L., Jiang, X. M., Yan, P., Wang, Y., Zhang, Y. M., Jia, X. F., and Yu, X. L.: Characteristics of atmospheric
 598 ammonia over Beijing, China, *Atmos. Chem. Phys.*, 11, 6139-6151, 10.5194/acp-11-6139-2011, 2011.

599 Miyazaki, K., Eskes, H. J., Sudo, K., Takigawa, M., Weele, M. V., and Boersma, K. F.: Simultaneous assimilation of satellite
 600 NO₂, O₃, CO, and HNO₃ data for the analysis of tropospheric chemical composition and emissions, *Atmos. Chem. Phys.*
 601 & Discussions, 264, 1017-1023, 2012.

602 Muller, J. F., Stavrakou, T., Bauwens, M., George, M., Hurtmans, D., Coheur, P. F., Clerbaux, C., and Sweeney, C.: Top-
 603 Down CO Emissions Based On IASI Observations and Hemispheric Constraints on OH Levels, *Geophys. Res. Lett.*, 45,
 604 1621-1629, 10.1002/2017gl076697, 2018.

605 Naik, V., Voulgarakis, A., Fiore, A. M., Horowitz, L. W., Lamarque, J. F., Lin, M., Prather, M. J., Young, P. J., Bergmann,
 606 D., Cameron-Smith, P. J., Cionni, I., Collins, W. J., Dalsoren, S. B., Doherty, R., Eyring, V., Faluvegi, G., Folberth, G.
 607 A., Josse, B., Lee, Y. H., MacKenzie, I. A., Nagashima, T., van Noije, T. P. C., Plummer, D. A., Righi, M., Rumbold, S.
 608 T., Skeie, R., Shindell, D. T., Stevenson, D. S., Strode, S., Sudo, K., Szopa, S., and Zeng, G.: Preindustrial to present-
 609 day changes in tropospheric hydroxyl radical and methane lifetime from the Atmospheric Chemistry and Climate Model
 610 Intercomparison Project (ACCMIP), *Atmos. Chem. Phys.*, 13, 5277-5298, 10.5194/acp-13-5277-2013, 2013.

611 Nemitz, E., Milford, C., and Sutton, M. A.: A two-layer canopy compensation point model for describing bi-directional
 612 biosphere-atmosphere exchange of ammonia, *Q. J. R. Meteorol. Soc.*, 127, 815-833, 10.1256/smsqj.57305, 2001.

613 Noije, T. P. C. V., Eskes, H. J., Dentener, F. J., Stevenson, D. S., Ellingsen, K., Schultz, M. G., Wild, O., Amann, M., Atherton,
 614 C. S., and Bergmann, D. J.: Multi-model ensemble simulations of tropospheric NO₂ compared with GOME retrievals for
 615 the year 2000, *Atmos. Chem. Phys.*, 6, 2943-2979, 2006.

616 Novelli, P. C., Masarie, K. A., and Lang, P. M.: Distributions and recent changes of carbon monoxide in the lower troposphere,
 617 *J. Geophys. Res.-Atmos.*, 103, 19015-19033, 10.1029/98jd01366, 1998.

618 Pan, Y., Tian, S., Zhao, Y., Zhang, L., Zhu, X., Gao, J., Huang, W., Zhou, Y., Song, Y., Zhang, Q., and Wang, Y.: Identifying
 619 ammonia hotspots in China using a national observation network, *Environ. Sci. Technol.*, 52, 3926-3934,
 620 10.1021/acs.est.7b05235, 2018.

621 Pan, Y. P., Wang, Y. S., Tang, G. Q., and Wu, D.: Wet and dry deposition of atmospheric nitrogen at ten sites in Northern
 622 China, *Atmos. Chem. Phys.*, 12, 6515-6535, 10.5194/acp-12-6515-2012, 2012.

623 Paulot, F., Jacob, D. J., Pinder, R. W., Bash, J. O., Travis, K., and Henze, D. K.: Ammonia emissions in the United States,
 624 European Union, and China derived by high-resolution inversion of ammonium wet deposition data: Interpretation with
 625 a new agricultural emissions inventory (MASAGE_NH3), *J. Geophys. Res.-Atmos.*, 119, 4343-4364,
 626 10.1002/2013jd021130, 2014.

627 Peters-Lidard, C. D., Kemp, E. M., Matsui, T., Santanello, J. A., Kumar, S. V., Jacob, J. P., Clune, T., Tao, W. K., Chin, M.,
 628 Hou, A., Case, J. L., Kim, D., Kim, K. M., Lau, W., Liu, Y. Q., Shi, J., Starr, D., Tan, Q., Tao, Z. N., Zaitchik, B. F.,
 629 Zavodsky, B., Zhang, S. Q., and Zupanski, M.: Integrated modeling of aerosol, cloud, precipitation and land processes at
 630 satellite-resolved scales, *Environ. Modell. Softw.*, 67, 149-159, 10.1016/j.envsoft.2015.01.007, 2015.

631 Petron, G., Granier, C., Khattatov, B., Lamarque, J. F., Yudin, V., Muller, J. F., and Gille, J.: Inverse modeling of carbon
 632 monoxide surface emissions using Climate Monitoring and Diagnostics Laboratory network observations, *J. Geophys.*
 633 *Res.-Atmos.*, 107, 23, 10.1029/2001jd001305, 2002.

634 Petron, G., Granier, C., Khattatov, B., Yudin, V., Lamarque, J. F., Emmons, L., Gille, J., and Edwards, D. P.: Monthly CO
 635 surface sources inventory based on the 2000-2001 MOPITT satellite data, *Geophys. Res. Lett.*, 31, 5,
 636 10.1029/2004gl020560, 2004.

637 Pielke, R. A., Cotton, W. R., Walko, R. L., Tremback, C. J., Lyons, W. A., Grasso, L. D., Nicholls, M. E., Moran, M. D.,
 638 Wesley, D. A., Lee, T. J., and Copeland, J. H.: A COMPREHENSIVE METEOROLOGICAL MODELING SYSTEM -
 639 RAMS, *Meteorol. Atmos. Phys.*, 49, 69-91, 10.1007/bf01025401, 1992.

640 Pinder, R. W., Adams, P. J., Pandis, S. N., and Gilliland, A. B.: Temporally resolved ammonia emission inventories: Current
 641 estimates, evaluation tools, and measurement needs, *J. Geophys. Res.-Atmos.*, 111, 14, 10.1029/2005jd006603, 2006.

642 Randerson, J. T., Werf, G. R. v. d., Giglio, L., Collatz, G. J., and Kasibhatla, P. S.: Global Fire Emissions Database, Version
 643 3 (GFEDv3.1). Data set. Available on-line [<http://daac.ornl.gov/>] from Oak Ridge National Laboratory Distributed Active
 644 Archive Center, Oak Ridge, Tennessee, USA. doi:10.3334/ORNLDAAAC/1191, 2013.

645 Rao, S. T., Galmarini, S., and Puckett, K.: Air Quality Model Evaluation International Initiative (AQMEII) Advancing the
 646 State of the Science in Regional Photochemical Modeling and Its Applications, *Bull. Amer. Meteorol. Soc.*, 92, 23-30,
 647 10.1175/2010bams3069.1, 2011.

648 Saito, K., Fujita, T., Yamada, Y., Ishida, J. I., Kumagai, Y., Aranami, K., Ohmori, S., Nagasawa, R., Kumagai, S., Muroi, C.,
 649 Kato, T., Eito, H., and Yamazaki, Y.: The operational JMA nonhydrostatic mesoscale model, *Mon. Weather Rev.*, 134,
 650 1266-1298, 10.1175/mwr3120.1, 2006.

651 Shao, M., Zhang, Y. H., Zeng, L. M., Tang, X. Y., Zhang, J., Zhong, L. J., and Wang, B. G.: Ground-level ozone in the Pearl
 652 River Delta and the roles of VOC and NO_x in its production, *J. Environ. Manage.*, 90, 512-518,
 653 10.1016/j.jenvman.2007.12.008, 2009.

654 Shen, J. L., Liu, X. J., Zhang, Y., Fangmeier, A., Goulding, K., and Zhang, F. S.: Atmospheric ammonia and particulate
655 ammonium from agricultural sources in the North China Plain, *Atmos. Environ.*, 45, 5033-5041,
656 10.1016/j.atmosenv.2011.02.031, 2011.

657 Sillman, S.: The relation between ozone, NO_x and hydrocarbons in urban and polluted rural environments, *Atmos. Environ.*,
658 33, 1821-1845, 10.1016/s1352-2310(98)00345-8, 1999.

659 Skamarock, W. C.: A description of the advanced research WRF version 3, *Near Technical*, 113, 7-25, 2008.

660 Stein, O., Schultz, M. G., Bouarar, I., Clark, H., Huijnen, V., Gaudel, A., George, M., and Clerbaux, C.: On the wintertime
661 low bias of Northern Hemisphere carbon monoxide found in global model simulations, *Atmos. Chem. Phys.*, 14, 9295-
662 9316, 10.5194/acp-14-9295-2014, 2014.

663 Steinfeld, J. I.: *Atmos. Chem. Phys.: From Air Pollution to Climate Change*, Wiley, 1595-1595 pp., 1998.

664 Sun, W., Shao, M., Granier, C., Liu, Y., Ye, C. S., and Zheng, J. Y.: Long-Term Trends of Anthropogenic SO₂, NO_x, CO,
665 and NMVOCs Emissions in China, *Earth Future*, 6, 1112-1133, 10.1029/2018ef000822, 2018.

666 Sun, Y. L., Wang, Z. F., Dong, H. B., Yang, T., Li, J., Pan, X. L., Chen, P., and Jayne, J. T.: Characterization of summer
667 organic and inorganic aerosols in Beijing, China with an Aerosol Chemical Speciation Monitor, *Atmos. Environ.*, 51,
668 250-259, 10.1016/j.atmosenv.2012.01.013, 2012.

669 Sun, Y. L., Wang, Z. F., Fu, P. Q., Yang, T., Jiang, Q., Dong, H. B., Li, J., and Jia, J. J.: Aerosol composition, sources and
670 processes during wintertime in Beijing, China, *Atmos. Chem. Phys.*, 13, 4577-4592, 10.5194/acp-13-4577-2013, 2013.

671 Tan, J., Fu, J. S., Carmichael, G. R., Itahashi, S., Tao, Z., Huang, K., Dong, X., Yamaji, K., Nagashima, T., Wang, X., Liu, Y.,
672 Lee, H. J., Lin, C. Y., Ge, B., Kajino, M., Zhu, J., Zhang, M., Hong, L., and Wang, Z.: Why models perform differently
673 on particulate matter over East Asia? – A multi-model intercomparison study for MICS-Asia III, *Atmos. Chem. Phys.*
674 *Discuss.*, 2019, 1-36, 10.5194/acp-2019-392, 2019.

675 Tang, G., Wang, Y., Li, X., Ji, D., Hsu, S., and Gao, X.: Spatial-temporal variations in surface ozone in Northern China as
676 observed during 2009-2010 and possible implications for future air quality control strategies, *Atmos. Chem. Phys.*, 12,
677 2757-2776, 10.5194/acp-12-2757-2012, 2012.

678 Tang, X., Zhu, J., Wang, Z. F., and Gbaguidi, A.: Improvement of ozone forecast over Beijing based on ensemble Kalman
679 filter with simultaneous adjustment of initial conditions and emissions, *Atmos. Chem. Phys.*, 11, 12901-12916,
680 10.5194/acp-11-12901-2011, 2011.

681 Tang, X., Zhu, J., Wang, Z. F., Wang, M., Gbaguidi, A., Li, J., Shao, M., Tang, G. Q., and Ji, D. S.: Inversion of CO emissions
682 over Beijing and its surrounding areas with ensemble Kalman filter, *Atmos. Environ.*, 81, 676-686,
683 10.1016/j.atmosenv.2013.08.051, 2013.

684 Uno, I., He, Y., Ohara, T., Yamaji, K., Kurokawa, J. I., Katayama, M., Wang, Z., Noguchi, K., Hayashida, S., Richter, A., and
685 Burrows, J. P.: Systematic analysis of interannual and seasonal variations of model-simulated tropospheric NO₂ in Asia
686 and comparison with GOME-satellite data, *Atmos. Chem. Phys.*, 7, 1671-1681, 10.5194/acp-7-1671-2007, 2007.

687 US EPA Office of Research and Development: CMAQv5.0, , doi:10.5281/zenodo.1079888, 2012.

688 Van Damme, M., Whitburn, S., Clarisse, L., Clerbaux, C., Hurtmans, D., and Coheur, P. F.: Version 2 of the IASI NH₃ neural
689 network retrieval algorithm: near-real-time and reanalysed datasets, *Atmos. Meas. Tech.*, 10, 4905-4914, 10.5194/amt-
690 10-4905-2017, 2017.

691 Van Damme, M., Clarisse, L., Whitburn, S., Hadji-Lazaro, J., Hurtmans, D., Clerbaux, C., and Coheur, P.-F.: Level 2 dataset
692 and Level 3 oversampled average map of the IASI/Metop-A ammonia (NH₃) morning column measurements (ANNI-
693 NH3-v2.1R-I) from 2008 to 2016. PANGAEA, 2018.

694 von Bobruzki, K., Braban, C. F., Famulari, D., Jones, S. K., Blackall, T., Smith, T. E. L., Blom, M., Coe, H., Gallagher, M.,
695 Ghalaieny, M., McGillen, M. R., Percival, C. J., Whitehead, J. D., Ellis, R., Murphy, J., Mohacsi, A., Pogany, A.,
696 Junninen, H., Rantanen, S., Sutton, M. A., and Nemitz, E.: Field inter-comparison of eleven atmospheric ammonia
697 measurement techniques, *Atmos. Meas. Tech.*, 3, 91-112, 10.5194/amt-3-91-2010, 2010.

698 Wang, G., Zhang, R., Gomez, M. E., Yang, L., Zamora, M. L., Hu, M., Lin, Y., Peng, J., Guo, S., and Meng, J.: Persistent
699 sulfate formation from London Fog to Chinese haze, *Proc. Natl. Acad. Sci. U. S. A. of America*, 113, 13630, 2016.

700 Wang, Z. F., Maeda, T., Hayashi, M., Hsiao, L. F., and Liu, K. Y.: A nested air quality prediction modeling system for urban
701 and regional scales: Application for high-ozone episode in Taiwan, *Water Air Soil Pollut.*, 130, 391-396,
702 10.1023/a:1013833217916, 2001.

703 Warner, J. X., Wei, Z., Strow, L. L., Dickerson, R. R., and Nowak, J. B.: The global tropospheric ammonia distribution as seen
704 in the 13-year AIRS measurement record, *Atmos. Chem. Phys.*, 16, 5467-5479, 10.5194/acp-16-5467-2016, 2016.

705 Warner, J. X., Dickerson, R. R., Wei, Z., Strow, L. L., Wang, Y., and Liang, Q.: Increased atmospheric ammonia over the
706 world's major agricultural areas detected from space, *Geophys. Res. Lett.*, 44, 2875-2884, 10.1002/2016gl072305, 2017.

707 Xu, W., Wu, Q. H., Liu, X. J., Tang, A. H., Dore, A., and Heal, M.: Characteristics of ammonia, acid gases, and PM_{2.5} for
708 three typical land-use types in the North China Plain, *Environ. Sci. Pollut. Res.*, 23, 1158-1172, 10.1007/s11356-015-
709 5648-3, 2016.

710 Xu, Z., Wang, T., Xue, L. K., Louie, P. K. K., Luk, C. W. Y., Gao, J., Wang, S. L., Chai, F. H., and Wang, W. X.: Evaluating
711 the uncertainties of thermal catalytic conversion in measuring atmospheric nitrogen dioxide at four differently polluted
712 sites in China, *Atmos. Environ.*, 76, 221-226, 10.1016/j.atmosenv.2012.09.043, 2013.

713 Xu, Z., Liu, M., Zhang, M., Song, Y., Wang, S., Zhang, L., Xu, T., Wang, T., Yan, C., Zhou, T., Sun, Y., Pan, Y., Hu, M.,
714 Zheng, M., and Zhu, T.: High efficiency of livestock ammonia emission controls in alleviating particulate nitrate during
715 a severe winter haze episode in northern China, *Atmos. Chem. Phys.*, 19, 5605-5613, 10.5194/acp-19-5605-2019, 2019.

716 Zhang, L., Wang, T., Zhang, Q., Zheng, J. Y., Xu, Z., and Lv, M. Y.: Potential sources of nitrous acid (HONO) and their
717 impacts on ozone: A WRF-Chem study in a polluted subtropical region, *J. Geophys. Res.-Atmos.*, 121, 3645-3662,
718 10.1002/2015jd024468, 2016.

719 Zhang, L., Li, Q. Y., Wang, T., Ahmadov, R., Zhang, Q., Li, M., and Lv, M. Y.: Combined impacts of nitrous acid and nitryl
720 chloride on lower-tropospheric ozone: new module development in WRF-Chem and application to China, *Atmos. Chem.*
721 *Phys.*, 17, 9733-9750, 10.5194/acp-17-9733-2017, 2017.

722 Zhang, L., Chen, Y. F., Zhao, Y. H., Henze, D. K., Zhu, L. Y., Song, Y., Paulot, F., Liu, X. J., Pan, Y. P., Lin, Y., and Huang,
 723 B. X.: Agricultural ammonia emissions in China: reconciling bottom-up and top-down estimates, *Atmos. Chem. Phys.*,
 724 18, 339-355, 10.5194/acp-18-339-2018, 2018.

725 Zhang, Q., Streets, D. G., Carmichael, G. R., He, K. B., Huo, H., Kannari, A., Klimont, Z., Park, I. S., Reddy, S., Fu, J. S.,
 726 Chen, D., Duan, L., Lei, Y., Wang, L. T., and Yao, Z. L.: Asian emissions in 2006 for the NASA INTEX-B mission,
 727 *Atmos. Chem. Phys.*, 9, 5131-5153, 10.5194/acp-9-5131-2009, 2009.

728 Zhang, Q., Pan, Y., He, Y., Zhao, Y., Zhu, L., Zhang, X., Xu, X., Ji, D., Gao, J., Tian, S., Gao, W., and Wang, Y.: Bias in
 729 ammonia emission inventory and implications on emission control of nitrogen oxides over North China Plain, *Atmos.*
 730 *Environ.*, 214, 116869, <https://doi.org/10.1016/j.atmosenv.2019.116869>, 2019.

731 Zhao, Y., Zhou, Y. D., Qiu, L. P., and Zhang, J.: Quantifying the uncertainties of China's emission inventory for industrial
 732 sources: From national to provincial and city scales, *Atmos. Environ.*, 165, 207-221, 10.1016/j.atmosenv.2017.06.045,
 733 2017.

734 Zheng, B., Zhang, Q., Zhang, Y., He, K. B., Wang, K., Zheng, G. J., Duan, F. K., Ma, Y. L., and Kimoto, T.: Heterogeneous
 735 chemistry: a mechanism missing in current models to explain secondary inorganic aerosol formation during the January
 736 2013 haze episode in North China, *Atmos. Chem. Phys.*, 15, 2031-2049, 10.5194/acp-15-2031-2015, 2015.

737 Zheng, B., Chevallier, F., Ciais, P., Yin, Y., Deeter, M. N., Worden, H. M., Wang, Y. L., Zhang, Q., and He, K. B.: Rapid
 738 decline in carbon monoxide emissions and export from East Asia between years 2005 and 2016, *Environ. Res. Lett.*, 13,
 739 9, 10.1088/1748-9326/aab2b3, 2018.

740 Zheng, B., Chevallier, F., Yin, Y., Ciais, P., Fortems-Cheiney, A., Deeter, M. N., Parker, R. J., Wang, Y. L., Worden, H. M.,
 741 and Zhao, Y. H.: Global atmospheric carbon monoxide budget 2000-2017 inferred from multi-species atmospheric
 742 inversions, *Earth Syst. Sci. Data*, 11, 1411-1436, 10.5194/essd-11-1411-2019, 2019.

743 Zhong, L. J., Louie, P. K. K., Zheng, J. Y., Wai, K. M., Ho, J. W. K., Yuan, Z. B., Lau, A. K. H., Yue, D. L., and Zhou, Y.:
 744 The Pearl River Delta Regional Air Quality Monitoring Network - Regional Collaborative Efforts on Joint Air Quality
 745 Management, *Aerosol Air Qual. Res.*, 13, 1582-U1232, 10.4209/aaqr.2012.10.0276, 2013.

746 Zhong, Q. R., Huang, Y., Shen, H. Z., Chen, Y. L., Chen, H., Huang, T. B., Zeng, E. Y., and Tao, S.: Global estimates of
 747 carbon monoxide emissions from 1960 to 2013, *Environ. Sci. Pollut. Res.*, 24, 864-873, 10.1007/s11356-016-7896-2,
 748 2017.

749

750 Tables

751 Table 1: Basic configurations of participating models in MICS-Asia III

No	Horizontal resolution	Vertical resolution	First layer height	Horizontal advection	Vertical advection	Horizontal Diffusion	Vertical Diffusion	Gas phase chemistry	Aerosol processes	Dry deposition of gases	Wet deposition of gases	Meteorology	Boundary condition	Online (Yes or No)
M1	45km	$40\sigma_p$ level	57 m	Yamo (Yamartino, 1993)	ppm (Collella and Woodward, 1984)	multiscale	ACM2 (Pleim, 2007)	SAPRC99 (Carter, 2000)	Aero6 (Binkowski and Roselle, 2003)	Wesely (1989)	Henry's law	Standard ^a	GEOS-Chem (Martin et al., 2002)	No
M2	45km	$40\sigma_p$ level	57 m	Yamo	ppm	multiscale	ACM2	SAPRC99	Aero6	Wesely (1989)	Henry's law	Standard ^a	Default	No
M3	45km	$40\sigma_p$ level	57 m	Yamo	Yamo	multiscale	ACM2	CB05 (Yarwood et al., 2005)	Aero5	Wesely (1989)	Henry's law	Standard ^a	GEOS-Chem	No
M4	45km	$40\sigma_p$ level	57 m	ppm	ppm	multiscale	ACM2_ inline	SAPRC99	Aero5	Wesely (1989)	Henry's law	Standard ^a	CHASER (Sudo et al., 2002a)	No
M5	45km	$40\sigma_p$ level	57 m	ppm	ppm	multiscale	ACM2_ inline	SAPRC99	Aero5	M3DRY (Pleim et al., 2001)	Henry's law	Standard ^a	CHASER	No
M6	45km	$40\sigma_p$ level	57 m	Yamo	Yamo	multiscale	ACM2_ inline	SAPRC99	Aero5	M3DRY	ACM	Standard ^a	CHASER	No
M7	45km	$40\sigma_p$ level	29 m	Monotonic	Monotonic	no diffusion	no diffusion	RACM-ESRL with KPP (Goliff et al., 2013)	MADE (Ackerman et al., 1998)	Wesely (1989)	Henry's law	WRF/NCEP ^a	Default	No
M8	45km	$40\sigma_p$ level	57 m	5 th order Monotonic	3 th order Monotonic	MYJ	MYJ	RACM with KPP	MADE	Wesely (1989)	AQCHEM	WRF/NCEP ^a	CHASER	Yes
M9	45km	$40\sigma_p$ level	16 m	5 th order Monotonic	3 th order Monotonic	Smagorinsky first order closure	YSU (Hong et al., 2006)	RADM2 (Stockwell et al., 1990)	MADE	Wesely (1989)	Easter et al., (2004)	WRF/NCEP ^a	GEOS-Chem	Yes
M10	45km	$60\sigma_p$ level	44 m	Monotonic	3 th order Monotonic	2 th order Monotonic	YSU	RADM2	GOCART	Wesely (1989)	Grell	WRF/MERRA2 ^a	MOZART + GOCART ^b	No
M11	45km	$20\sigma_z$ level	50 m	Walcek and Aleksic (1998)	Walcek and Aleksic (1998)	multiscale	K-theory	CBMZ (Zaveri et al., 1999)	ISORROPI A1.7 (Nenes et al., 1998)	Wesely (1989)	Henry's law	Standard ^a	CHASER	No

M12	45km	40 σ_p level	54 m	Walcek and Aleksic (1998)	Walcek and Aleksic (1998)	FTCS	FTCS	SAPRC99	Kajino et al. (2012)	Zhang et al. (2003)	Henry's law	Standard ^a	CHASER	No
M13	0.5°×0.667°	47 σ_p level	60 m	ppm	ppm	Lin and McElroy, 2010	Lin and McElroy, 2010	NO _x -O ₃ -HC	ISORROPI A2.0 (Fountoukis and Nenes, 2007)	Wesely	Henry's law	GEOS-5 ^a	Geos-Chem	No
M14	64km	15 σ_z level	100 m	ppm	ppm	multiscale	ACM2	SAPRC99	ISORROPI A1.7	Wesely (1989)	Henry's law	RAMS/NCEP ^a	Geos-Chem	No

^a Standard represents the reference meteorological field provided by MICS-Asia III project; WRF/NCEP and WRF/MERRA represents the meteorological field of the participating model itself, which was run by WRF driven by the NCEP and Modern Era Retrospective-analysis for Research and Applications (MERRA) reanalysis dataset. RAMS/NCEP is the meteorology field run by RAMS driven by the NCEP reanalysis dataset.

^b Boundary conditions of M10 are from MOZART and GOCART (Chin et al., 2002; Horowitz et al., 2003), which provided results for gaseous pollutants and aerosols, respectively.

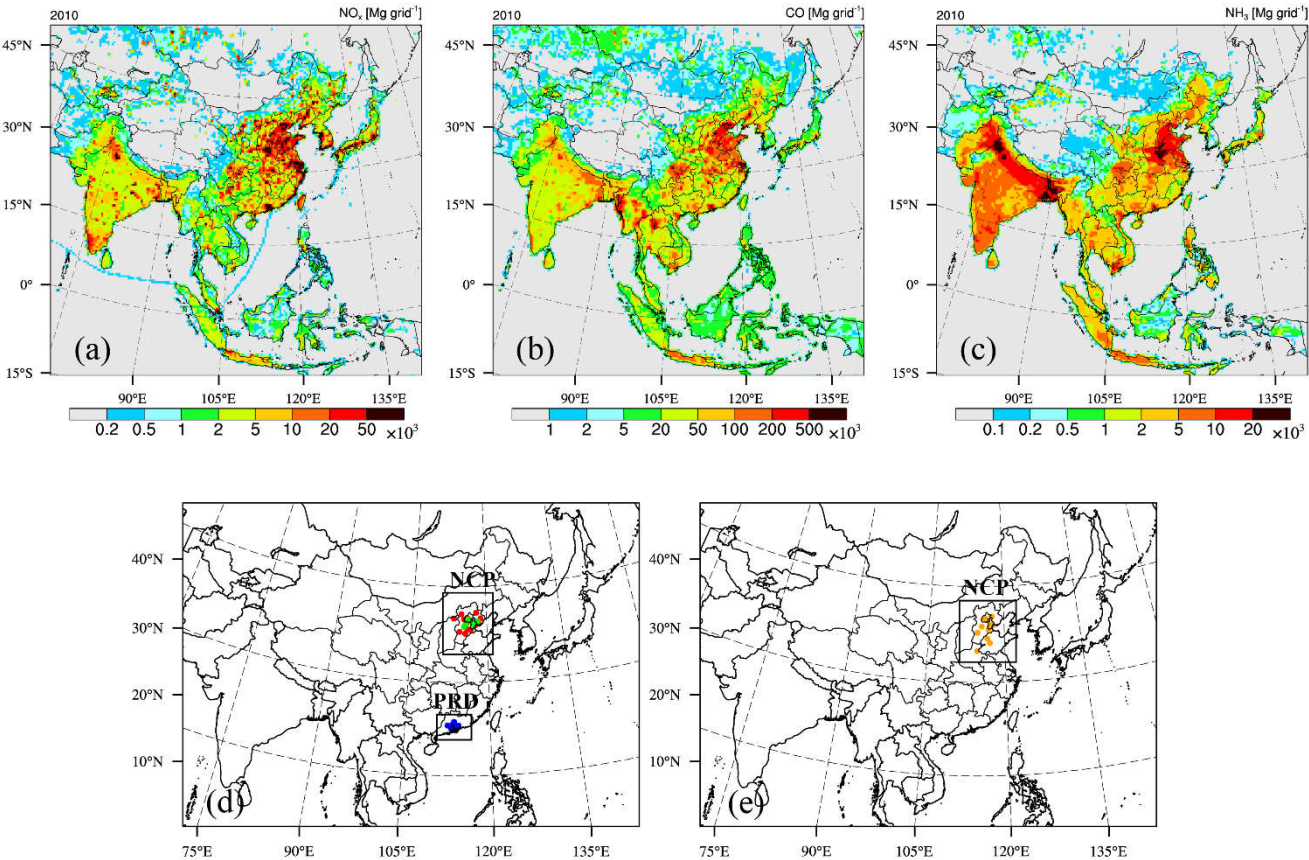
767 **Table 2: Statistics of simulated annual mean concentrations over the NCP and PRD regions.**

Species	Regions	Statistics	Model													
			M1	M2	M4	M5	M6	M7	M8	M9	M10	M11	M12	M13	M14	Ense
NO ₂	NCP	R(spatial) ^a	0.63	0.67	0.67	0.67	0.67	0.70	0.70	0.59	0.57	0.66	0.69	-	0.70	0.67
		R(temporal) ^b	0.82	0.92	0.93	0.86	0.92	0.81	0.28	0.85	0.95	0.75	0.90	-	0.96	0.91
		MBE	-4.11	-5.66	-6.54	1.86	-5.12	-5.04	3.30	8.28	-2.45	0.00	-3.81	-	-2.99	-1.86
		NMB(%)	-17.8	-24.5	-28.4	8.0	-22.2	-21.9	14.2	35.9	-10.6	0.02	-16.5	-	-13.0	-8.0
		RMSE	7.40	8.25	8.79	6.75	8.01	7.55	6.54	12.74	7.72	6.37	7.38	-	6.68	6.36
	PRD	R(spatial) ^a	0.12	0.06	0.07	0.07	0.06	0.12	0.20	0.38	0.00	0.08	0.12	-	0.02	0.10
		R(temporal) ^b	0.93	0.80	0.86	0.88	0.79	0.68	0.83	0.95	0.74	0.74	0.75	-	0.52	0.86
		MBE	-6.73	-9.84	-7.21	1.96	-6.66	-3.99	3.24	-7.61	-1.84	3.02	-5.49	-	-5.03	-3.85
		NMB(%)	-30.1	-44.0	-32.3	8.8	-29.8	-17.9	14.5	-34.0	-8.2	13.5	-24.6	-	-22.5	-17.2
		RMSE	11.31	13.14	12.00	10.80	11.84	10.60	8.73	10.69	10.72	10.51	11.68	-	12.00	10.15
CO	NCP	R(spatial) ^a	0.35	0.48	0.27	0.34	0.36	0.22	0.19	0.48	0.49	0.33	0.35	-0.13	0.29	0.37
		R(temporal) ^b	0.94	0.96	0.92	0.22	0.90	0.77	0.94	0.92	0.82	0.85	0.94	0.85	0.88	0.92
		MBE	-1.53	-1.35	-1.59	-1.69	-1.52	-1.64	-1.29	-1.16	-1.55	-1.37	-1.38	-1.53	-1.51	-1.47
		NMB(%)	-68.9	-60.9	-71.4	-76.2	-68.2	-73.7	-58.2	-52.0	-70.0	-61.6	-62.3	-68.9	-68.0	-66.2
		RMSE	1.71	1.54	1.77	1.86	1.70	1.82	1.51	1.36	1.74	1.57	1.58	1.74	1.70	1.66
	PRD	R(spatial) ^a	0.04	-0.24	-0.25	-0.23	-0.22	-0.05	0.08	0.55	-0.02	-0.01	-0.22	0.09	-0.21	-0.06
		R(temporal) ^b	0.96	0.91	0.93	0.84	0.95	0.90	0.90	0.96	0.83	0.87	0.93	0.76	0.82	0.94
		MBE	-0.66	-0.64	-0.65	-0.64	-0.62	-0.64	-0.51	-0.57	-0.50	-0.51	-0.58	-0.52	-0.67	-0.59
		NMB(%)	-68.4	-67.0	-67.0	-66.7	-64.7	-66.5	-53.3	-59.7	-52.3	-52.7	-60.7	-54.1	-69.6	-61.7
		RMSE	0.70	0.70	0.70	0.69	0.67	0.69	0.57	0.62	0.56	0.57	0.64	0.58	0.72	0.65
NH ₃	NCP	R(spatial) ^a	0.72	0.70	0.69	0.70	0.71	0.65	-	0.70	0.57	0.62	0.67	0.61	0.58	0.69
		R(temporal) ^b	-0.48	-0.22	-0.45	-0.55	-0.41	0.04	-	-0.19	0.64	0.08	-0.37	0.65	-0.04	-0.17
		MBE	-0.69	2.95	-6.14	-6.61	-3.89	4.94	-	21.8	10.5	-0.07	0.31	-5.19	-12.2	0.47
		NMB(%)	-3.8	16.1	-33.5	-36.0	-21.2	26.9	-	118.7	57.1	-0.4	1.69	-28.3	-66.3	2.59
		RMSE	7.20	10.04	8.95	9.24	7.48	8.78	-	29.24	13.48	8.30	7.33	8.82	14.48	7.20

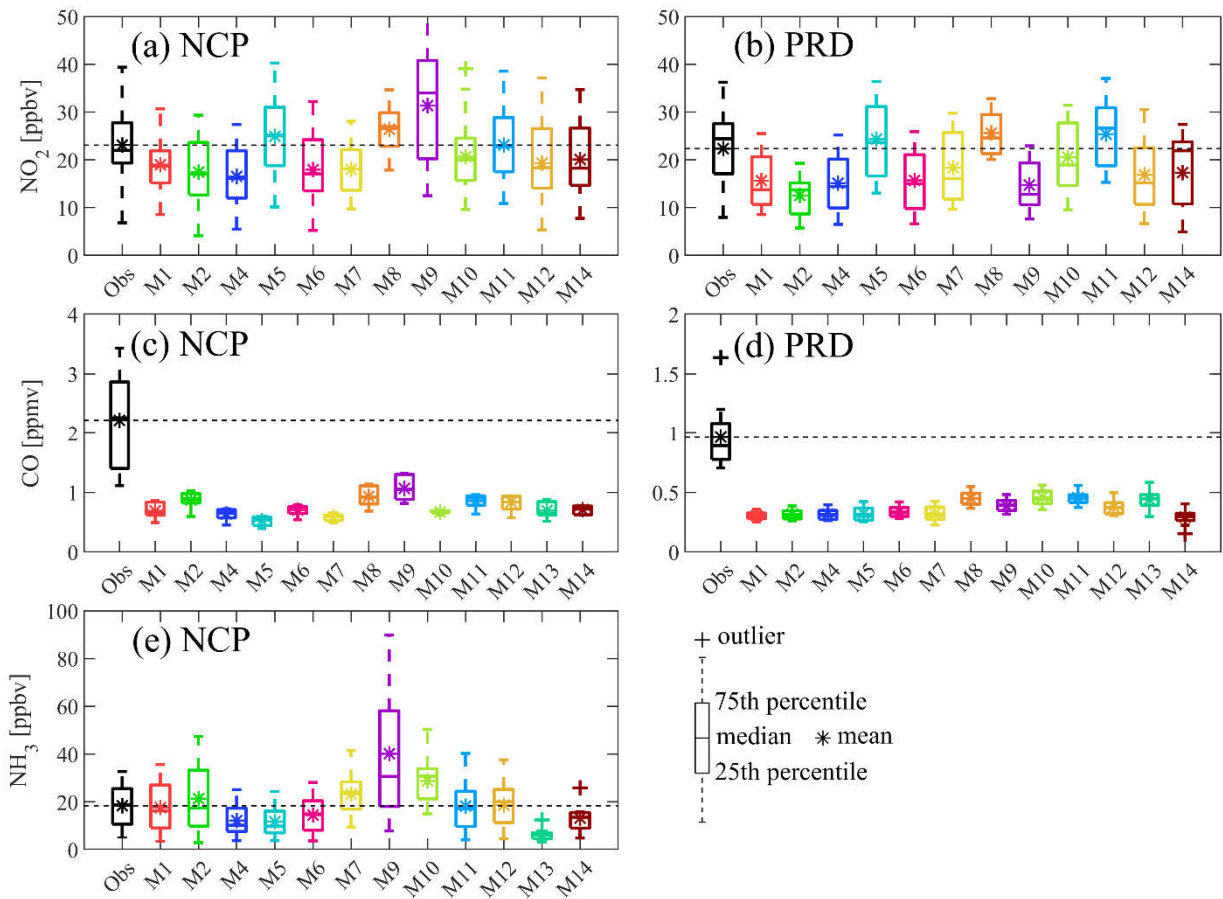
768 ^a R(spatial) represents the spatial correlation coefficients between simulated and observed concentrations sampled from different stations in NCP or PRD;

769 ^b R(temporal) represents the temporal correlation coefficients between simulated and observed monthly mean concentrations from January to December in 2010;

770



772
773 **Figure 1: Modeling domains of the participated models except M13 and M14 along with spatial distributions of the total emissions**
774 **of (a) NO_x , (b) CO and (c) NH_3 in 2010 provided by MICS-Asia III (upper panel), and the distributions of observation stations of (d)**
775 **NO_2 and CO over the NCP and PRD regions, as well as (e) NH_3 over the NCP region (lower panel). The horizontal resolution is**
776 **45km \times 45km. Note that domains of M13 and M14 are shown in fig. 7 and only six of nineteen observational sites (green) over the**
777 **NCP region have CO measurements.**



778

779 **Figure 2: Boxplot of simulated and observed annual mean NO₂, CO and NH₃ concentrations sampled from different stations over**
 780 **the NCP (a, c, e) and PRD (b, d) regions. The outlier was defined as values larger than $q_3 + 1.5 \times (q_3 - q_1)$ or less than $q_1 -$**
 781 **$1.5 \times (q_3 - q_1)$, where q_3 denotes the 75th percentile, and q_1 the 25th percentile. This approximately corresponds to 99.3 percent**
 782 **coverage if the data are normally distributed.**

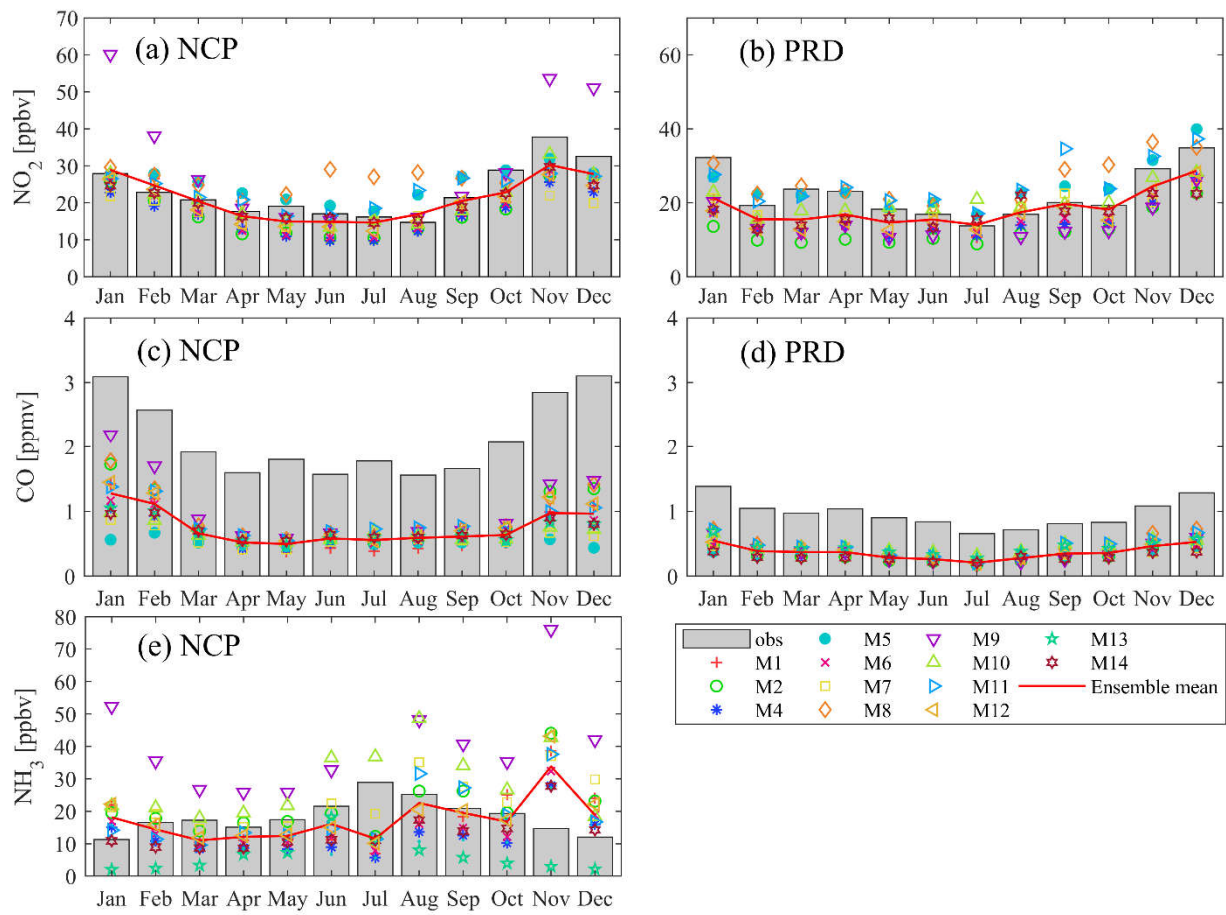


Figure 3: Timeseries of regional mean NO₂, CO concentrations over the NCP (a, c) and PRD (b, d) regions as well as NH₃ concentrations over the NCP (e) region from January to December in year 2010.

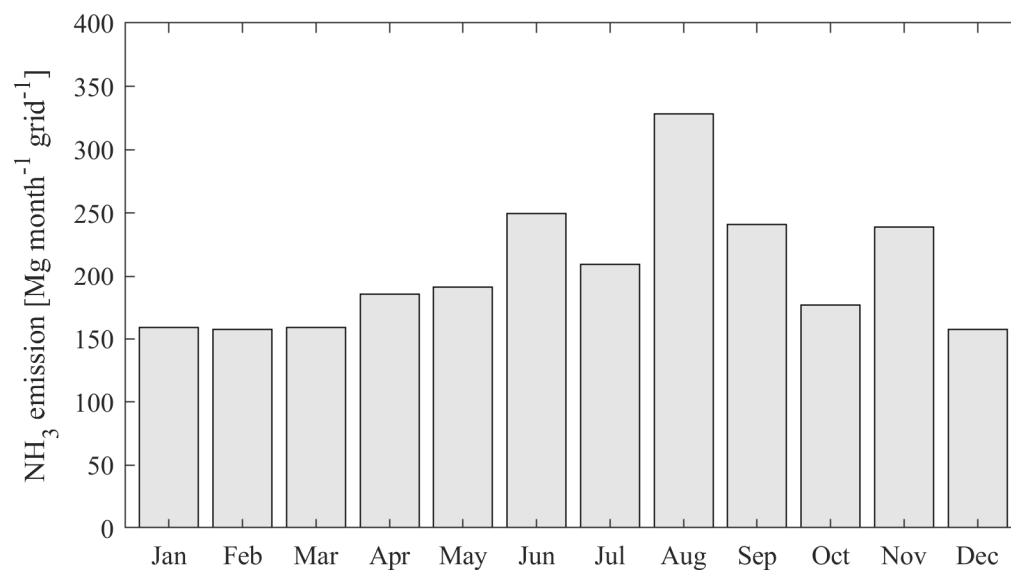


Figure 4: Timeseries of NH₃ emissions over the NCP region provided by MICS-Asia III on a horizontal resolution of 45km×45km from January to December in year 2010.

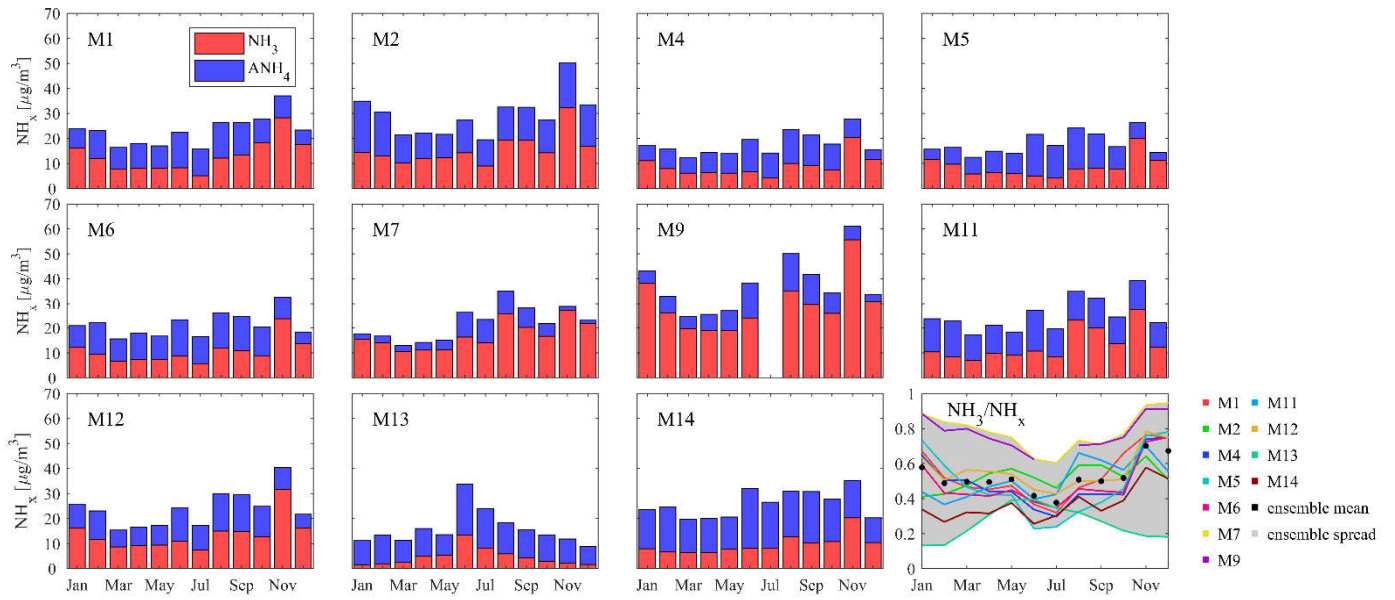
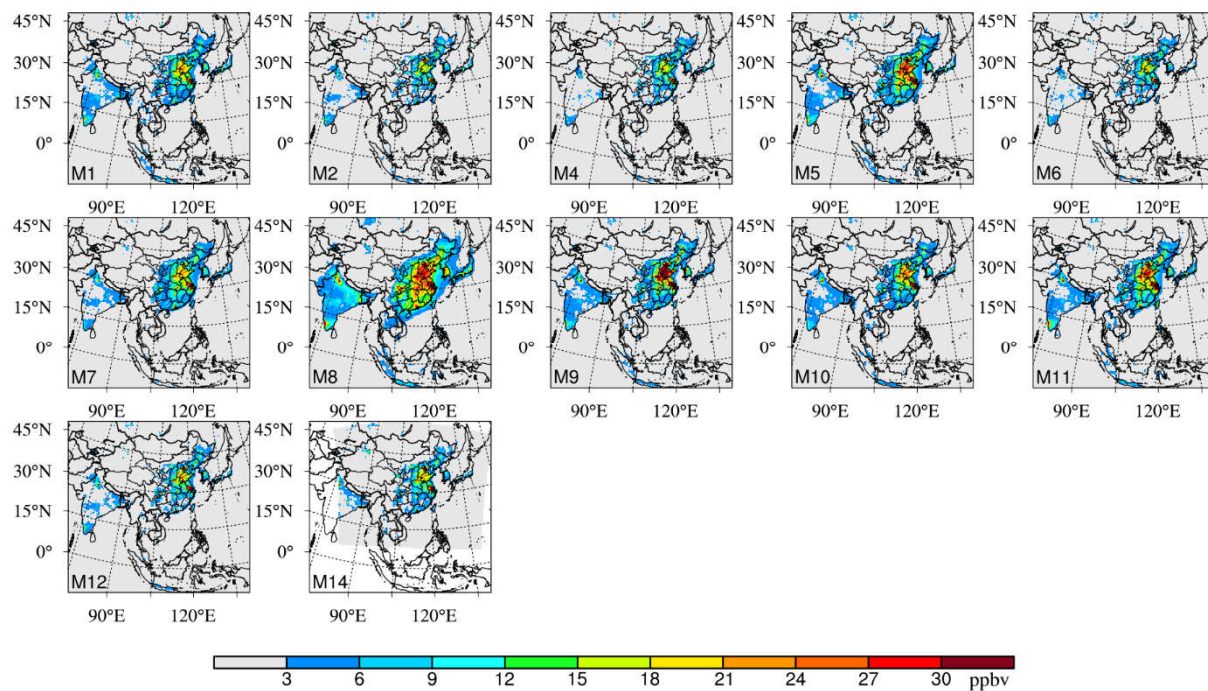


Figure 5: Timeseries of the multi-model simulated total ammonium ($\text{NH}_x = \text{NH}_3 + \text{NH}_4^+$) in atmosphere along with the ratio of gaseous NH_3 to the total ammonium over the NCP region from January to December in year 2010.



814

815 **Figure 6: Spatial distribution of the annual mean NO₂ concentrations from each modeling results of MICS-Asia III. Note that M13**

816 **are not included in this figure.**

817

818

819

820

821

822

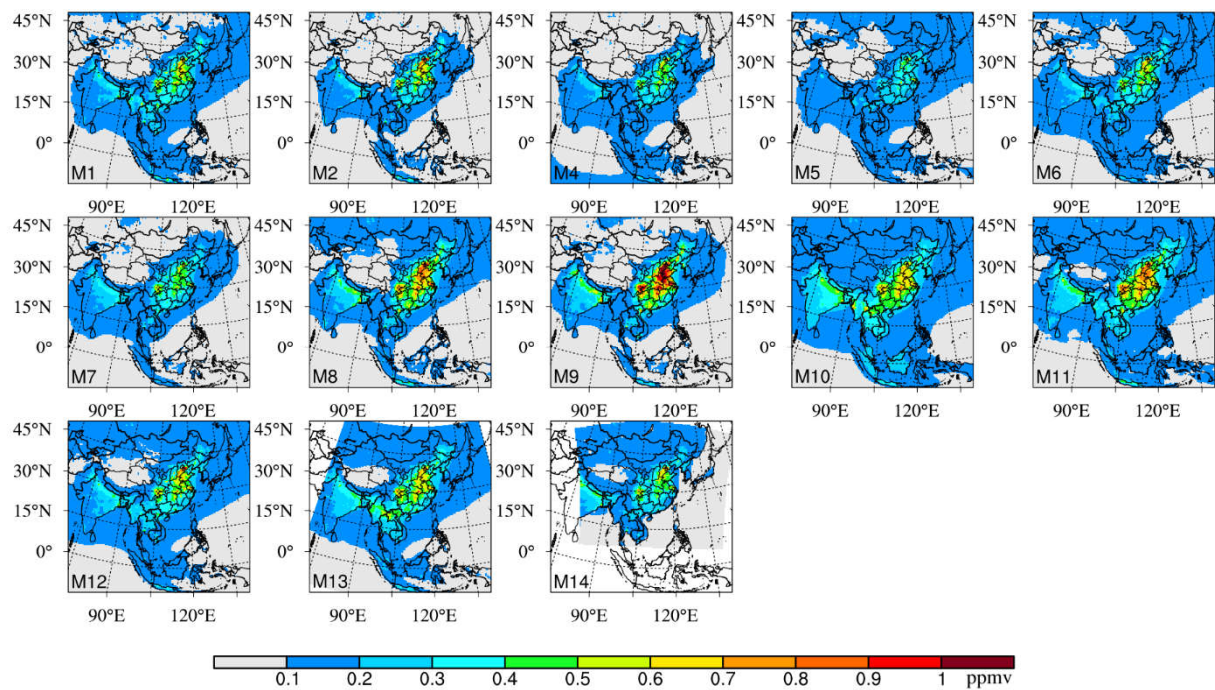
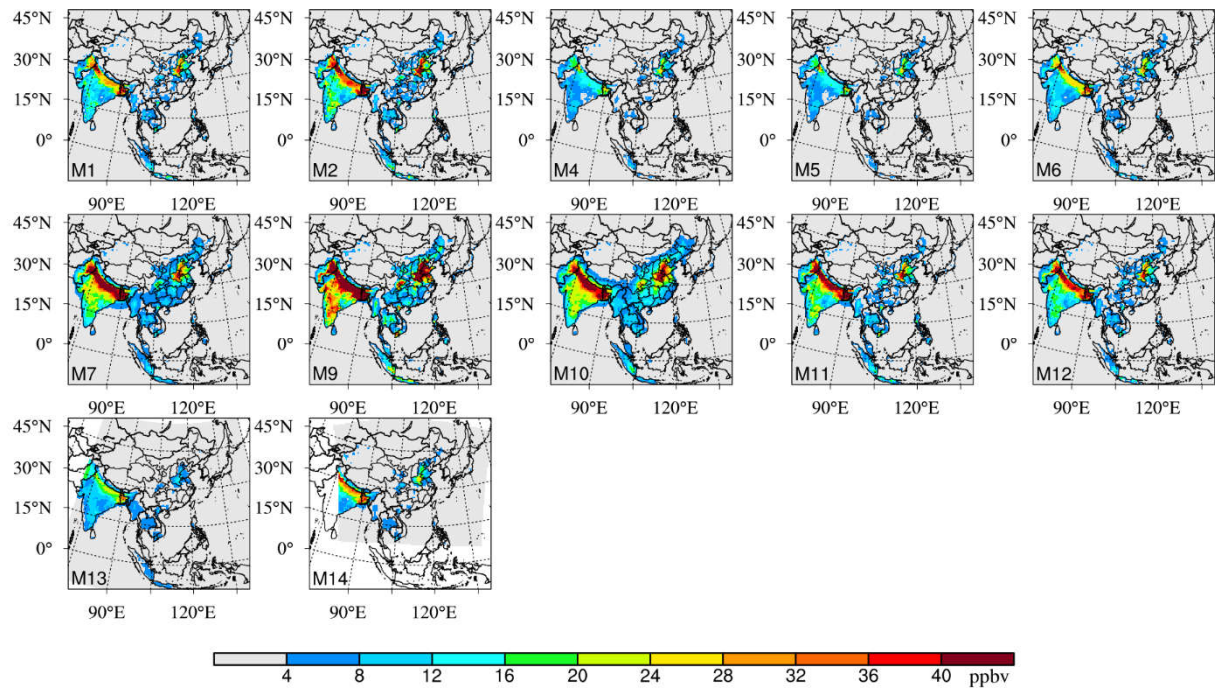


Figure 7: Spatial distribution of the annual mean CO concentrations from each modeling results of MICS-Asia III.

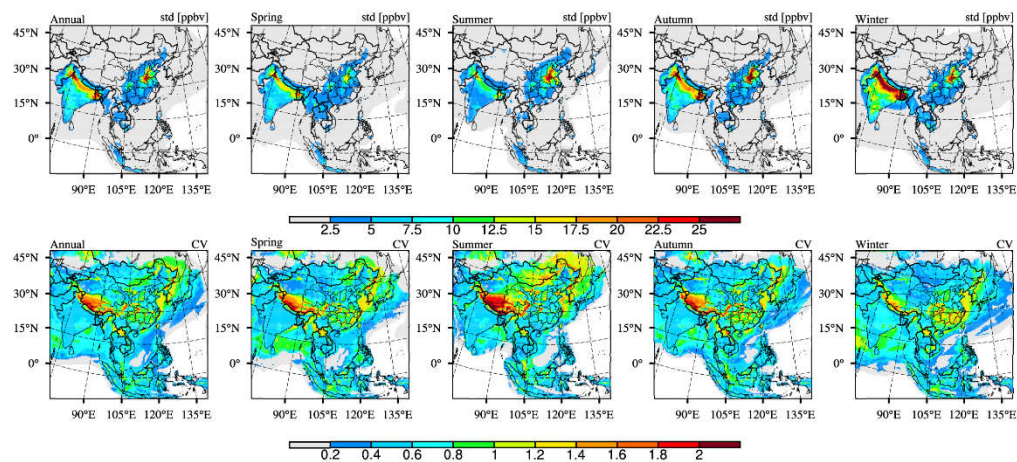


832

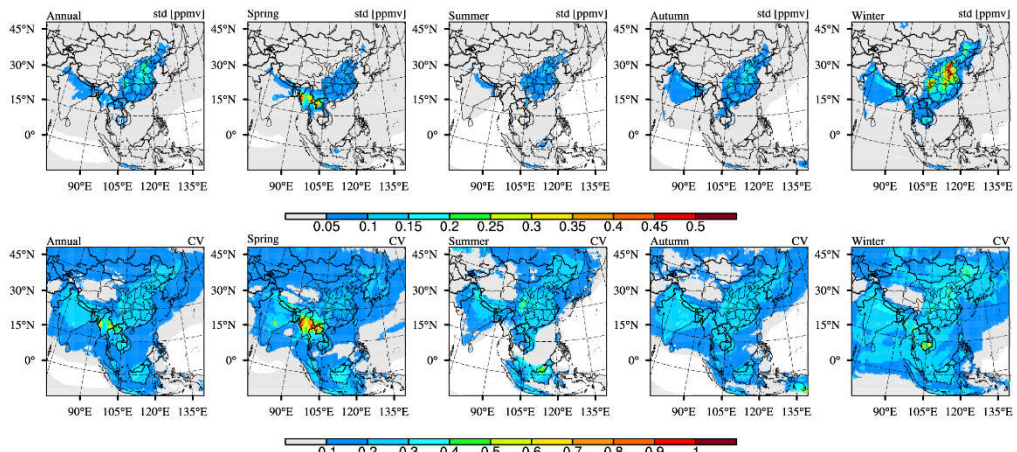
833 **Figure 8: Spatial distribution of the annual mean NH_3 concentrations from each modeling results of MICS-Asia III.**

834

(a) NH_3 :



(b) CO :



(c) NO_2 :

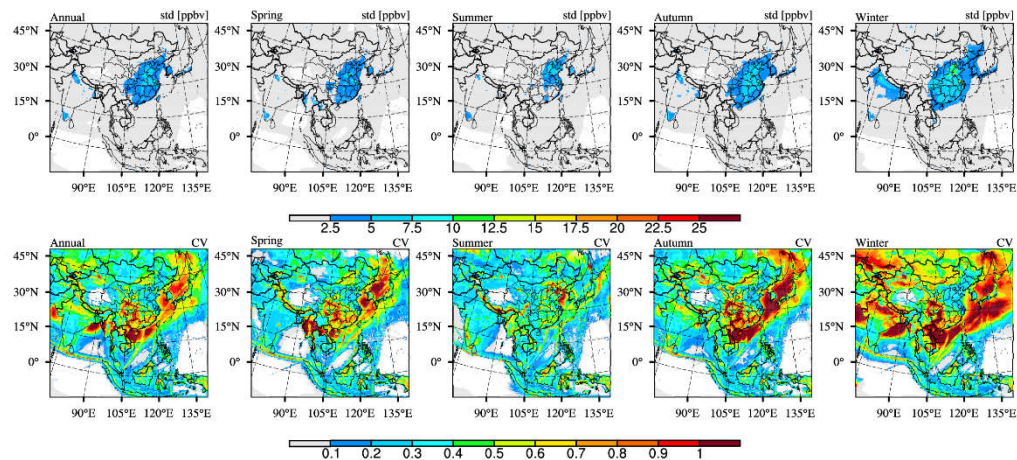


Figure 9: Spatial distribution of the standard deviation of (a) NH_3 , (b) CO and (c) NO_2 multi-model predictions in MICS-Asia III, as well as the corresponding distribution of CV on the annual and seasonal basis.

Supplementary Material

Sect. S1 Evaluations of the standard meteorological simulations

Meteorological simulations have large impacts on the simulations of atmospheric chemistry. The simulated wind speed (u-wind and v-wind), relative humidity (RH) and air temperature (T) from the standard meteorological fields were evaluated against the observations over the NCP and PRD regions. These parameters are all important factors that influences the simulations of NO₂, CO and NH₃. For example, the wind speed determines the transport of species and the air temperature influences the reaction rates of thermal chemical reactions. The RH and T also influence the thermodynamic equilibrium of gases and aerosols.

Three-hourly meteorological observations from the Integrated Surface Database (ISD) compiled by the National Oceanic and Atmospheric Administration (NOAA), U.S. (Smith et al., 2011) were used in meteorological evaluations with observation sites in the NCP and PRD regions shown in fig S1. Figure S2 shows the averaged time series of the simulated and observed meteorological parameters over the NCP region from January, 2010 to December, 2010. The evaluation statistics, including correlation coefficient (R), mean bias error (MBE) and root of mean square error (RMSE), were summarized in Table S2. It clearly shows that the standard meteorology simulations well captured the main features of the observed meteorological conditions in NCP throughout the year with high correlation coefficient, small biases and low errors for all meteorological parameters. Similar results could be obtained from the evaluations of meteorological conditions over the PRD region (fig. S3). These results suggested that the standard meteorological simulations can well reproduce the meteorological conditions of the NCP and PRD regions.

Sect. S2 Descriptions of the IASI measurement of NH₃ total columns

The ANNI-NH₃-v2.1R-I retrieval product (Van Damme et al., 2017; Van Damme et al., 2018) was used in this study to quantitatively evaluate the modeled monthly variations of NH₃ concentrations. It is a reanalysis version of NH₃ retrievals from IASI instruments and provides the daily morning (~9:30 am local time) NH₃ total columns from year 2008 to 2016. The morning orbit was used since IASI is generally more sensitive to the atmospheric boundary layer at this time due to more favorable thermal conditions, which could provide more information on the NH₃ concentrations in the boundary layer where NH₃ is emitted. The dataset was produced by Van Damme et al., 2018 based on the conversion of hyperspectral range indices (HRIs) using an Artificial Neural Network (Whitburn et al., 2016). It uses the ERA-interim ECWMF meteorological input data rather than the operationally provided EUMETSAT IASI Level 2 (L2) data used for the standard near-real-time version, which is more coherent in time and suitable for the study of temporal variations. To facilitate comparisons, the NH₃ total columns

873 were averaged to monthly data at 45km × 45km MICS-Asia grids.

874 **Sect. S3 Sensitivity experiments of high-resolution simulation in the PRD region**

875 To investigate the impacts of horizontal resolution on the simulations of gas concentrations over the PRD region, a full-
876 year run with finer horizontal resolutions has been conducted using the NAQPMS model, which is one of the participating
877 CTMs in MICS-Asia III. In our experiment, two nested domains with finer horizontal resolutions were added to the original
878 modeling domain of MICS-Asia III, which are shown in Fig. S4. The first domain (D1) is identical to the modeling domain of
879 MICS-Asia III with horizontal resolution of 45km. The second domain (D2) covers most part of southeast China with
880 horizontal resolution of 15km. The third domain has the finest horizontal resolution (5km) which covers the PRD region and
881 its surrounding areas. The chemical configurations of NAQPMS in each modeling domain were completely identical to those
882 used in MICS-Asia III. Meteorological fields for each modeling domain were simulated by the WRF model version 3.4.1,
883 same as the standard meteorological model in MICS-Asia III. The WRF configurations were also kept same as those used in
884 the standard meteorological simulations except two additional nested domains were added (Fig. S4). The emission inventories
885 and boundary conditions in D1 were provided by the standard input datasets of MICS-Asia III. Since MICS-Asia III only
886 provided the 45km-resolution emission inventories and boundary conditions, the emission rates ($\mu\text{g}/\text{m}^2/\text{s}$) and boundary
887 conditions over one model grid in D2 and D3 were simply obtained from the corresponding model grid in its parent domain.
888 This means that although we used the finer horizontal resolutions in D2 and D3, the resolutions of emission inventories and
889 boundary conditions in D2 and D3 were the same as those used in D1. Therefore, the horizontal resolutions were only
890 dynamically increased in D2 and D3. The modeling results from different modeling domains were then compared with each
891 other to investigate the dynamical impacts of horizontal resolution on the model performance.

892 Figure S5 shows the spatial distributions of the observed annual mean NO₂ concentrations in PRD region overlay the
893 simulated concentrations with different horizontal resolutions. We can clearly see that the coarse modeling results (D1) cannot
894 resolve the high spatial variability of NO₂ concentrations in the PRD region. For simulations using finer horizontal resolutions
895 (D2 and D3), although the spatial scales of NO₂ observations can be resolved by the 15km and 5km resolutions, the modeling
896 results still show poor performance in capturing the observed spatial variability of NO₂ concentrations, with calculated
897 correlation coefficient only of 0.03 and 0.02, respectively (Table S3), even worse than the coarse modeling results. Similar
898 results could be obtained from the comparisons of CO observations and simulations using different horizontal resolutions (Fig.
899 S6). These results indicated that the poor model performance in PRD may not be attributed to the resolution of model but more
900 related to the resolution and/or spatial allocation of emission inventories in the PRD region. These results also suggested that
901 only increasing the resolution of model may not help improve the model performance.

902

903

904 **Tables:**

905 Table S1 Configurations of the standard meteorological model and different WRF-Chem models

No	Microphysics		Longwave radiation		Shortwave radiation		Boundary layer	Cumulus physics			surface physics		
Standard	Lin et al. scheme		RRTMG scheme		Goddard shortwave scheme		YSU scheme	Grell 3D ensemble scheme			Unified Noah land-surface model		
M7	Lin et al. scheme		RRTM scheme		Goddard shortwave		YSU scheme	Grell 3D ensemble scheme			Unified Noah land-surface model		
M8	Lin et al. scheme		RRTMG scheme		RRTMG scheme		Mellor-Yamada-Janjic TKE scheme	Grell 3D ensemble scheme			Unified Noah land-surface model		
M9	Lin et al. scheme		RRTMG scheme		RRTMG scheme		YSU scheme	Grell 3D ensemble scheme			Unified Noah land-surface model		
M10	Goddard Ensemble	Cumulus	Goddard scheme	longwave	Goddard scheme	shortwave	YSU scheme	Grell 3D ensemble scheme			Unified Noah land-surface model		

906

907 Table S2 Evaluation metrics of the standard meteorological simulation

	NCP			PRD		
	R	MBE	RMSE	R	MBE	RMSE
temp (°C)	1.00	0.21	1.08	1.00	-0.22	0.71
RH (%)	0.97	-0.16	5.15	0.97	3.42	4.82
u-wind (m/s)	0.91	-0.08	0.63	0.82	-0.20	0.53
v-wind (m/s)	0.93	0.33	0.76	0.93	0.05	0.81

908

909 Table S3: Evaluation metrics of the simulated annual mean NO₂ and CO concentrations over the PRD region with different
910 horizontal resolutions.

	NO ₂ (ppbv)				CO (ppmv)			
	Spatial R	MBE	NMB (%)	RMSE	Spatial R	MBE	MBE (%)	RMSE
45km	0.09	2.99	13.37	10.53	0.00	-0.51	-52.85	0.57
15km	0.03	2.19	9.81	10.15	0.00	-0.54	-56.25	0.60
5km	0.02	0.58	2.59	10.23	-0.10	-0.58	-59.23	0.62

911

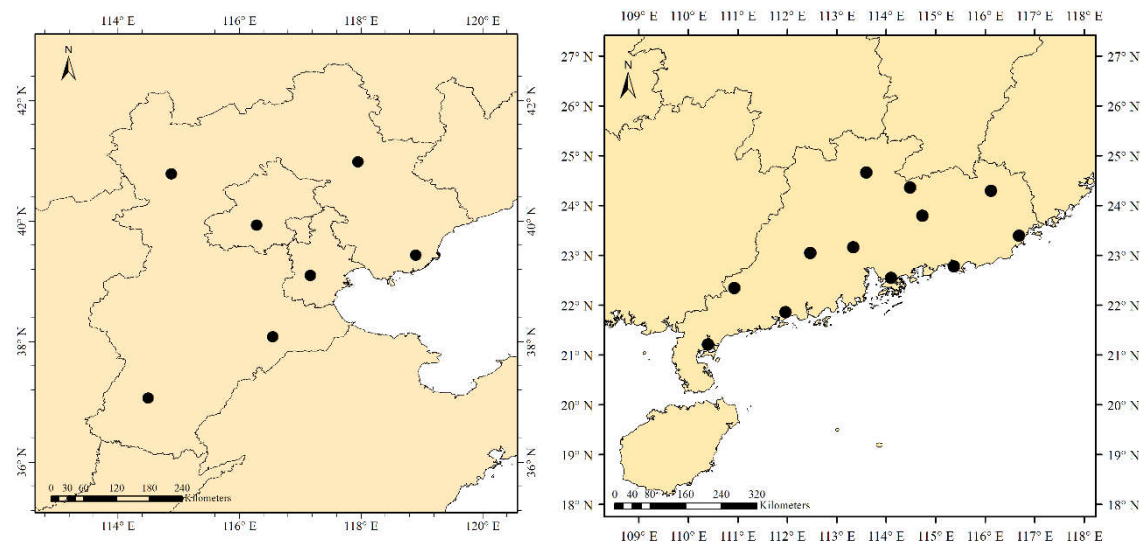
912

913

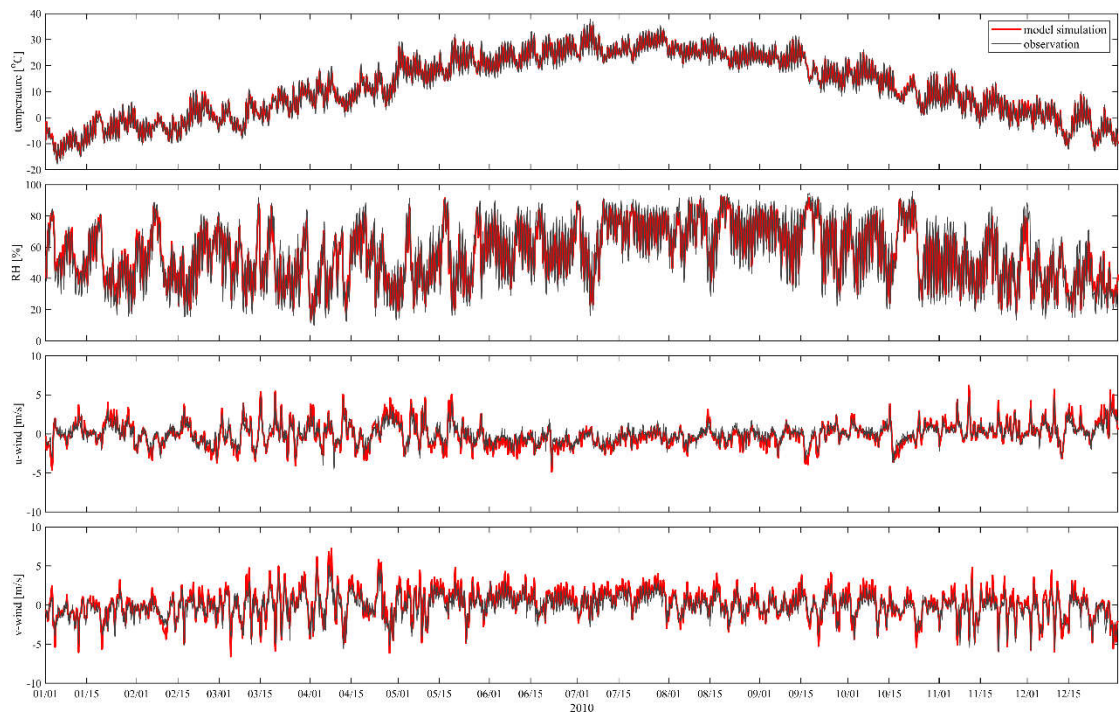
914

915

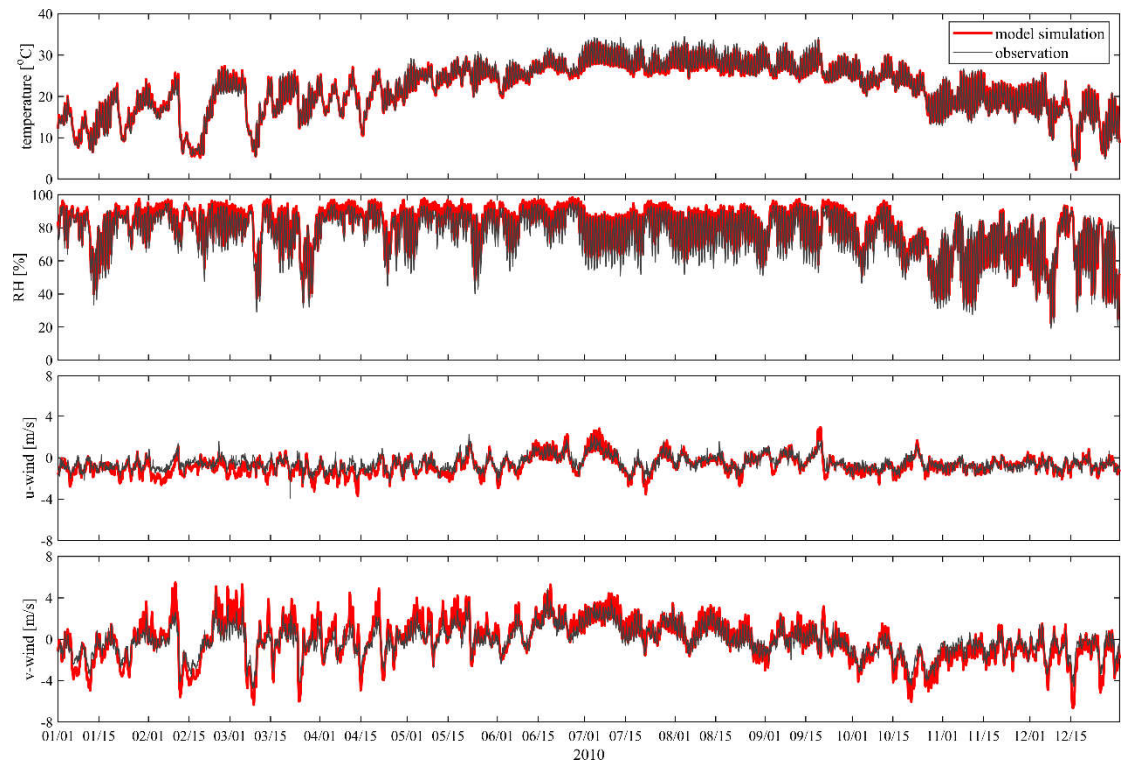
916 **Figures:**



917
918 **Figure S1: spatial distributions of the meteorological observation sites from the ISD over the NCP region (left panel) and the PRD**
919 **region (right panel).**

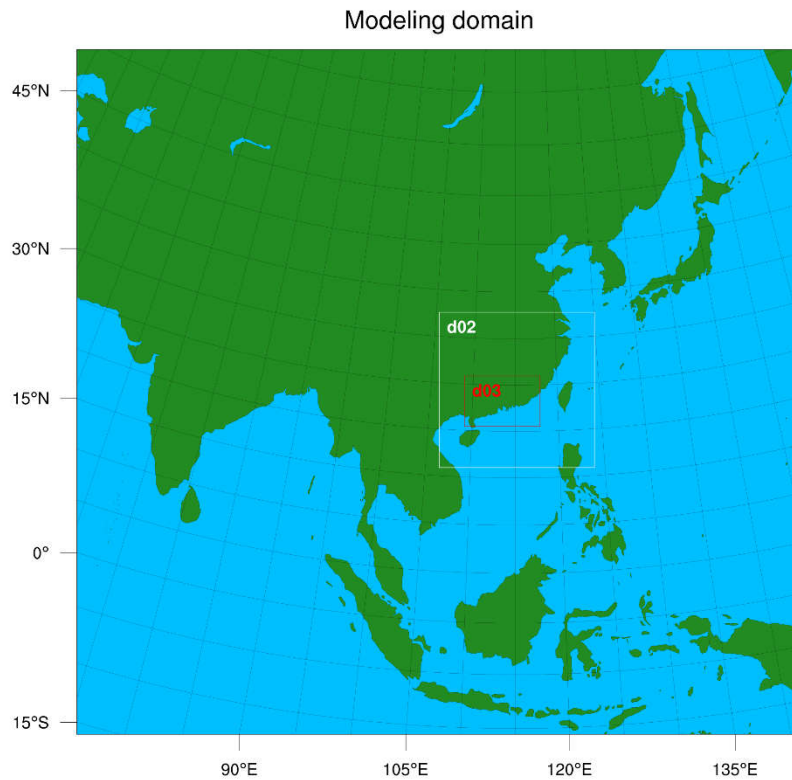


921
922 **Figure S2: Time series of the simulated and observed meteorological parameters over the NCP region form January 2010 to**
923 **December 2010 with an interval of three hours.**



924

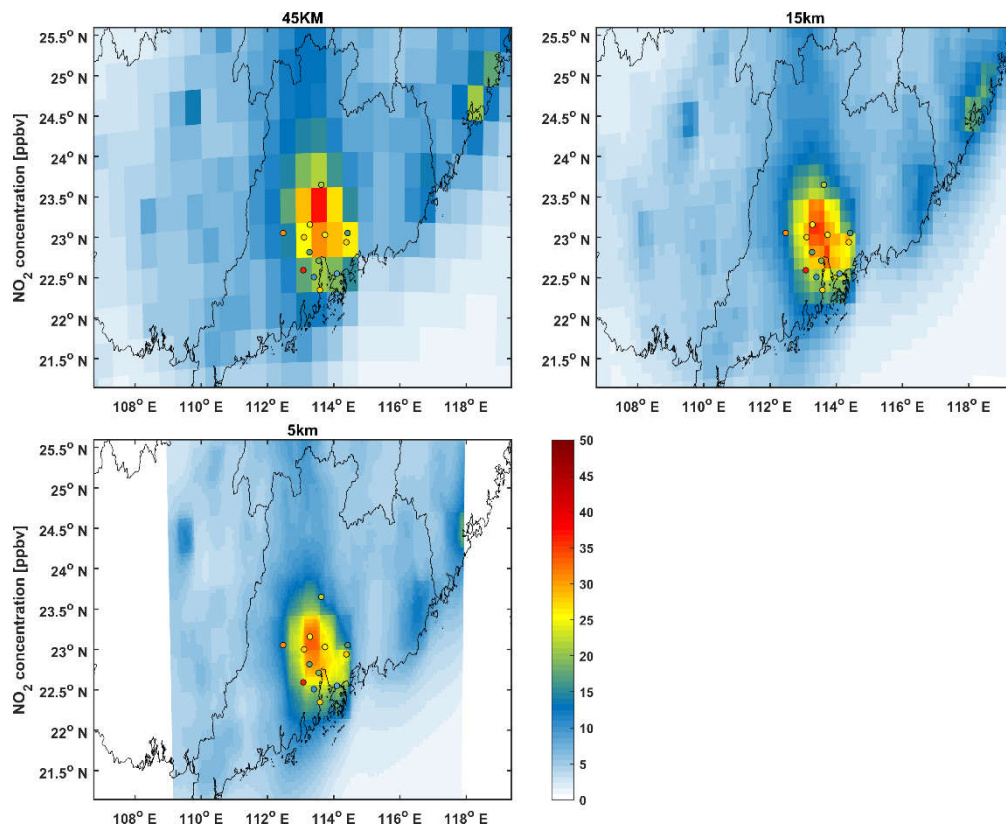
925 **Figure S3: Same as Figure S* but for the PRD region.**



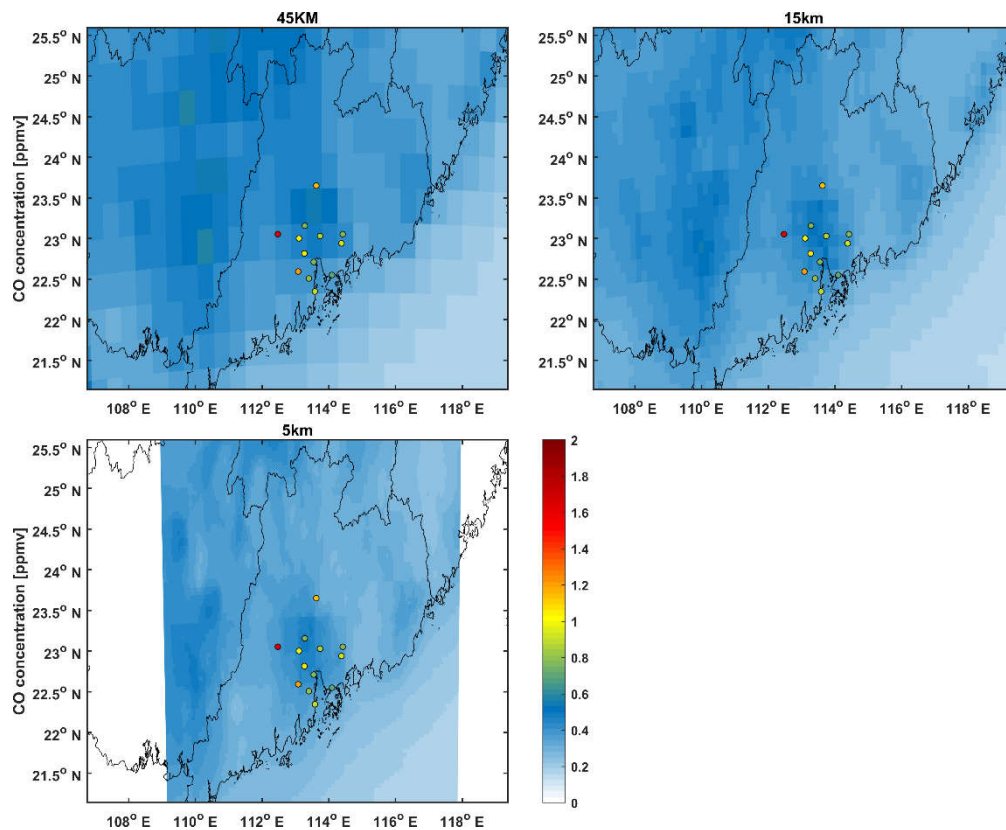
926

927 **Figure S4: Modeling domain of the sensitivity experiment using different horizontal resolutions. The first domain (D1) is identical**
 928 **to the modeling domain of MICS-Asia III with horizontal resolution of 45km. The second domain (D2) covers most part of southeast**
 929 **China with horizontal resolution of 15km, and the third domain has the finest horizontal resolution (5km) covering the PRD region**
 930 **and its surrounding areas.**

931



932
 933 **Figure S5: Spatial distributions of the observed and multi-resolution simulated annual mean NO_2 concentrations over the PRD**
 934 **region.**



935
 936 **Figure S6: Same as fig.S6 but for CO concentrations.**

937

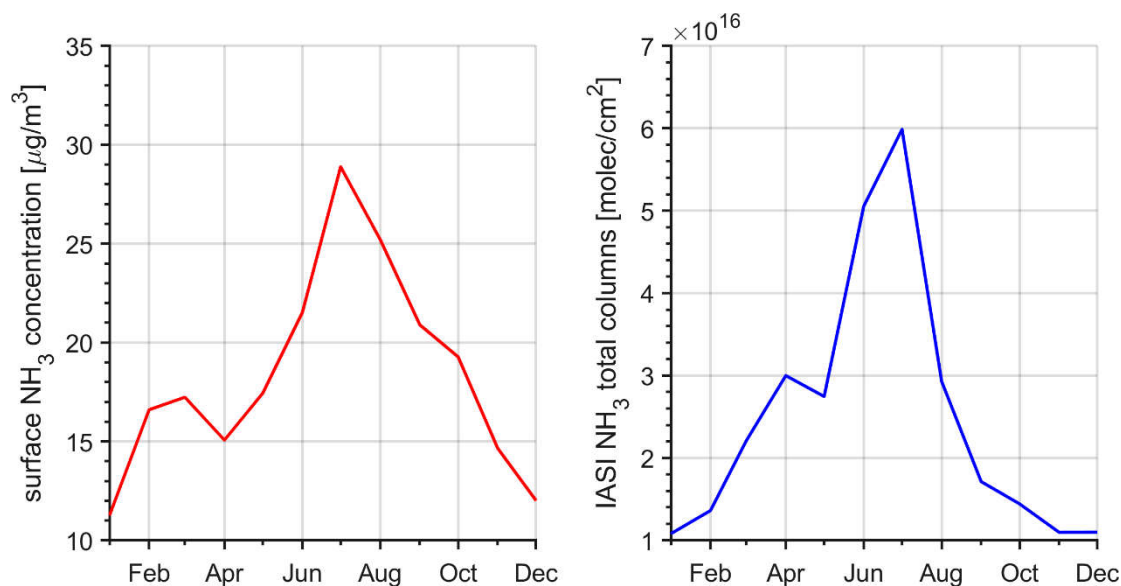


Figure S7: Time series of the surface NH₃ concentrations (left panel) from AMoN-China and NH₃ total columns from IASI (right panel) over the NCP region during September 2015 – August 2016. Note that we reordered the months to better characterise the monthly variations.

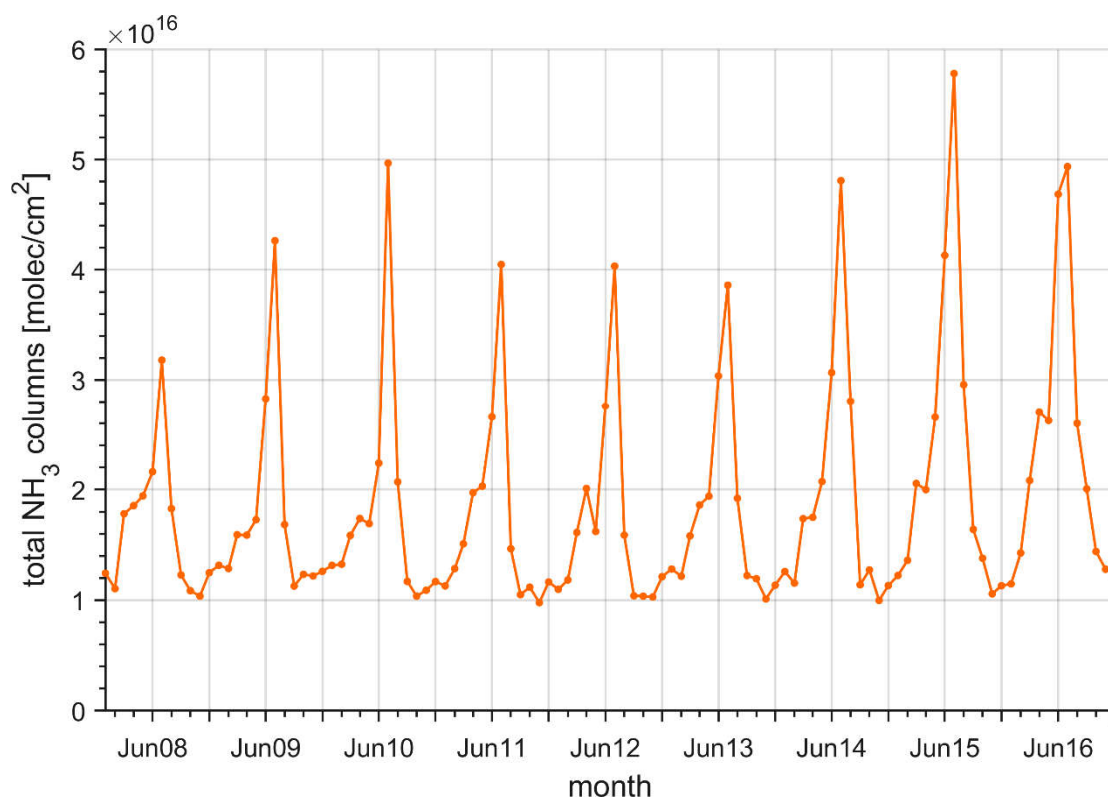


Figure S8: Monthly series of IASI measured NH₃ total columns over the NCP region from year 2008 to 2016

References

- Smith, A., Lott, N., and Vose, R.: The Integrated Surface Database Recent Developments and Partnerships, Bull. Amer. Meteorol. Soc., 92, 704-708, 10.1175/2011bams3015.1, 2011.
- Van Damme, M., Whitburn, S., Clarisse, L., Clerbaux, C., Hurtmans, D., and Coheur, P. F.: Version 2 of the IASI NH₃ neural network retrieval algorithm: near-real-time and reanalysed datasets, Atmos. Meas. Tech., 10, 4905-4914, 10.5194/amt-10-4905-2017, 2017.

952 Van Damme, M., Clarisse, L., Whitburn, S., Hadji-Lazaro, J., Hurtmans, D., Clerbaux, C., and Coheur, P.-F.: Level 2 dataset
953 and Level 3 oversampled average map of the IASI/Metop-A ammonia (NH₃) morning column measurements (ANNI-
954 NH3-v2.1R-I) from 2008 to 2016. PANGAEA, 2018.

955 Whitburn, S., Van Damme, M., Clarisse, L., Bauduin, S., Heald, C. L., Hadji-Lazaro, J., Hurtmans, D., Zondlo, M. A., Clerbaux,
956 C., and Coheur, P. F.: A flexible and robust neural network IASI-NH₃ retrieval algorithm, J. Geophys. Res.-Atmos., 121,
957 6581-6599, 10.1002/2016jd024828, 2016.

958

959